AWARD NUMBER: W81XWH-13-1-0409

TITLE: The Role of Skp2 in the Prostate Tumorigenesis Following Rb and p53 Loss

PRINCIPAL INVESTIGATOR: Hongling Zhao

CONTRACTING ORGANIZATION: Albert Einstein College of Medicine
Bronx, NY 10461

REPORT DATE: December 2015

TYPE OF REPORT: Final Report

PREPARED FOR: U.S. Army Medical Research and Materiel Command
Fort Detrick, Maryland 21702-5012

REPORT DOCUMENTATION PAGE

Form Approved
OMB No. 0704-0188

1. REPORT DATE	**2. REPORT TYPE**	**3. DATES COVERED**
December 2015	Final Report	26 Sep 2013 - 25 Sep 2015

4. TITLE AND SUBTITLE

The Role of Skp2 in the Prostate Tumorigenesis Following Rb and p53 Loss

5a. CONTRACT NUMBER

5b. GRANT NUMBER
W81XWH-13-1-0409

5c. PROGRAM ELEMENT NUMBER

6. AUTHOR(S)

Hongling Zhao

E-Mail:Hongling.zhao@einstein.yu.edu

5d. PROJECT NUMBER

5e. TASK NUMBER

5f. WORK UNIT NUMBER

7. PERFORMING ORGANIZATION NAME(S) AND ADDRESS(ES)

Albert Einstein College of Medicine of Yeshiva University
Department of Developmental and
Molecular Biology
Room 521 Ullmann
1300 Morris Park Avenue
Bronx, NY 10461-1975

8. PERFORMING ORGANIZATION REPORT NUMBER

9. SPONSORING / MONITORING AGENCY NAME(S) AND ADDRESS(ES)

U.S. Army Medical Research and Materiel Command
Fort Detrick, Maryland 21702-5012

10. SPONSOR/MONITOR'S ACRONYM(S)

11. SPONSOR/MONITOR'S REPORT NUMBER(S)

12. DISTRIBUTION / AVAILABILITY STATEMENT

Approved for Public Release; Distribution Unlimited

13. SUPPLEMENTARY NOTES

14. ABSTRACT

Prostate cancer is the most commonly diagnosed male cancer and the second highest cause of cancer death in the West. The most unique and fundamental aspect of prostate cancer is its initial androgen-dependence (AD) and inevitable progression to androgen-independent (AI) disease when subjected to androgen ablation therapy. Currently, AI prostate cancer is incurable and kills thirty thousand men annually in the US. pRb and p53 are two major tumor suppressors, and have been associated with human prostate cancers. Inactivation of both genes in mouse prostate results in rapidly developing carcinomas, with median survival of 226 days. Supported by DOD postdoctoral training grant, I found that p53 activates expression of Pirh2 and KPC1, two of the ubiquitin ligases for p27. Loss of p53 in the absence of Skp2, the third ubiquitin ligase for p27, shrinks the cellular pool of p27 ubiquitin ligases to accumulate p27 protein. In the absence of pRb and p53, p27 was unable to inhibit DNA synthesis in spite of its abundance, but could inhibit division of cells that maintain DNA replication with re-replication. This mechanism blocked pRb and p53 doubly deficient prostate tumorigenesis lastingly coexistent with BrdU-labeling neoplastic lesions, revealing an unconventional cancer cell vulnerability when pRb and p53 are inactivated. Overexpression of Skp2 coupled with under expression of p27 is frequent characteristics of cancer cells. Ubiquitination of p27 by SCF^{Skp2} requires Cks1 and depends on the interaction between the Skp2/Cks1 pocket and the phosphorylated Thr187 of p27. I further identify p27 ubiquitination by SCFSkp2/Cks1 becomes rate limiting in pRb and p53 deficient (DKO) prostate tumorigenesis . Thus, p27 protein accumulated in prostate when p27T187A KI mice underwent DKO prostate tumorigenesis. p27T187A KI or Skp2 knockdown (KD) induced similar degrees of p27 protein accumulation in DKO prostate cells, and Skp2 KD did not increase p27 protein in DKO prostate cells that contained p27T187A KI (AADKO prostate cells). p27T187A KI activated an E2F1-p73 apoptosis axis in DKO prostate tumorigenesis, slowed disease progression, and significantly extended survival. An Skp2/Cks1 pocket inhibitor preferentially collapsed DKO prostate tumor organoids over AA DKO organoids, which spontaneously disintegrated over time when DKO prostate tumor organoids grew larger. Querying TCGA of prostate cancer for the genetic status of five prostate cancer drivers revealed statistically significant co-occurrences of TP53 inactivation and MYC activation in primary prostate cancer. With disease progression to metastatic castration resistant prostate cancer (mCRPC), co-inactivation of RB1 and TP53 became the only statistically significant co-occurrences. Our findings identify targeting the Skp2/Cks1 pocket as a potential therapy strategy for mCRPC.

15. SUBJECT TERMS

pRb, p53, Skp2, ubiquitin ligase, p27, $p27^{T187A/T187A}$, p27 phophorylation, Skp2/Cks1 inhibitors, prostate cancer, tumorigenesis, organoid culture.

16. SECURITY CLASSIFICATION OF:			17. LIMITATION OF ABSTRACT	18. NUMBER OF PAGES	19a. NAME OF RESPONSIBLE PERSON
					USAMRMC
a. REPORT	b. ABSTRACT	c. THIS PAGE	UU	91	19b. TELEPHONE NUMBER *(include area code)*
U	U	U			

Table of Contents

INTRODUCTION:

pRb and p53 are the two of the best known tumor suppressor proteins. They play key roles in providing most and best of the cells' intrinsic antitumor mechanisms, such as proliferation arrest, cellular senescence, and apoptosis. pRb and p53 are frequently inactivated in cancer[1,2,3,4,5,6,7,8]. Reactivating pRb and p53 is a major goal of anticancer strategies. When pRb and p53 are genetically inactivated, cells would permanently lose the antitumor mechanisms provided by them. The Cancer Genome Atlas projects have shown that genetic inactivation of RB1 and TP53 is very common. Moreover, these mutations often co-occur, and the co-occurrences become more frequent in more advanced cancer, which likely explains why advanced cancer are more likely to resist current anticancer therapies. Finding successful treatments for more advanced and multi-therapy resistant cancers will likely depend on our ability to discover antitumor mechanisms that are effective when pRb and p53 are genetically inactivated. S phase kinase-associated protein 2 (Skp2) is an F-box protein in the Skp1-Cul1-Fbox (SCF) E3 ubiquitin ligase, responsible for ubiquitination of p27 and other substrates. Elevated Skp2 protein expression is frequent in human prostate cancers, and is associated with loss of p27 and reduced survival. Pandolfi Lab found that targeting Skp2 suppresses pten-deficient prostate cancer[9]. Our lab showed that Skp2 is essential for survival of Rb-deficient melanotrophs[10]. The purpose of this research is to determine whether deletion of Skp2 can block tumorigenesis following loss of pRb and p53 in mouse prostate tumor model. The scope of the research is from the determine the role of Skp2 in prostate tumorigenesis induced by loss of both pRb and p53, and to dissect the detail molecular mechanisms of the roles of Skp2 in the tumorigenesis by investigating whether the effects of Skp2 loss on prostate tumorigenesis is p27-dependent. Finally, we will determine the other mechanisms of Skp2 in prostate tumorigenesis in pRb and p53 double deficient mice.

KEYWORDS:

pRb, p53, ,Skp2, p27, $p27^{T187A/T187A}$, p27 phophorylation, Tumor Suppressors, Ubiquitin Ligase, Tumorigenesis, Safeguard, Antitumor Mechanism, Skp2/Cks1 inhibitors, prostate cancer, tumorigenesis, organoid culture.

OVERALL PROJECT SUMMARY:

Task 1. To determine the roles of Skp2 in prostate tumorigenesis induced by loss of both pRb and p53 (Timeline 1-3 months).

I have finished Task 1. Please see attached paper in appendices for detail "Cancer Cell 2013 Nov 11;24(5):645-59".

Task 2. To determine whether Skp2's repressive effects on the prostate tumorigenesis is p27-dependent (Timeline: months 1-24).

Task 2a. p27T187A/T187A knock-in mice are available in our lab. We have set up breeding colonies in order to generate DKO;p27T187A/T187A (AADKO) male mice.

I have finished Task 2a, and is going to submit the manuscript for publication. Please see attached manuscript "p27T187A knockin mutation identifies Skp2/Cks1 pocket inhibitors for advanced prostate cancer". In this manuscript, we further identified E2F1-p73 axis is responsible for the apoptosis in DKO prostate following Skp2 deletion or p27T187A knockin.

Task 2b. To determine whether p27 is necessary for prostate tumorigenesis in this DKO model (Timeline: 1-24 months). We will generate at least 5 TKO;p27-/- male mice and littermate control.

As shown in manuscript "p27T187A knockin mutation identifies Skp2/Cks1 pocket inhibitors for advanced prostate cancer", p27T187A KI or Skp2 knockdown (KD) induced similar degrees of p27 protein accumulation in DKO prostate cells, and Skp2 knockdown did not increase p27 protein in DKO prostate cells that contained p27T187A KI (AADKO prostate cells). Moreover, even though p27T187A/T187A knockin delays tumor progression and prolongs the survival of DKO mice, it cannot completely phenocopy the effect of Skp2 deletion in blocking prostate tumorigenesis in DKO mice. Above evidence indicates that the other functions of Skp2 might also contribute to the blockage of tumorigenesis. So next, I decided to further investigate what functions of Skp2 might play roles in our prostate tumor mouse model instead do further crossing to get TKO;p27-/- male mice.

In addition to mediating ubiquitination and degradation of p27 to activate cyclin/CDKs, Skp2 can also ubiquitinate Akt1 to promote anaerobic glycolysis[11], and E-cadherin to promote cell migration[12]. Based on this platform, we identified multiple antitumor mechanisms of Skp2 deletion, including apoptosis by p73, blocking anaerobic glycolysis by targeting LDH-A, and dynamic control of EMT. We believe that we will identify multiple antitumor mechanisms of Skp2 in our pRb and p53 double deficient mouse prostate tumor model, which will be considered in designing therapies for advanced and multi-therapy resistant cancer.

So new task 2b is to identify multiple antitumor mechanisms of Skp2 deletion in our pRb and p53 double deficient mouse prostate tumor model.

Task 2b1. To determine significances and mechanisms of Skp2 functions in promoting anaerobic glycolysis.

A paradigm shifting finding for Skp2 function, reported in 2012, shows that Skp2 uses K63 linked ubiquitination to activate (rather than degrade) Akt function in promoting anaerobic glycolysis[11]. Since we learned that p27T187A KI only partially

phenocopies Skp2 KO in blocking DKO tumorigenesis, and a number of glucose metabolism steps have recently been identified as potential targets for anticancer therapy[13,14,15], this task 2b1 will reveal whether they could remain effective when pRb and p53 are both genetically inactivated. We established primary cultures of DKO prostate cancer cells (Figure 1) to study the functional significances of a select group of glucose metabolism enzymes. This included hexokinase 2 (HK2), the first enzyme that commits glucose to the glycolytic pathways when it is transported inside cells; lactate dehydrogenase A (LDH-A) the last enzyme in the anaerobic glycolysis pathway converting pyruvate to lactate for excretion; and glycine decarboxylase (GLDC), functioning in a branch of glycolysis for anabolic biosynthesis involving glycine, serine, and tetrahydrofolate. A search for their expression status in human prostate cancer tissues analyzed by TCGA revealed recurrences in their overexpression in 8-16% of the cases (Figure 1A). Some LDH-A overexpression co-occurred with HK2 overexpression. Figure 1B shows the relative expression levels of these three genes (each normalized with GAPDH in the same cells) in cultured DKO prostate cancer cells M1 and M21.

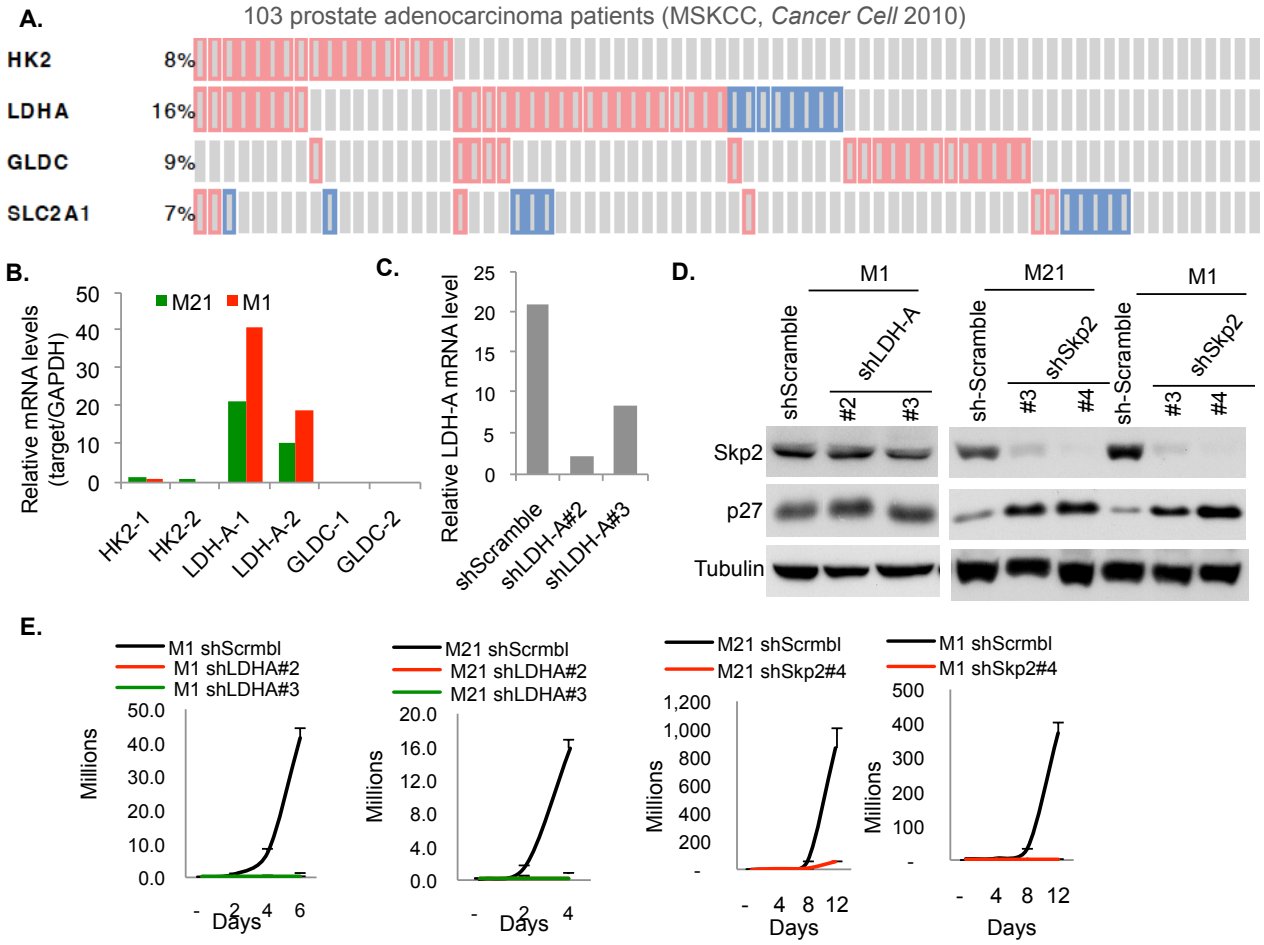

Figure 1. A, mRNA expression data from TCGA, every column represents one prostate cancer patient, red indicates higher expression than paired normal tissue, blue indicates lower expression. SLC2A1 encodes Glut1. B, Expression of the three indicated genes, measured byRT-qPCR with two sets of primers for each, in M1 and M21 DKO prostate cancer cells in culture. C, Knockdown of LDH-A measured by RT-qPCR. D, Effects of LDH-A knockdown on Skp2 and p27 protein in M1 cells. Effects of Skp2 knockdown on Skp2 and p27 protein in M21 and M1 DKO cells. E. Effects of knockdown of LDH-A and Skp2 on proliferation of M1 and M21 cells.

Interestingly, LDH-A expression stood out far above those of HK2 and GLDC. We next determined the functional significance of high expression of LDH-A. Remarkably, knockdown of LDH-A (Figure 1C) efficiently inhibited proliferation of M1 and M21 to similar extent as knockdown of Skp2 (Figure 1E). Unlike Skp2 knockdown, LDH-A knockdown did not reduce Skp2 protein and did not significantly increase p27 protein (Figure 1D). These results are consistent with Skp2 functions in these DKO cells to promote anaerobic glycolysis (anaerobic glycolysis: pyruvate is converted to lactate by lactate dehydrogenase).

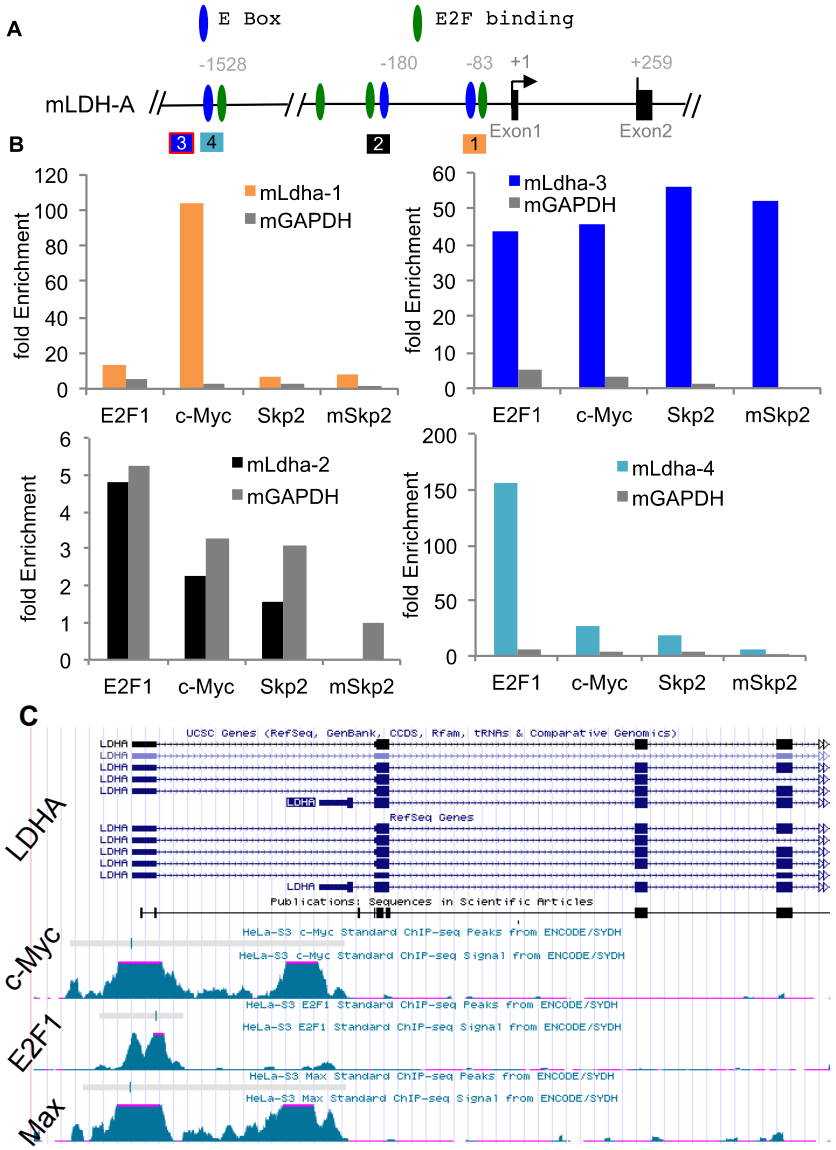

Figure 2. Skp2 and c-Myc co-localize on *LDHA* promoter. A. Schematic diagram of the promoter of mouse *LDHA.* Blue Ovals (E Box) indicates the consensus binding sites of c-MYC and the green ovals indicates the consensus binding sites of E2F1 (another upregulated gene in our DKO prostate cells). 1,2,3,4 in different color boxes indicate 4 primer sets used to detect c-Myc binding sites on *LDHA* promoter. B. Chromatin Immunoprecipitation (CHIP) results for *LDHA* promoter using E2F1, c-Myc, 2 Skp2 antibodies compared to control IgG using 4 pairs of primer (mLdha1-mLdha4). GAPDH primer was used as a negative control. C. ENCODE database revealed binding sites of Myc, Max and E2F1 on human LDHA promoter

It has been shown that Skp2 activates c-MYC by ubiquitination

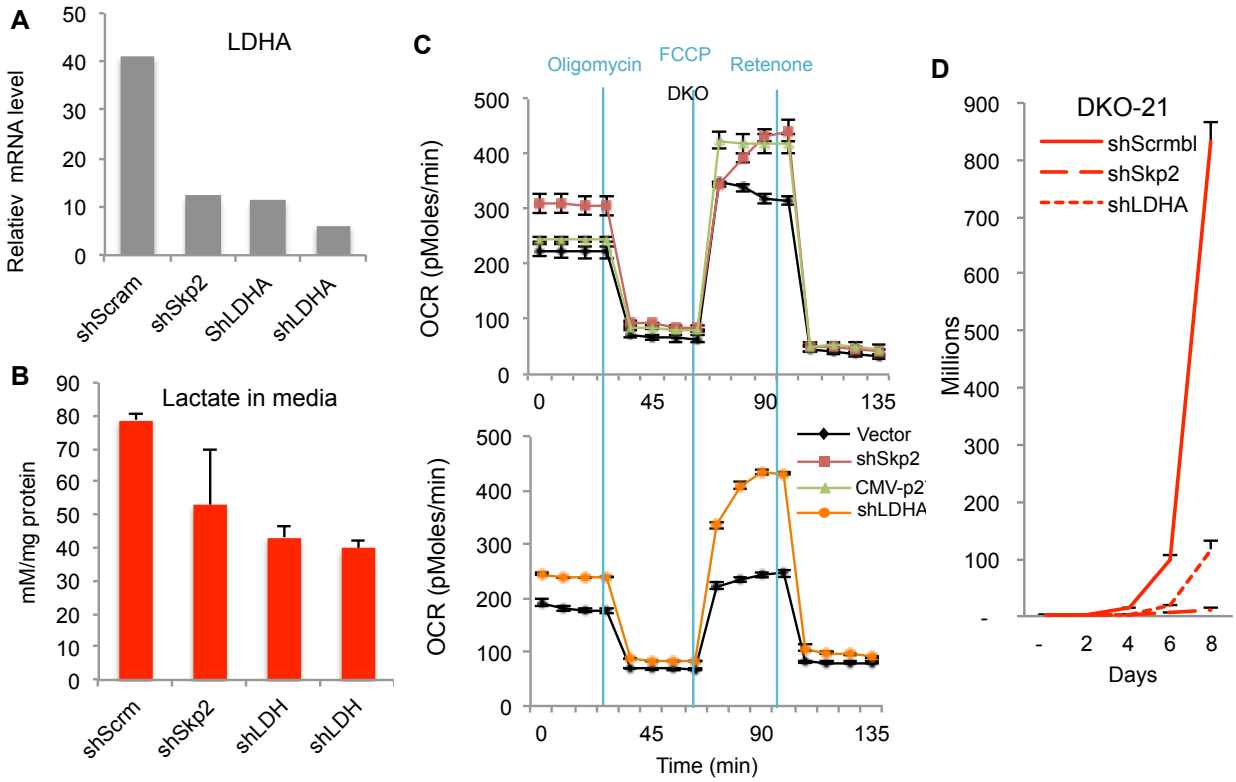

Figure 3. Knockdowns of Skp2 and LDHA phenocopies each other in mouse DKO prostate cancer cells. **(A)** RT-qPCR for LDHA expression. **(B)** Lactate production following indicated treatment. **(C)** Oxygen consumption rate (OCR) determination under indicated conditions. The value was normalized to total protein. **(D)** Cell proliferation of DKO prostate cancer cells in response to Skp2 or LDHA knockdown.

and is required for c-Myc to transactivate certain target genes[16,17]. LDHA is an established c-Myc target gene[18]. We hypothesize that in addition to targeting p27 proteasome degradation, Skp2 might also activate c-Myc-dependent LDHA expression. Using our early passage DKO prostate cancer cells, we performed ChIP and found Skp2 and c-Myc co-localized on the LDHA promoter, indicated by primer set #3 (Figure 2B). Interestingly, the mouse LDHA promoter also contains several E2F binding sequences (Figure 2A) and at least one of them recruited E2F1 to the promoter (the sequence 3 box, Figure 2B). Search of ENCODE database revealed E2F1 ChIP on human LDHA promoter as well (Figure 2C), suggesting pRb inactivation also contributed to LDHA expression activation. RT-qPCR showed that Skp2 knockdown reduced LDHA expression as efficiently as LDHA knockdown (Figure 3A). Similarly, knockdowns of Skp2 and LDHA phenocopied each other in mouse DKO prostate cancer cells regarding to the inhibitory effects on lactate production, oxygen consumption rate and cell proliferation (Figure 3B, 3C and 3D). These data suggest that Skp2 is an important co-activator of c-Myc in activation of LDHA transcription. Next we will determine whether the effects of Skp2 knockdown on LDHA expression is dependent on c-Myc and what role E2F1 plays in LDHA expression in DKO prostate

cancer cells. We will knockdown c-Myc and/or E2F1 in our DKO prostate cancer cells to determine whether Skp2 is still on the LDHA promoter. We will further determine the molecular mechanisms linking Skp2 to LDHA and the therapeutic effects of inhibiting LDHA using mouse and human prostate cancer cell cultures and organoid cultures. We will validate functional results from cell culture studies in DKO prostate tumorigenesis using an LDH-Alox mice, which was recently reported by Dr. Pankaj Seth's group[19]. Global deletion of LDH-A results in non-lethal hemolytic anemia. We will use PB4-Cre to delete LDH-A in prostate and determine whether it could inhibit DKO tumorigenesis. It is tantalizing that if deletion of LDH-A partially blocks DKO prostate tumorigenesis, and combining LDH-A deletion with p27T187A KI enhances the block to levels similar to those achieved by Skp2 KO. LDH-A may not be the only metabolic enzyme deregulated in DKO tumorigenesis. To more systematically determine the metabolism reprogramming in DKO tumorigenesis and how Skp2 deletion affects it, we will use M1 and M21 cells to perform metabolite profiling without Skp2 knockdown to identify additional metabolism reprograming features, and with Skp2 knockdown to identify how Skp2 functions in reprogramming. Einstein Diabetes Center has established expertise in metabolomics.

Task 2b2. To determine the role of Skp2 in EMT.

Another major advance in Skp2 function studies, also reported in 2012[12], is the identification of E-cadherin as an ubiquitination and degradation target of Skp2 after casein kinase I (CKI) mediated phosphorylation. DKO prostate tumorigenesis quickly progress to invasive and metastatic cancer[5]. It is possible that Skp2 promotes degradation of E-cadherin to promote this progression and, therefore, Skp2 deletion might block DKO prostate tumorigenesis by preventing E-cadherin degradation. An interesting uncertainty is that while ectopically expressed Skp2 can reduce E-cadherin protein levels, it did not lead to increased mesenchymal expression[5], suggesting that Skp2 might not be able to promote the entire EMT process.

In Figure 4, we stained prostate sections with EMT markers. Expression of E-cadherin and its membranous localization is clearly seen in WT and Skp2 KO prostate epithelium. In DKO PINs, some epithelial cells show reduced E-cadherin expression with loss of membranous localization. In several areas, entire acinus had lost E-cadherin expression. Interestingly, the loss of E-cadherin is not accompanied with gain of mesenchymal expression. Co-expression of E-cadherin and vimentin, which was seen in prostate cancer models by FGFR-1 activation[20] or by Pten deletion and KRAS activation[21], was not detected. These findings are consistent with Skp2 being promoting E-cadherin degradation without promoting gain of mesenchymal expression in LNCaP cells[12]. Significantly, in DKO PINs that were blocked by Skp2 deletion, multilayered epithelium maintained normal expression and membranous localization of E-cadherin lasting well into old age. At the invasive fronts of DKO tumor mass, tumor epithelial cells

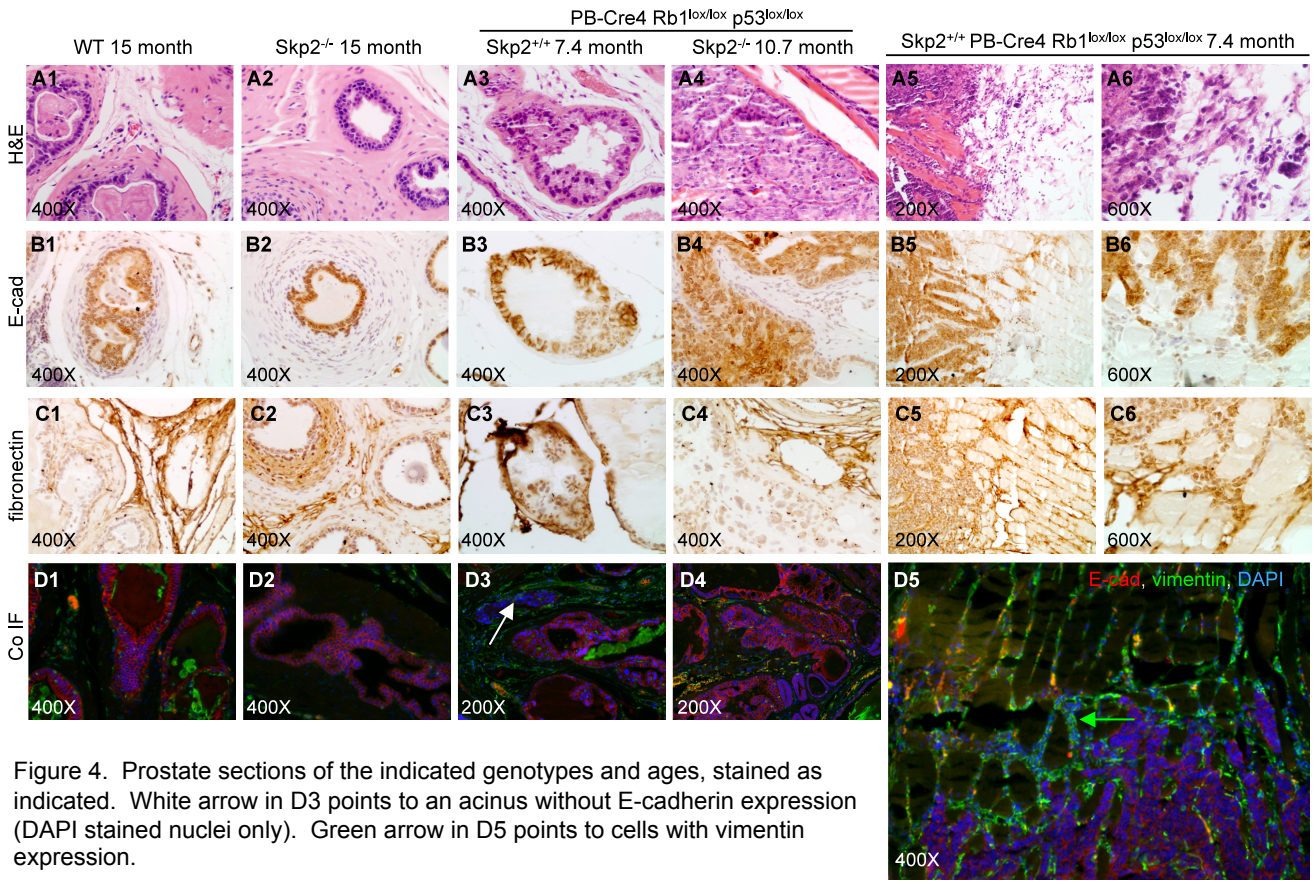

Figure 4. Prostate sections of the indicated genotypes and ages, stained as indicated. White arrow in D3 points to an acinus without E-cadherin expression (DAPI stained nuclei only). Green arrow in D5 points to cells with vimentin expression.

showed reduced E-cadherin expression but these cells did not express vimentin at the same time. Rather, in front of the DKO cancer cells that were weakly expressing E-cadherin we observed cells with strong cytoplasmic expression of vimentin. The epithelial origin of these cells are being determined with RosaR-YFP tracking.

When monolayer cultures of DKO tumor cells were established, they contained islands of cells with epithelial morphology among cells with spindly morphology (Figure 5). Cells with epithelial morphology expressed E-cadherin but not fibronectin and cells with spindly morphology expressed fibronectin but not E-cadherin. We clonally isolated cells in epithelial islands using cloning rings. However, upon expansion, all clones again showed a mixture of epithelial like and spindly like cells, suggesting a tendency to transit from epithelial to mesenchymal with loss of E-cadherin.

We will determine the role of Skp2 in the loss of E-cadherin expression in DKO prostate cancer cells. In culture, we will use Skp2 knockdown or Skp2 inhibitors C1 and C25 to determine whether these treatments could block the tendency to lose E-cadherin expression and transit to mesenchymal morphology. The first two such experiments showed positive results. In vivo, we will introduce the Cdh1lox allele to DKO prostate tumorigenesis to determine whether targeted deletion of Cdh1 could fasten progression to invasion and metastasis and whether Skp2 deletion could still block the DKO prostate tumorigenesis, or how long the block can last. If we obtain positive results, we will

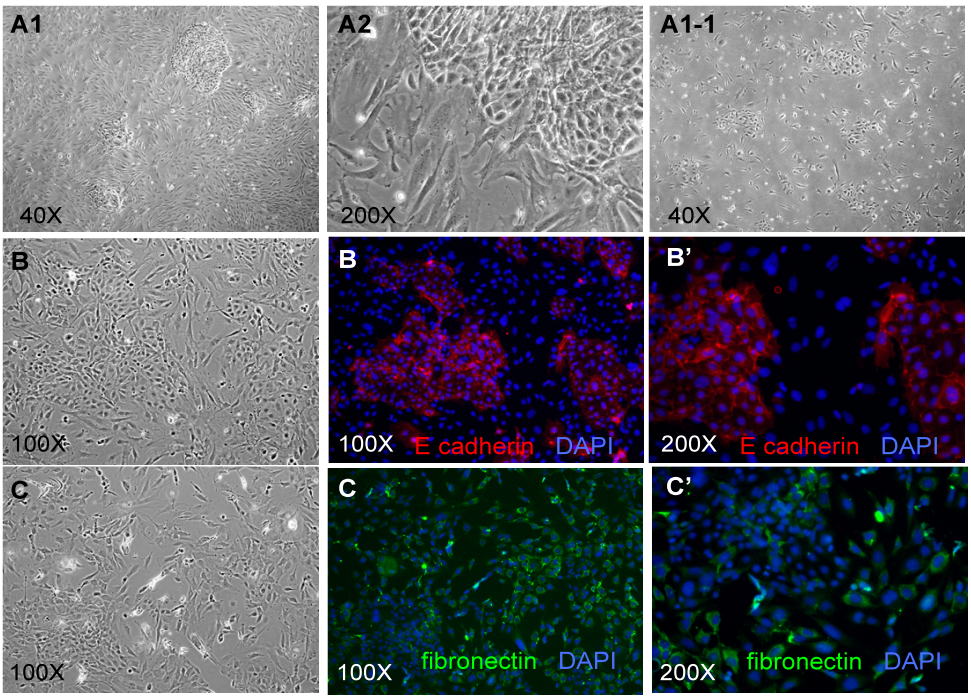

Figure 5. M21 cells cultured as monolayer show islands of cells with epithelial morphology and cell-cell connection in A1 with enlarged view of an epithelial cell island in A2. After clonal isolation of epithelial island cells, the cell culture again contains both epithelial cells and mesenchymal like cells in A1-1. IF staining as indicated is shown with phase contrast images of the same field at 100X.

perform the gain-of-function experiment by generating a Rosa26-LSL-Cdh1 mouse to ectopically express E-cadherin from the Rosa26 locus (which is unlikely to be repressed by the EMT transcription factor) during DKO prostate tumorigenesis. If expression of a WT E-cadherin is unable to maintain E-cadherin expression in DKO prostate tumorigenesis, we will express E-cadherin6A, which cannot be phosphorylated by CKI and therefore is resistant to Skp2 mediated ubiquitination and degradation[12]. We will then determine whether maintaining E-cadherin expression alone, or in combination with p27T187A KI could block DKO prostate tumorigenesis and to what extent.

Task 3. To determine the role of Skp2 in prostate stem cell and prostate cancer stem cell compartments (Timeline 1-12 months).

Most prostate cancers undergo temporary remissions after androgen ablation therapy, but they invariably recur as AI prostate cancers, which are more aggressive and currently incurable. The mechanisms involved in AI cancer progression are poorly understood. It has been demonstrated that targeting basal epithelial stem cells can efficiently inhibit prostate cancer initiation[22]. Prostate cancer in this DKO model arises exclusively from the proximal region of the prostatic ducts, which is the compartment highly enriched for prostatic stem cells with high Sca-1[23]. In addition, these tumors are androgen ablation–resistant from very early stage[23]. All these evidence indicates that

Rb and p53 are important for the regulation of prostatic stem cell population, and the transformation of prostate stem cell by loss of Rb and p53 may lead to aggressive cancers. A transiently proliferating subcompartment (stem cell derived) within the basal cell compartment of human prostate has been identified by reduced p27 protein levels[24]. Furthermore, our showed that Skp2 knockout can delay or block DKO tumorigenesis and there are dramatic increases in p27 protein levels in TKO prostates and MEFs[25]. Based on these evidence, we hypothesize that Skp2 might play essential roles in prostate stem cell and/or prostate cancer stem cell compartment.

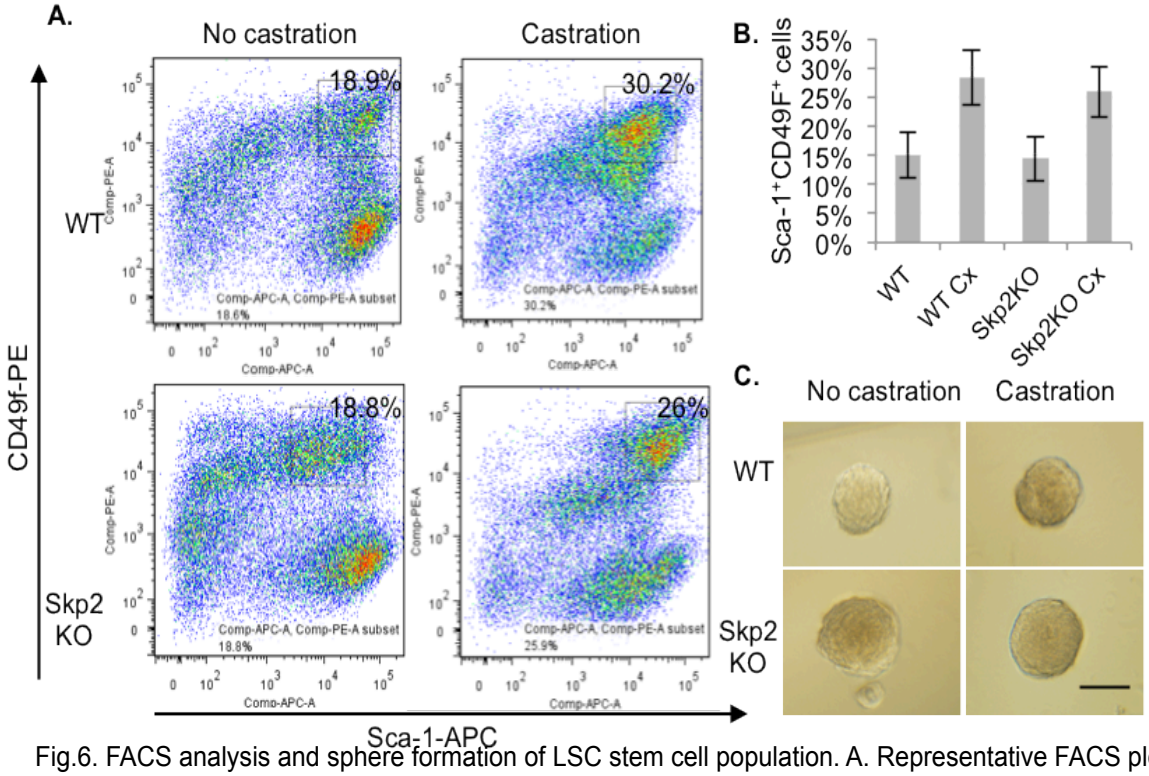

Fig.6. FACS analysis and sphere formation of LSC stem cell population. A. Representative FACS plots show the percentage of Sca-1 and CD49f double positive stem cell population (using Lin^- gate). B. Summary of $Sca\text{-}1^+CD49f^+$ population from indicated prostates. (n=3) C. Representative images of spheres from sorted Sca-1 and CD49f double positive cells after 10 days in culture (scale: 50μM, 200X original magnification).

Even though we didn't detect significant difference in the prostate stem cell population between wild type and Skp2KO prostates (Figure 6), we found there are more prostate cancer stem cell populations in DKO context based on the increased stem cell marker expression: CD49f and Sca-1, which can be decreased by Skp2 deletion (Figure 7). Now we are further characterizing the quantity and quality difference of these stem cells populations between DKO and TKO prostates by performing colony-forming assay, sphere-forming assay and in vivo prostate-regeneration assays.

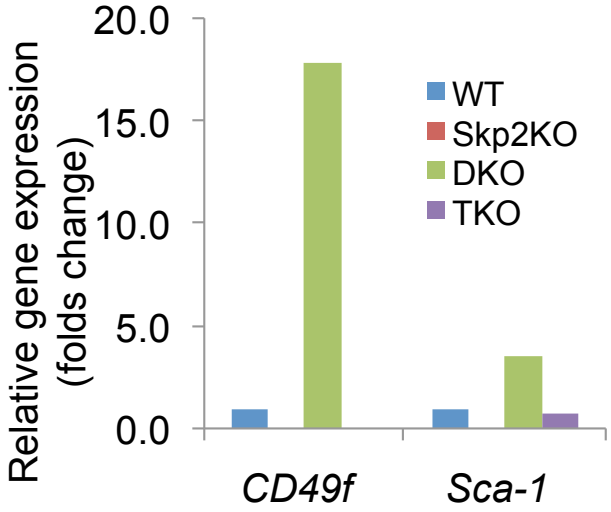

Figure 7. Quantitative analysis of (Q-PCR) prostate stem cell marker genes (*CD49f* and *Sca-1*) in prostates from 3-4 month old mice

KEY RESEARCH ACCOMPLISHMENTS:

1. Identification of KPC1 as a p53 target gene.
2. Identification of p27 as an antitumor safeguard following p53 inactivation, which usually masked by the presence of Skp2.
3. Identification additional antitumor mechanisms those remain effective when both pRb and p53, two major tumor suppressors, are genetically inactivated.
4. p27T187A knocking partially phenocopies the effects of Skp2 deletion in blocking DKO prostate tumorigenesis.
5. Identification of other antitumor mechanisms of Skp2 deletion, such as inhibition of anaerobic glycolysis and EMT.

CONCLUSION:

pRb and p53 are the two of the best known tumor suppressor proteins. They play key roles in provide most and best of the cells' intrinsic antitumor mechanisms, such as proliferation arrest, cellular senescence, and apoptosis. pRb and p53 are frequently inactivated in cancer. Reactivating pRb and p53 is a major goal of anticancer strategies. While many investigators have studied and successfully demonstrated the importance of pRb and p53 in tumor suppression by deleting Rb1 or TP53 to establish various mouse tumor models, very few cancer researchers have attempted to inhibit tumorigenesis in models that mutate both pRb and p53. Indeed, it was not known whether pRb and p53 doubly deficient tumorigenesis could be blocked without resorting

to severe measures that are incompatible with normal cell proliferation.

This research demonstrated unequivocally that pRb and p53 doubly deficient tumorigenesis can be completely blocked (at least in the mouse prostate). Moreover, this research has achieved this by deleting a molecule (Skp2) that can be targeted without causing major defects in cell proliferation and mouse development. Thus, in this work, I have identified a vulnerability of pRb and p53 doubly deficient tumor cells, which can potentially be exploited therapeutically. In addition, this study provides a cause for optimism, by showing that we can anticipate finding therapeutic strategies that are effective against highly aggressive cancers, such as those lacking RB1 and TP53. Using p27T187A knockin mouse model, we identified Skp2/Cks1 pocket inhibitors for advanced prostate cancer.

I further identified other functions of Skp2 in tumorigenesis. I took advantage of our primary prostate tumor cells isolated from our DKO and AADKO mouse models and further characterized the roles of Skp2 in anaerobic glycolysis and EMT, which will benefit the design strategies for targeting Skp2 in cancer treatment in the future.

PUBLICATIONS, ABSTRACTS, AND PRESENTATIONS:

Manuscripts submitted for publication during the period covered by this report resulting from this project.

1. Peer-Reviewed Scientific Journals*:*

- **Hongling Zhao**, Frederick Bauzon, Hao Fu, Zhonglei Lu, Jinhua Cui, Keiko Nakayama, Keiich I. Nakayama, Joseph Locker, and Liang Zhu "Skp2 deletion unmasks a p27 safeguard that blocks tumorigenesis in the absence of pRb and p53 tumor suppressors" Cancer Cell 2013 Nov 11;24(5):645-59.
- **Hongling Zhao**, Frederick Bauzon, Enguang Bi, J. Jessica Yu, Hao Fu, Zhonglei Lu, Jinhua Cui, Hyungjun Jeon, Xingxing Zang, B. Hilda Ye and Liang Zhu "Substituting Threonine187 With Alanine in p27Kip1 Prevents Pituitary Tumorigenesis By Two-Hit Loss Of Rb1 And Enhances Humoral Immunity In Old Age" *J Biol Chem* 290:5797-809.

2. To be submitted manuscript:

- **Hongling Zhao**, Zhonglei Lu, Frederick Bauzon, Hao Fu, Jinhua Cui, Joseph Locker, and Liang Zhu "p27T187A knockin mutation identifies specific $SCF^{Skp2/Cks1}$inhibitors for advanced prostate cancer" 2015

3. Abstracts: Submitted abstract for **"**Cell Symposium, Hallmarks of Cancer: Asia, November 9-11, 2-14-Beijing, China" Please see appendices for detail

INVENTIONS, PATENTS AND LICENSES: Nothing to report

REPORTABLE OUTCOMES: Nothing to report

OTHER ACHIEVEMENTS:

Because of the research I have done supported by this award, I was selected as a recipient of the Dennis Shields Postdoctoral Research Prizes in 2014. Please see appendices for detail.

Opportunities for training and professional development:

1. Cancer center seminar, departmental weekly working in progress and journal club give me opportunities to developmental presentation skills and group discussion, which broaden my knowledge.
2. Discussion of project with my mentor, Dr. Liang Zhu, on daily basis, which make sure the project is on the right track and solves problems in the experiments.
3. Learning project thinking flow and grant writing with my mentor, Dr. Liang Zhu, and preparation for grant writing and develop my own academic career.

REFERENCES:

1. Marino, S., Vooijs, M., van Der Gulden, H., Jonkers, J., and Berns, A. (2000). Induction of medulloblastomas in p53-null mutant mice by somatic inactivation of Rb in the external granular layer cells of the cerebellum. Genes Dev. 14, 994–1004.
2. Meuwissen, R., Linn, S.C., Linnoila, R.I., Zevenhoven, J., Mooi, W.J., and Berns, A. (2003). Induction of small cell lung cancer by somatic inactivation of both Trp53 and Rb1 in a conditional mouse model. Cancer Cell 4, 181–189.
3. Walkley, C.R., Qudsi, R., Sankaran, V.G., Perry, J.A., Gostissa, M., Roth, S.I., Rodda, S.J., Snay, E., Dunning, P., Fahey, F.H., et al. (2008). Conditional mouse osteosarcoma, dependent on p53 loss and potentiated by loss of Rb, mimics the human disease. Genes Dev. 22, 1662–1676.
4. Berman, S.D., Calo, E., Landman, A.S., Danielian, P.S., Miller, E.S., West, J.C., Fonhoue, B.D., Caron, A., Bronson, R., Bouxsein, M.L., et al. (2008). Metastatic osteosarcoma induced by inactivation of Rb and p53 in the osteoblast lineage. Proc. Natl. Acad. Sci. USA 105, 11851–11856.
5. Zhou, Z., Flesken-Nikitin, A., Corney, D.C., Wang, W., Goodrich, D.W., Roy-Burman, P., and Nikitin, A.Y. (2006). Synergy of p53 and Rb deficiency in a conditional mouse model for metastatic prostate cancer. Cancer Res. 66, 7889–7898.
6. Flesken-Nikitin, A., Choi, K.C., Eng, J.P., Shmidt, E.N., and Nikitin, A.Y. (2003). Induction of carcinogenesis by concurrent inactivation of p53 and Rb1 in the mouse ovarian surface epithelium. Cancer Res. 63, 3459–3463.
7. Jiang, Z., Deng, T., Jones, R., Li, H., Herschkowitz, J.I., Liu, J.C., Weigman, V.J., Tsao, M.S., Lane, T.F., Perou, C.M., and Zacksenhaus, E. (2010). Rb deletion in mouse mammary progenitors induces luminal-B or basal-like/ EMT tumor subtypes depending on p53 status. J. Clin. Invest. 120, 3296–3309.
8. McClendon, A.K., Dean, J.L., Ertel, A., Fu, Z., Rivadeneira, D.B., Reed, C.A., Bourgo, R.J., Witkiewicz, A., Addya, S., Mayhew, C.N., et al. (2011). RB and p53 cooperate to prevent liver tumorigenesis in response to tissue damage. Gastroenterology 141, 1439–1450.
9. Lin, H. K., Z. Chen, G. Wang, C. Nardella, S. W. Lee, C. H. Chan, W. L. Yang, J. Wang, A. Egia, K. I.Nakayama, C. Cordon-Cardo, J. Teruya-Feldstein, and P. P. Pandolfi. 2010. Skp2 targeting suppresses tumorigenesis by Arf-p53-independent cellular senescence. Nature 464:374-379.
10. Wang, H., Bauzon, F., Ji, P., Xu, X., Sun, D., Locker, J., Sellers, R.S., Nakayama, K., Nakayama, K.I.,Cobrinik, D., and Zhu, L. (2010) Skp2 is required for survival of aberrantly proliferating Rb1-deficient cells and for tumorigenesis in Rb1+/- mice. Nature Genetics, 42:83-88.

11. Chia-Hsin Chan, Chien-Feng Li, et al (2012). The Skp2-SCF E3 ligase regulates Akt ubiquitination, glycolysis, Herceptin sensitivity and tumorigenesis. Cell 149, 1098-1111.
12. Inuzuka, H., D. Gao, L. W. Finley, W. Yang, L. Wan, H. Fukushima, Y. R. Chin, B. Zhai, S. Shaik, A.W. Lau, Z. Wang, S. P. Gygi, K. Nakayama, J. Teruya-Feldstein, A. Toker, M. C. Haigis, P. P.Pandolfi, and W. Wei. 2012. Acetylation-dependent regulation of Skp2 function. Cell 150:179-193.
13. Anastasiou, D., Y. Yu, W. J. Israelsen, J. K. Jiang, M. B. Boxer, B. S. Hong, W. Tempel, S. Dimov,M. Shen, A. Jha, H. Yang, K. R. Mattaini, C. M. Metallo, B. P. Fiske, K. D. Courtney, S. Malstrom, T.M. Khan, C. Kung, A. P. Skoumbourdis, H. Veith, N. Southall, M. J. Walsh, K. R. Brimacombe, W.Leister, S. Y. Lunt, Z. R. Johnson, K. E. Yen, K. Kunii, S. M. Davidson, H. R. Christofk, C. P.Austin, J. Inglese, M. H. Harris, J. M. Asara, G. Stephanopoulos, F. G. Salituro, S. Jin, L. Dang, D.S. Auld, H. W. Park, L. C. Cantley, C. J. Thomas, and M. G. Vander Heiden. 2012. Pyruvate kinaseM2 activators promote tetramer formation and suppress tumorigenesis. Nature chemical biology 8:839-847.
14. Patra, K. C., Q. Wang, P. T. Bhaskar, L. Miller, Z. Wang, W. Wheaton, N. Chandel, M. Laakso, W. J.Muller, E. L. Allen, A. K. Jha, G. A. Smolen, M. F. Clasquin, R. B. Robey, and N. Hay. 2013. Hexokinase 2 is required for tumor initiation and maintenance and its systemic deletion is therapeutic in mouse models of cancer. Cancer Cell 24:213-228.
15. Zhang, W. C., N. Shyh-Chang, H. Yang, A. Rai, S. Umashankar, S. Ma, B. S. Soh, L. L. Sun, B. C.Tai, M. E. Nga, K. K. Bhakoo, S. R. Jayapal, M. Nichane, Q. Yu, D. A. Ahmed, C. Tan, W. P. Sing, J.Tam, A. Thirugananam, M. S. Noghabi, Y. H. Pang, H. S. Ang, W. Mitchell, P. Robson, P. Kaldis, R.A. Soo, S. Swarup, E. H. Lim, and B. Lim. 2012. Glycine decarboxylase activity drives non-small cell lung cancer tumor-initiating cells and tumorigenesis. Cell 148:259-272.
16. von der Lehr, N. *et al.* The F-box protein Skp2 participates in c-Myc proteosomal degradation and acts as a cofactor for c-Myc-regulated transcription. *Mol. Cell* **11**, 1189-1200 (2003).
17. Kim, S. Y., Herbst, A., Tworkowski, K. A., Salghetti, S. E. & Tansey, W. P. Skp2 regulates Myc protein stability and activity. *Mol. Cell* **11**, 1177-1188 (2003).
18. Shim, H. *et al.* c-Myc transactivation of LDH-A: implications for tumor metabolism and growth. *Proc Natl Acad Sci U S A* **94**, 6658-6663 (1997).
19. Xie, H., J. Hanai, J. G. Ren, L. Kats, K. Burgess, P. Bhargava, S. Signoretti, J. Billiard, K. J. Duffy,A. Grant, X. Wang, P. K. Lorkiewicz, S. Schatzman, M. Bousamra, 2nd, A. N. Lane, R. M. Higashi,T. W. Fan, P. P. Pandolfi, V. P. Sukhatme, and P. Seth. 2014. Targeting lactate dehydrogenase--ainhibits tumorigenesis and tumor progression in mouse models of lung cancer and impacts tumorinitiating cells. Cell Metab 19:795-809.

20. Acevedo, V. D., R. D. Gangula, K. W. Freeman, R. Li, Y. Zhang, F. Wang, G. E. Ayala, L. E.Peterson, M. Ittmann, and D. M. Spencer. 2007. Inducible FGFR-1 activation leads to irreversible prostate adenocarcinoma and an epithelial-to-mesenchymal transition. Cancer Cell 12:559-571.
21. Mulholland, D. J., N. Kobayashi, M. Ruscetti, A. Zhi, L. M. Tran, J. Huang, M. Gleave, and H. Wu. 2012. Pten loss and RAS/MAPK activation cooperate to promote EMT and metastasis initiated from prostate cancer stem/progenitor cells. Cancer Res 72:1878-1889.
22. Lawson DA, Zong Y, Memarzadeh S, Xin L, Huang J, Witte ON. Basal epithelial stem cells are efficient targets for prostate cancer initiation. Proc Natl Acad Sci USA; 107:2610-5.
23. Zhou, Z., Flesken-Nikitin, A., and Nikitin, A.Y. (2007). Prostate cancer associated with p53 and Rb deficiency arises from the stem/progenitor cell-enriched proximal region of prostatic ducts. Cancer Res. 67, 5683-5690.
24. Lukacs RU, Goldstein AS, Lawson DA, Cheng D, Witte ON. Isolation, cultivation and characterization of adult murine prostate stem cells. Nat Protoc;5:702-13.
25. Zhao, H., F. Bauzon, H. Fu, Z. Lu, J. Cui, K. Nakayama, K. I. Nakayama, J. Locker, and L. Zhu. 2013. Skp2 Deletion Unmasks a p27 Safeguard that Blocks Tumorigenesis in the Absence of pRb and p53 Tumor Suppressors. Cancer Cell 24:645-659.

APPENDICES:

Cancer Cell
Article

Skp2 Deletion Unmasks a p27 Safeguard that Blocks Tumorigenesis in the Absence of pRb and p53 Tumor Suppressors

Hongling Zhao,[1,2,3,4] Frederick Bauzon,[1,2,3,4] Hao Fu,[1,2,3,4] Zhonglei Lu,[1,2,3,4] Jinhua Cui,[1,2,3,4] Keiko Nakayama,[5] Keiich I. Nakayama,[6] Joseph Locker,[7] and Liang Zhu[1,2,3,4,*]
[1]Department of Developmental and Molecular Biology, Albert Einstein College of Medicine, Bronx, NY 10461, USA
[2]Department of Medicine, Albert Einstein College of Medicine, Bronx, NY 10461, USA
[3]Albert Einstein Cancer Center, Albert Einstein College of Medicine, Bronx, NY 10461, USA
[4]Marion Bessin Liver Research Center, Albert Einstein College of Medicine, Bronx, NY 10461, USA
[5]Division of Cell Proliferation, Advanced Research and Translational Medicine, Tohoku University Graduate School of Medicine, Sendai 980-8575, Japan
[6]Department of Molecular and Cellular Biology, Medical Institute of Bioregulation, Kyushu University, Fukuoka 812-8582, Japan
[7]Department of Pathology, University of Pittsburgh School of Medicine, Pittsburgh, PA 15261, USA
*Correspondence: liang.zhu@einstein.yu.edu
http://dx.doi.org/10.1016/j.ccr.2013.09.021

SUMMARY

pRb and p53 are two major tumor suppressors. Here, we found that p53 activates expression of Pirh2 and KPC1, two of the three ubiquitin ligases for p27. Loss of p53 in the absence of Skp2, the third ubiquitin ligase for p27, shrinks the cellular pool of p27 ubiquitin ligases to accumulate p27 protein. In the absence of pRb and p53, p27 was unable to inhibit DNA synthesis in spite of its abundance, but could inhibit division of cells that maintain DNA replication with rereplication. This mechanism blocked pRb/p53 doubly deficient pituitary and prostate tumorigenesis lastingly coexistent with bromodeoxyuridine-labeling neoplastic lesions, revealing an unconventional cancer cell vulnerability when pRb and p53 are inactivated.

INTRODUCTION

The prototype tumor suppressor retinoblastoma protein (pRb) is a transducer between the cell's environment and gene expression machinery (Burkhart and Sage, 2008). Fully active pRb recruits chromatin-modifying proteins to the promoters of E2F target genes to repress genes for DNA replication, which can be sufficiently potent and permanent to induce cellular senescence (Chicas et al., 2010). Upstream, pRb is regulated by phosphorylation by cyclin-dependent kinases (CDKs). Various signaling pathways can activate expression of relevant CDKs and cyclin-dependent kinase inhibitors (CKIs) to inactivate pRb (such as by cyclin D1/Cdk4 to induce tumorigenesis) or to activate pRb (such as by p16Ink4A to induce senescence) (Sherr, 2012).

The other major tumor suppressor, p53, is activated by oncogenic stress, such as the loss of pRb, directly or indirectly via Arf (Sherr, 2012). Activated p53 switches on its target genes to induce cell-cycle arrest, senescence, and apoptosis to safeguard against tumorigenesis.

In experimental settings, most of the cell's intrinsic antitumor mechanisms seem to function via p53, pRb, or both. Indeed, combined deletion of *Rb1* (encoding pRb) and *Trp53* (encoding p53) is very effective in inducing tumors in a wide spectrum of tissues in mice. Clinically, inactivation of both pRb and p53 is frequent in various cancers and may explain, in large part, why cancers are difficult to treat. In recent studies, investigators have discovered that deleting *Skp2*, a subunit of the Skp1, Cullin1, F-box protein complex, Cullin-Ring ubiquitin ligase 1 (SCF CRL1) E3 ubiquitin ligase, can induce apoptosis to block

Significance

Because pRb and p53 together are responsible for most antitumor mechanisms, their combined loss is frequent in cancers and explains in large part why cancers are difficult to treat. We discovered that deleting *Skp2* in mice allowed a p27 safeguard to be activated by the loss of p53 and pRb to block the otherwise aggressive tumorigenesis. This block of tumorigenesis lasted well into mouse old age. A counterintuitive feature of this block is that DNA synthesis persisted in the blocked neoplastic cells before they were eliminated by apoptosis. Thus, pRb/p53 doubly deficient tumors might be effectively treated by Skp2 inhibitors, but inhibition of DNA synthesis might not be a useful diagnostic criterion as traditionally practiced.

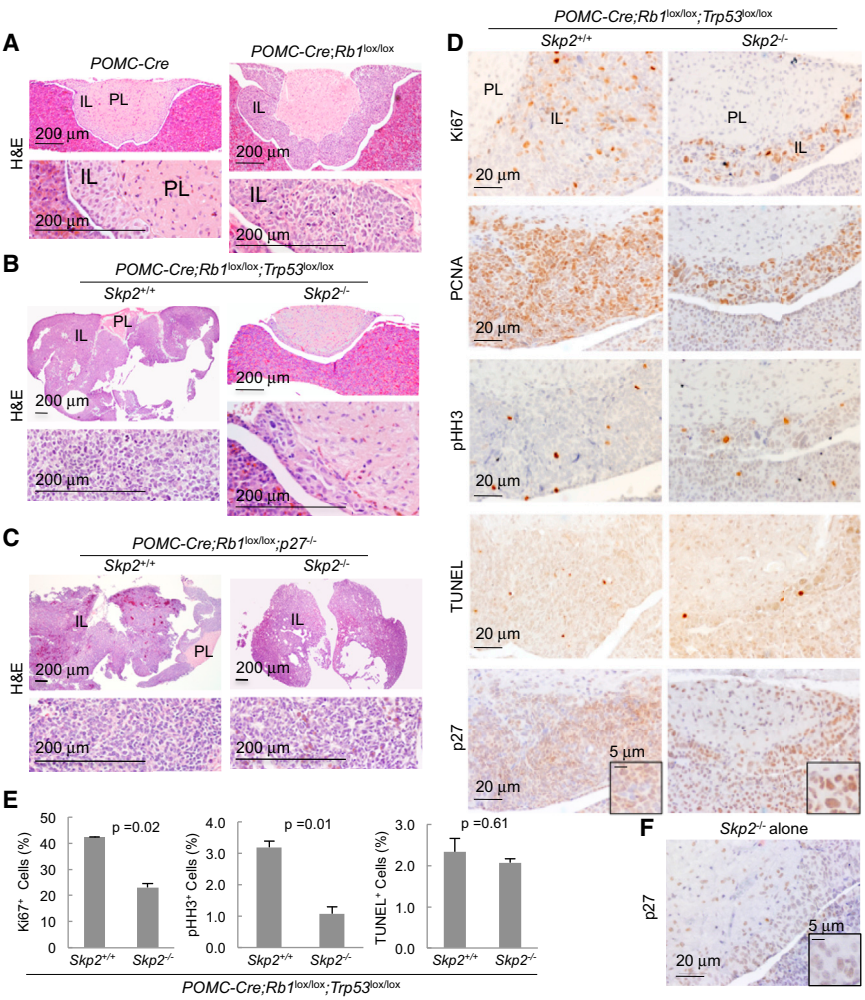

Figure 1. *Skp2* Deletion Blocks pRb/p53 Doubly Deficient, but Not pRb/p27 Doubly Deficient, Pituitary Tumorigenesis

(A–C) Hematoxylin and eosin (H&E)–stained sections of pituitary samples at 7 weeks of age. Higher-magnification views of the intermediate lobe (IL) are presented under lower-magnification ones. PL, posterior lobe.

(D) Pituitary sections of indicated genotypes were stained as indicated. For the *Skp2*$^{+/+}$;*POMC-Cre*;*Rb1*$^{lox/lox}$;*Trp53*$^{lox/lox}$ genotype, we selected pituitaries that were not deformed by macroscopic tumors. PCNA, proliferating cell nuclear antigen; pHH3, phosphohistone 3; TUNEL, terminal deoxynucleotidyl transferase deoxyuridine triphosphate nick-end labeling.

(E) Quantification of cells shown in (D) that stained positive with Ki67, pHH3, or TUNEL.

(F) A representative image of *Skp2*$^{-/-}$ pituitaries stained for p27.

Scale bars are as marked. Quantitative data are presented as averages ± SEM. Statistical analyses were carried out by Student's t test. See also Figure S1.

pRb-deficient pituitary tumorigenesis (Wang et al., 2010) or induce p53-independent senescence to block tumorigenesis in *Arf*$^{-/-}$ mice or *Pten*-deficient prostate (Lin et al., 2010). These two findings might have conformed to the existing paradigm that p53 is activated to inhibit pRb-deficient tumorigenesis, and, vice versa, that pRb is activated to inhibit p53-deficient tumorigenesis, when Skp2 is absent. *Skp2* deletion, however, was found not to block tumorigenesis by *N*-ethyl-*N*-nitrosourea (Wang et al., 2010) or by Myc-driven lymphomagenesis (Old et al., 2010).

In this study, we sought to determine whether combined loss of pRb and p53 would leave cells defenseless against tumorigenesis in the absence of Skp2.

RESULTS

Skp2 Deletion Blocks pRb/p53 Doubly Deficient Pituitary Tumorigenesis

Deleting *Rb1* using *POMC-Cre* was sufficient to induce melanotroph tumorigenesis across the entire intermediate lobe (IL) in the pituitary (Figure 1A), whereas deleting *Trp53* did not do so (Figure S1A available online). Combined deletion of *Rb1* and *Trp53* greatly accelerated IL tumorigenesis (Figure 1B), demonstrating the safeguarding role of p53 following loss of *Rb1*. Remarkably, *Skp2* deletion still blocked this tumorigenesis (Figure 1B). In comparison, *p27* knockout (KO) induced IL hyperplasia (Fero et al., 1996; Kiyokawa et al., 1996; Nakayama et al., 1996) (Figure S1B) and accelerated pRb-deficient IL tumorigenesis to an extent similar to deletion of *Trp53*, but *Skp2* was dispensable in this context (Figure 1C).

Surprisingly, although the Skp2KO ILs did not develop tumors following co-deletion of *Rb1* and *Trp53* in them, they appeared to contain as much of the proliferation markers Ki67 and proliferating cell nuclear antigen (PCNA) as the Skp2 wild-type (WT), pRb/p53 doubly deficient ILs, which were undergoing rapid tumorigenesis (Figure 1D). Quantification of Ki67-positive cells on a percentage basis showed a reduction of about or less than twofold, but this finding was statistically significant (Figure 1E). In the same samples, the mitotic marker phosphohistone 3 (pHH3) was reduced threefold, suggesting a more significant inhibition in cell division (Figures 1D and 1E). Consistent with the substantial presence of proliferation markers, senescence-associated β-galactosidase (SA-β-gal) staining was negative in *Skp2*$^{-/-}$;*POMC-Cre*;*Rb1*$^{lox/lox}$;*Trp53*$^{lox/lox}$ IL (data not shown). Apoptosis was similarly infrequent in these two genotypes as measured by terminal deoxynucleotidyl transferase deoxyuridine triphosphate nick-end labeling (TUNEL) staining (Figures 1D and 1E), demonstrating that, indeed, p53 functioned to induce apoptosis in *Rb1*-deficient pituitary tumorigenesis in the absence of *Skp2* (Wang et al., 2010). Thus, the complete blocking of the highly accelerated tumorigenesis coexisted, unexpectedly, with abundant proliferation markers (also see Figure S1C).

Another unexpected finding was that *Skp2*$^{-/-}$;*POMC-Cre*;*Rb1*$^{lox/lox}$;*Trp53*$^{lox/lox}$ melanotrophs contained more p27 protein

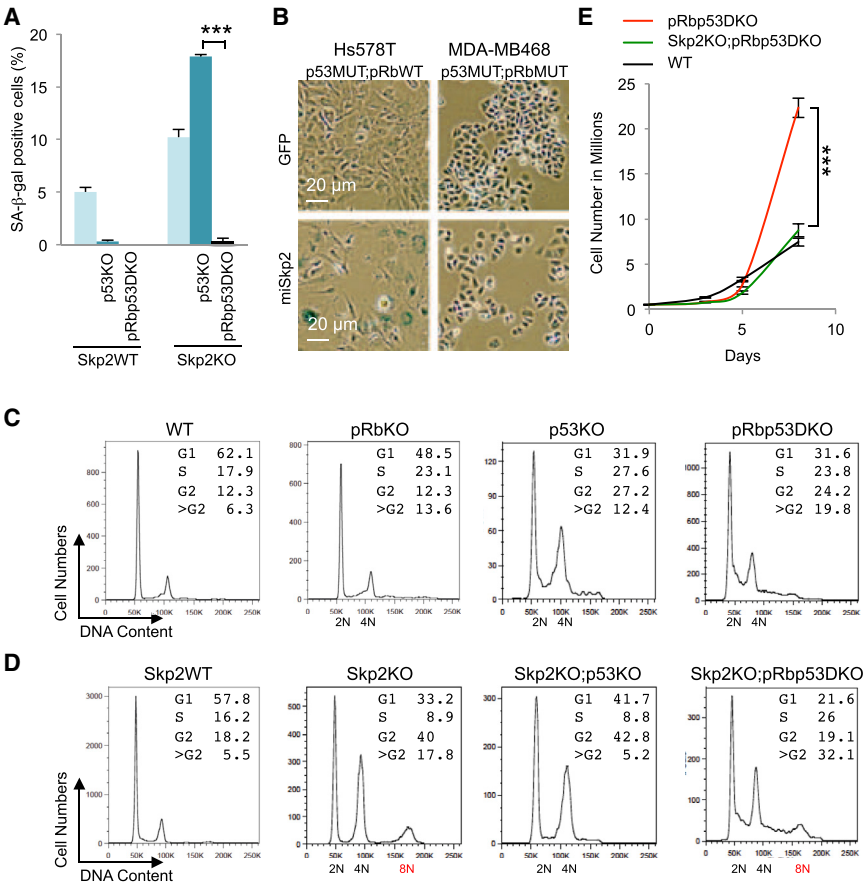

Figure 2. *Skp2/Rb1/Trp53* Triply Deficient Mouse Embryo Fibroblasts Show Higher DNA Replication and Rereplication, Accumulation at 8N, and Proliferation Speed of Wild-Type Mouse Embryo Fibroblasts

(A) Quantification of senescence-associated β-galactosidase (SA-β-gal) marker in mouse embryo fibroblasts (MEFs) of the indicated genotypes. DKO, double-knockout; KO, knockout.

(B) Human breast cancer cell lines with known pRb and p53 status (as indicated) were transduced with lentiviruses expressing green fluorescent protein (GFP) or miRNA hairpins targeting Skp2 (miSkp2). Five days after transduction, the same number of cells were plated. SA-β-gal staining was performed 3 days later.

(C and D) DNA content assessed by fluorescence-activated cell sorting (FACS) analysis of MEFs with the indicated genotypes. WT, wild type.

(E) Cell proliferation of the indicated MEFs is measured by counting cell numbers.

Quantitative data are presented as averages ± SEM. Statistical analyses were carried out by Student's t test. ***$p < 0.002$. FACS analysis results are representative of three experiments. See also Figure S2.

than *Skp2*$^{-/-}$ melanotrophs (Figures 1D and 1F; Figure S1C). This finding was controlled with staining of *p27*$^{-/-}$ pituitary (Figure S1D). p27 accumulated in the nuclei, and p27-abundant nuclei were larger, suggesting accumulation of more DNA.

Taken together, these results provide indications that, in the absence of Skp2, codeletion of *Rb1* and *Trp53* could further increase p27 protein levels, resembling a safeguard response, but that this high-level p27 is unable to inhibit expression of proliferation markers and induce senescence in the absence of pRb and p53. Nevertheless, the highly accelerated tumorigenesis was blocked.

Deleting *Trp53* in Skp2KO Mouse Embryo Fibroblasts Activates a pRb Safeguard to Induce Senescence

To further investigate the above-described unexpected findings, we generated mouse embryo fibroblasts (MEFs) of the same genotypes to study how *Skp2* deletion blocked pRb/p53 doubly deficient tumorigenesis. We used adeno-Cre to delete *Trp53*, *Rb1*, or both in MEFs controlled by parallel infection with adenovirus expressing green fluorescent protein (adeno-GFP). To simplify the text, we hereinafter refer to the various MEFs as p53KO, double-knockout pRbp53DKO, or Skp2KO; pRbp53DKO, for example.

Inactivation of p53 can immortalize Skp2WT MEFs but, to the contrary, it induces senescence in Skp2KO MEFs (Lin et al., 2010). In Figures 2A and S2A and 2B, we show, as measured by SA-β-gal staining, that Skp2WT;p53KO MEFs were prevented from senescence but that Skp2KO;p53KO MEFs senesced more than Skp2KO MEFs. To study how p53KO paradoxically induced more senescence in Skp2KO MEFs, and to determine whether combined deletion of *Rb1* would disable the senescence, we deleted *Rb1* in Skp2KO;p53KO MEFs (resulting in Skp2KO;pRbp53DKO MEFs) and prevented senescence (Figure 2A). To model therapeutic inhibition of Skp2, we performed Skp2 knockdown in the human breast cancer cell lines Hs578T and HCC1143, which contain functional pRb but are deficient for p53, and MDA-MB468 and BT549, which are deficient for both pRb and p53. Two tandem microRNA 30 (miR30)-based hairpins targeting Skp2 effectively reduced Skp2 protein and increased p27 protein in these cell lines (Sun et al., 2006) (Figure S2C). SA-β-gal staining revealed senescence in Hs578T cells, but not in MDA-MB468 cells, following Skp2 knockdown (Figures 2B and S2D). Thus, inactivation of p53 and Skp2 together activated a pRb safeguard to induce senescence. With additional loss of pRb, this line of antitumor defense is disabled, consistent with the abundant presence of proliferation markers in *Skp2*$^{-/-}$;*POMC-Cre*;*Rb1*$^{lox/lox}$;*Trp53*$^{lox/lox}$ IL.

Deleting *Trp53* and *Rb1* Induces DNA Rereplication

Notably, although the Skp2KO;pRbp53DKO genotype disabled senescence in MEFs and induced proliferation markers in IL, it induced no tumorigenesis. We subjected MEFs of relevant genotypes to fluorescence-activated cell sorting (FACS) analysis to study this unusual phenotype. As expected, deletion of *Rb1* or *Trp53* increased S phase cells (DNA content between 2N and 4N) and G_2 phase cells (4N) (Figure 2C).

Unexpectedly, deletion of *Rb1* or *Trp53* also generated more cells with DNA content larger than 4N (>G_2). Combined deletion of *Rb1* and *Trp53* increased this population to 20% (Figure 2C). The continuous distribution of the larger DNA content indicated DNA rereplication, which is defined as refiring of certain DNA replication origins before the entire set of chromosomes was fully duplicated (Arias and Walter, 2007). These findings reveal that pRb inhibits DNA rereplication and p53 safeguards against it. Notably, though combined loss of pRb and p53 did not synergistically increase S phase cells, it did for DNA rereplication (Figure 2C). Thus, a significant portion of elevated DNA synthesis activity during tumorigenesis following loss of pRb and p53 might be in the form of rereplication.

Codeleting *Trp53* and *Rb1* in Skp2KO Mouse Embryo Fibroblasts Induces Accumulation of DNA Rereplicating Cells by Mitotic Entry Delay

Consistent with previous reports that increased p27 in Skp2KO MEFs inhibited mitotic cyclin-Cdk (Nakayama et al., 2004), Skp2KO MEFs showed an increased G_2 population and an 8N peak. There was no accumulation of cells between 4N and 8N (Figure 2D), however. This profile indicates no DNA rereplication (as defined above), but the fully duplicated chromosomes failed to segregate into daughter cells before they were fully duplicated again.

Deletion of *Trp53* in Skp2KO MEFs, which induced senescence in them (Figure 2A), induced less DNA rereplication than p53KO MEFs (Figures 2C and 2D). Because pRb was activated in Skp2KO;p53KO MEFs to induce senescence (Figure 2A), a more active pRb might have inhibited DNA rereplication as well. Deletion of *Trp53* also abolished the 8N peak, suggesting that a more active pRb also blocked chromosome reduplication, likely due to the inhibition of DNA synthesis.

Skp2KO;pRbp53DKO MEFs, which were prevented from senescence, showed more S phase cells and DNA rereplication than Skp2KO;p53KO MEFs with return of the 8N peak, resulting in a total of 32% cells with DNA content larger than 4N (Figure 2D). This profile, together with the events leading to it, suggests that Skp2KO;pRbp53DKO allowed DNA rereplication to generate cells with more than 4N DNA content, and these cells gradually accumulated to an 8N peak. We further found that pHH3-positive cells were reduced from 1.13% in pRbp53DKO MEFs to 0.69% in Skp2KO;pRbp53DKO MEFs. These findings indicate the presence of a mitotic entry delay and are consistent with the significant decrease in pHH3-positive cells in *Skp2*$^{-/-}$;*POMC-Cre*;*Rb1*$^{lox/lox}$;*Trp53*$^{lox/lox}$ ILs (Figure 1D), whereas increased S phase and DNA rereplication explains the abundant presence of Ki67-positive and PCNA-positive cells (Figures 1D and 1E).

We counted cells to determine actual proliferation. We found that Skp2KO;pRbp53DKO MEFs proliferated at the speed of WT MEFs, despite much larger S phase populations. pRbp53DKO MEFs, despite S phase size similar to Skp2KO;pRbp53DKO MEFs, proliferated much faster than the latter, resulting in about threefold more cells at day 8 (Figure 2E). This difference in cell numbers resembled the tumorigenic potentials of these two genotypes in the pituitary. Similarly, human breast cancer cell lines MDA-MB468 and BT549 (mimicking pRbp53DKO) proliferated much faster than MDA-MB468-miSkp2 and BT549-miSkp2 (mimicking Skp2KO;pRbp53DKO), although the latter did not senesce (Figure 2B; Figures S2D and S2E).

These MEF studies modeled findings from the pituitary and provide insights into the unusual phenotypes of the Skp2KO;pRbp53DKO genotype. Chromosome separation failure restricted actual cell proliferation, whereas DNA rereplication sustained the presence of abundant proliferation markers.

p53 Loss Induces a p27 Safeguard

We next determined the molecular mechanisms for the phenotypes of Skp2KO;pRbp53DKO MEFs. Our finding that p27 protein levels were higher in *Skp2*$^{-/-}$;*POMC-Cre*;*Rb1*$^{lox/lox}$;*Trp53*$^{lox/lox}$ IL than in *Skp2*$^{-/-}$ IL (Figures 1D and 1F) suggested an elevation of a p27 safeguard by combined deletion of *Rb1* and *Trp53*. We performed western blot analysis to determine whether p27 protein levels in Skp2KO;pRbp53DKO MEFs also mimicked those in the pituitary. As expected, Skp2KO MEFs contained more p27 protein than Skp2WT MEFs (Figure 3A, lanes 1 and 3) (Nakayama et al., 2000). Combined deletion of *Rb1* and *Trp53* did not change p27 protein levels in Skp2WT MEFs (Figure 3A, lanes 1 and 2), but further increased p27 protein levels in Skp2KO MEFs (Figure 3A, lanes 3 and 4). Thus, MEFs again mimicked IL.

We investigated whether deleting *Rb1* or *Trp53* alone could further increase p27 protein in Skp2KO MEFs. We found that Skp2KO;p53KO MEFs (Figure 3A, lane 12), but not Skp2KO;pRbKO MEFs (Figure 3A, lane 8), contained increased p27 protein levels. Because p53 is gradually activated with passages of cultured MEFs (Figure S3A, lanes 1 and 2), deletion of *Trp53* in late-passage Skp2KO MEFs induced higher amounts of p27 (Figure S3A, lanes 6 and 7). Deletion of *Rb1* activated p53 in early-passage MEFs (Figure S3A, lane 3), which might explain why combined deletion of *Trp53* and *Rb1* induced the most p27 protein in Skp2KO MEFs (Figure 3A).

These findings explain why deletion of *Trp53* in Skp2KO MEFs induced higher levels of p27, which inhibits S phase cyclin-dependent kinases. Consequently, pRb is less phosphorylated and therefore more active. The activated pRb in turn inhibits DNA synthesis to induce senescence. This role of pRb as a transducer between inhibition of S phase cyclin-dependent kinases and inhibition of DNA synthesis is essential because Skp2KO;pRbp53DKO MEFs resumed DNA synthesis and failed to senesce. In comparison, because Skp2KO;pRbp53DKO MEFs are delayed for mitotic entry, the inhibition of mitotic cyclin-dependent kinases (by high p27 levels) can inhibit mitotic entry without activated pRb.

To determine the functional significance of the high p27 in blocking mitotic entry, we knocked down p27 in Skp2KO;pRbp53DKO MEFs with two p27-targeting hairpins (Figure S3B). Short hairpin 2 (sh2) reduced p27 protein in Skp2KO;pRbp53DKO MEFs to below that in Skp2WT;pRbp53DKO MEFs, abolished the 8N peak and reduced 4N to 8N cells (Figure S3C), and increased proliferation of Skp2KO;pRbp53DKO MEFs faster than Skp2WT;pRbp53DKO MEFs (Figure S3D). sh1 knocked down p27 to a lesser degree and reduced 4N to 8N cells and increased proliferation to a smaller extent. Thus, accumulation of 4N to 8N DNA content and inhibition of proliferation of pRbp53DKO MEFs by *Skp2* deletion was highly dependent on high p27 protein levels. When we used a

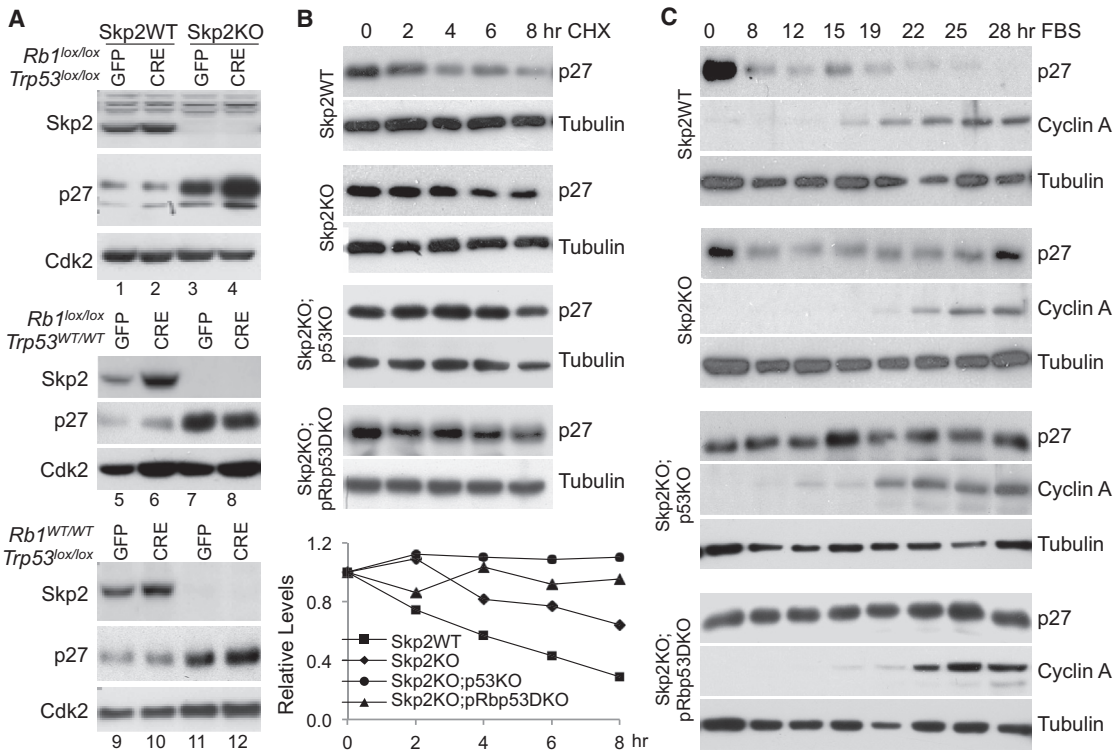

Figure 3. Deletion of *Trp53* Triggers Further Stabilization of p27 Protein in Skp2KO Mouse Embryo Fibroblasts

(A) Western blot analysis of indicated proteins in mouse embryo fibroblasts (MEFs) of indicated genotypes transduced in parallel by adenovirus expressing green fluorescent protein (adeno-GFP) or adeno-Cre (CRE). KO, knockout; WT, wild type.

(B) Cell extracts were prepared from MEFs of indicated genotypes at the indicated time points following the addition of cycloheximide (CHX), and the amounts of p27 protein were measured by western blot analysis in comparison to tubulin. p27 protein level quantification is presented under the gels.

(C) Cell extracts were prepared from MEFs of indicated genotypes at indicated time points after being cultured in serum-containing media following serum starvation for 3 days. The p27 protein level was determined by western blot analysis. The cyclin A protein level is shown to indicate cell-cycle progression, and the tubulin level is shown to indicate loading amounts. FBS, fetal bovine serum.

See also Figure S3.

cytomegalovirus (CMV) promoter to overexpress p27 in Skp2WT;pRbp53DKO MEFs (Figure S3E), p27 protein levels increased less than twofold (Figure S3F), cells did not accumulate 8N DNA content (data not shown), and proliferation rates were only slightly reduced (Figure S3G), suggesting that p27 protein degradation is the major regulator of p27 levels and functions in Skp2WT;pRbp53DKO MEFs.

The further increases in p27 protein levels were not associated with increases in p27 mRNA levels (Figure S3H), but they were associated with more stable p27 proteins (Figure 3B). This finding indicated that Skp2-independent p27 degradation mechanisms were reduced by deletion of *Trp53* in Skp2KO MEFs. That deletion of *Trp53* did not induce higher p27 in Skp2WT MEFs suggests that Skp2 possesses sufficient p27 degradation activity to compensate for reduction in other p27 protein degradation mechanisms.

In addition to Skp2, p27 is ubiquitinated by KPC1 and Pirh2 ubiquitin ligases, which function primarily at early time points of cell-cycle entry (Hattori et al., 2007; Kamura et al., 2004). We used serum starvation release to determine whether *Trp53* deletion affected p27 protein degradation within this time window. Figure 3C shows that Skp2KO did not prevent reduction of p27 protein levels at early time points (hours 8, 12, and 15), but prevented its further reduction at hours 22 and 25. *Trp53* deletion or combined *Trp53* and *Rb1* deletion did not affect the kinetics of p27 protein reduction in Skp2WT MEFs (data not shown), but prevented p27 protein reduction at hours 8, 12, and 15 in Skp2KO MEFs (Figure 3C). This finding suggests that *Trp53* deletion impaired the ability of KPC1 and/or Pirh2 to degrade p27.

Interestingly, Pirh2 was previously identified as a p53 target gene (Leng et al., 2003). We used the Transcription Regulatory Element Database (Xuan et al., 2005) to study whether the KPC1 gene promoter contains a p53 binding site, which is a ten-nucleotide consensus sequence repeated once with a spacer of 0 to 13 nucleotides (el-Deiry et al., 1992; Wei et al., 2006) (Figure S4A). The promoter of p21, a canonical p53 target gene, contains a p53 binding site with a matched first half and one mismatched second half. (We call it a 0,1 site.) The Pirh2 promoter contains a 0,1 site, and the KPC1 promoter contains a 1,1 site (Figure S4B). Skp2 and p27 promoters contain a 1,2 site and a 2,1 site, respectively.

The chromatin immunoprecipitation (ChIP) experiments shown in Figure 4A demonstrate that activation of p53 in WT MEFs by doxorubicin (DOX) stimulated recruitment of p53 to the promoters of p21, Pirh2, and KPC1, but not Skp2 and

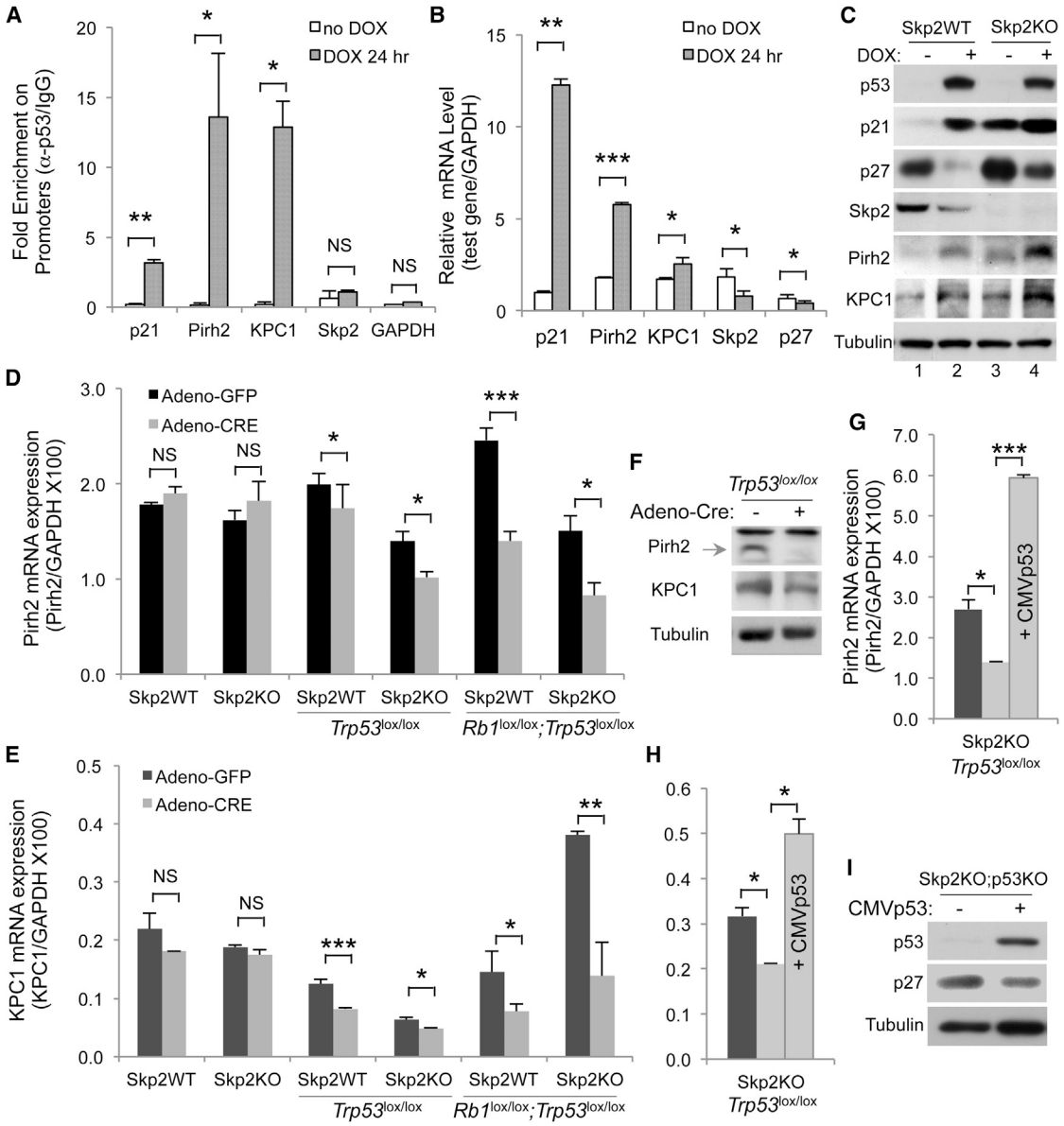

Figure 4. p27 Ubiquitin Ligases Pirh2 and KPC1 Are p53 Target Genes

(A) The results of chromatin immunoprecipitation assays with anti-p53 and control immunoglobulin G (IgG) following doxorubicin (DOX) treatment of wild-type (WT) mouse embryo fibroblasts (MEFs). Fold enrichment (anti-p53/IgG) for the indicated promoters is presented. GAPDH, glyceraldehyde 3-phosphate dehydrogenase.

(B) RT-quantitative PCR (RT-qPCR) of the indicated genes in WT MEFs following DOX treatment, normalized with GAPDH.

(C) Western blot of the indicated MEFs following treatment with DOX as in (B). KO, knockout.

(D and E) Expression of Pirh2 (D) and KPC1 (E) in MEFs transduced in parallel by adeno-GFP and adeno-Cre. Values were normalized with GAPDH.

(F) Western blots of Pirh2 and KPC1 before and after deletion of *Trp53*.

(G and H) Same as (D) and (E) with an additional sample in which p53 was ectopically expressed, as marked inside the bars. CMV, cytomegalovirus.

(I) Western blots of Skp2KO;p53KO MEFs without or with ectopic p53 expression.

Quantitative data are presented as average ± SEM. Student's t test was used for statistical analysis. *p < 0.05; **p < 0.01; ***p < 0.002; NS, p > 0.05. See also Figure S4.

glyceraldehyde 3-phosphate dehydrogenase. In agreement with the ChIP results, the expression levels of Pirh2 and KPC1 were stimulated by DOX, although to smaller degrees than the stimulation of p21 expression; but DOX did not stimulate expression of Skp2 or p27 (Figure 4B). The western blots show that p53, p21, Pirh2, and KPC1 proteins were increased, and that Skp2 protein was decreased, by DOX treatment (Figure 4C). We then confirmed that DOX counterintuitively decreased p27 protein levels (Figure 4C, lanes 1 and 2). Notably, DOX also reduced p27 protein levels in Skp2KO MEFs (Figure 4C, lanes 3 and 4). Thus, strong p53 activation and acute *Trp53* deletion have opposite effects on p27 protein levels. We explored the possibility that

these changes in protein levels were due to changes in cell-cycle profiles by DOX. We found that under the conditions we used, DOX did not dramatically change cell-cycle profiles of WT or Skp2KO MEFs (Figure S4C).

We next determined the effects of *Trp53* deletion on the expression of Pirh2 and KPC1. Figures 4D and 4E show that *Trp53* deletion alone or with *Rb1* reduced mRNA levels of Pirh2 and KPC1 in both Skp2WT and Skp2KO MEFs. The effects of *Trp53* deletion were smaller than *Trp53* and *Rb1* codeletion, likely because p53 was not highly activated in cultured MEFs before *Rb1* was deleted (Figures 3A and S3A). The western blots show that Pirh2 and KPC1 protein levels also decreased following deletion of *Trp53* (Figure 4F). Skp2 expression was not reduced following *Trp53* deletion or codeletion with *Rb1* (Figure S4D). When we reexpressed p53 in Skp2KO;p53KO MEFs, expression of Pirh2 and KPC1 increased (Figures 4G and 4H) and p27 protein levels decreased (Figure 4I). These results suggest that the combined reduction in Pirh2 and KPC1 expression shrinks the pool of the ubiquitin ligases for p27 further in Skp2KO;p53KO MEFs and therefore further increases p27 protein accumulation.

Knockdown of Pirh2 or KPC1 can increase p27 protein in various human and mouse cells (Hattori et al., 2007; Kamura et al., 2004). For our study, we ectopically expressed Pirh2 and KPC1 in Skp2KO;pRbp53DKO MEFs to determine their negative effects on high p27 levels. Although we succeeded in increasing Pirh2 levels by expression of CMV-huPirh2, expression of CMV-huKPC1 increased KPC1 protein levels only slightly in these MEFs (Figure S4E). Under these conditions, expression of Pirh2, KPC1, or both reproducibly decreased p27 protein levels, reduced 4N to 8N cells, and increased proliferation (Figures S4E–S4G), but all these effects were smaller than those observed with p27 knockdown (Figures S3B–S3D). In MDA-MB468 and BT549 breast cancer cell lines with Skp2 knockdown (mimicking Skp2KO;pRbp53DKO MEFs), expression of CMV-huPirh2 and CMV-huKPC1 also increased proliferation, most effectively in BT549 cells (Figures S4H–S4K). These results confirmed the functions of Pirh2 and KPC1 in promoting p27 degradation and proliferation, but the extent of their overexpression and phenotypes is cell type–dependent.

Skp2 Deletion Blocks pRb/p53 Doubly Deficient Prostate Tumorigenesis

We sought to determine whether our findings regarding the pituitary and MEFs were applicable to another tissue. Although *Rb1* deletion is sufficient to induce pituitary tumorigenesis, it requires combined deletion of *Trp53* to induce tumorigenesis in the brain (Marino et al., 2000), lung (Meuwissen et al., 2003), bone (Walkley et al., 2008; Berman et al., 2008), prostate (Zhou et al., 2006), ovary (Flesken-Nikitin et al., 2003), breast (Jiang et al., 2010), and liver (McClendon et al., 2011), suggesting that these tissues may mount a stronger p53 safeguard following *Rb1* deletion. We studied the prostate. *PB-Cre4*;*Rb1*$^{lox/lox}$;*Trp53*$^{lox/lox}$ mice developed rapid and invasive prostate cancer (Zhou et al., 2006). The prostate tumors became lethal from 6 months and killed all hosts (n = 58) within 1 year (Figure 5A) (Zhou et al., 2006). In contrast, all *Skp2*$^{-/-}$;*PB-Cre4*;*Rb1*$^{lox/lox}$;*Trp53*$^{lox/lox}$ mice (n = 32) survived, as WT mice did, for the 19-month period (Figure 5A). Pathological diagnoses for these two cohorts are shown in Figure 5B. Prostatic intraepithelial neoplasias (PINs) were divided into four grades (Park et al., 2002). At 3 to 4 months, PINs developed in both cohorts (also see Figure S5A). PINs in *PB-Cre4*;*Rb1*$^{lox/lox}$;*Trp53*$^{lox/lox}$ mice were of higher grades and quickly progressed to invasive carcinoma (Figures 5B and 5C; Figure S5B) and gross tumors during the 5- to 7-month period, when 20 of 42 mice died. In the 8- to 9-month period, most tumors had become macroscopic and all mice died by the end of the ninth month. In contrast, PINs in *Skp2*$^{-/-}$;*PB-Cre4*;*Rb1*$^{lox/lox}$;*Trp53*$^{lox/lox}$ mice never progressed beyond the PIN stage in a total of 26 mice examined, 6 of which were examined at 15 to 22 months.

Figures 5D and 5F show that PIN lesions in *Skp2*$^{-/-}$;*PB-Cre4*;*Rb1*$^{lox/lox}$;*Trp53*$^{lox/lox}$ mice contained higher levels of p27, as measured by immunohistochemical and western blot analysis of dissected ventral and anterior lobes, than they did in *Skp2*$^{-/-}$ glands. Nuclei expressing higher p27 protein levels were larger. PCNA expression was also high in *Skp2*$^{-/-}$;*PB-Cre4*;*Rb1*$^{lox/lox}$;*Trp53*$^{lox/lox}$ PINs (Figure 5E).

We used Ki67 staining to compare the proliferation status of PINs. Normal glands of WT and *Skp2*$^{-/-}$ mice contained few Ki67-positive cells, and PINs contained more of them (Figures 6A and 6B). Remarkably, the abundance of Ki67-positive cells was similar between PINs in *PB-Cre4;Rb1*$^{lox/lox}$;*Trp53*$^{lox/lox}$ mice and PINs in *Skp2*$^{-/-}$;*PB-Cre4*;Rb1$^{lox/lox}$;*Trp53*$^{lox/lox}$ mice. The presence of pHH3, on the other hand, was significantly reduced from 2.23% to 1.26% (Figures 6C and 6F). If PINs in *Skp2*$^{-/-}$;*PB-Cre4*;*Rb1*$^{lox/lox}$;*Trp53*$^{lox/lox}$ mice were undergoing DNA rereplication with mitotic entry block, as demonstrated by the MEF model of this genotype (Figure 2D), their nuclei should accumulate larger amounts of DNA. We used 4′,6-diamidino-2-phenylindole (DAPI) and Feulgen stains to study this and found that nuclei in PINs of the *Skp2*$^{-/-}$;*PB-Cre4*;*Rb1*$^{lox/lox}$;*Trp53*$^{lox/lox}$ genotype contained significantly more DAPI and Feulgen staining than the other three genotypes (Figures 6D, 6E, and 6G).

Thus, the ability of *Skp2* deletion to block pRb/p53 doubly deficient tumorigenesis and the mechanisms underlying this block were essentially the same in the prostate and the pituitary, as modeled in MEFs.

Lifelong Block in Bromodeoxyuridine Labeling Prostatic Intraepithelial Neoplasias

We next addressed the possibility that S phase Skp2KO;pRbp53DKO MEFs (as determined by DNA content) and proliferating *Skp2*$^{-/-}$;*PB-Cre4*;*Rb1*$^{lox/lox}$;*Trp53*$^{lox/lox}$ PINs (as determined by Ki67 and PCNA expression) might not actually be synthesizing DNA as reasons for slow proliferation of MEFs and absence of tumorigenesis for PINs. Cells containing more than 4N DNA content due to rereplication were found to cease DNA synthesis by activating p53-dependent checkpoints (Zhu et al., 2004). If cells of the Skp2KO;pRbp53DKO genotype had ceased DNA synthesis, a mechanism to inhibit DNA synthesis (and therefore tumorigenesis) following rereplication in the absence of pRb and p53 would be implicated.

We first addressed this issue by analyzing bromodeoxyuridine (BrdU)-labeled (30 minutes) Skp2KO;pRbp53DKO MEFs in parallel with WT and pRbp53DKO MEFs. For these three genotypes, cells defined as being in S phase by DNA content on the *x*-axis (positions indicated by yellow arrows) were shifted upward to become BrdU-positive on the *y*-axis (positions indicated by red

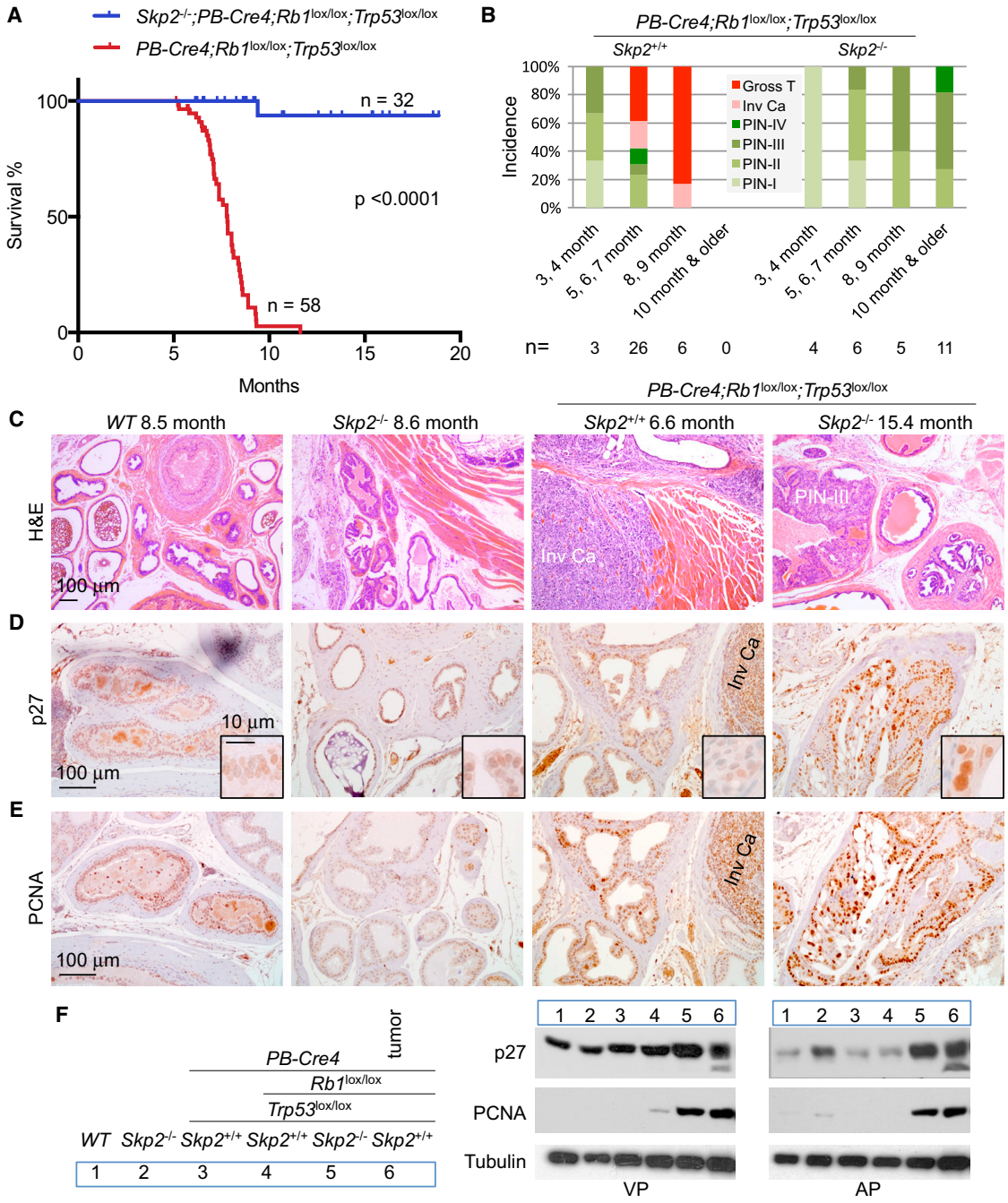

Figure 5. Deletion of *Skp2* Blocks pRb/p53 Doubly Deficient Prostate Tumorigenesis inside Prostatic Intraepithelial Neoplasia Stages

(A) Kaplan-Meier survival analysis of two cohorts of mice with indicated genotypes. One *Skp2*$^{-/-}$;*PB-Cre4*;*Rb1*$^{lox/lox}$;*Trp53*$^{lox/lox}$ mouse died from fighting at 9.4 months without prostate tumors.

(B) Pathological diagnoses of prostate lesions in mice of indicated genotypes in four age groups. Each prostate was serially sectioned and the most advanced lesions were the diagnoses. PIN, prostatic intraepithelial neoplasia.

(C–E) Sections of prostates from mice of four genotypes at the indicated ages stained with hematoxylin and eosin (H&E) (C), anti-p27 (D), and anti-proliferating cell nuclear antigen (anti-PCNA; E). Invasive carcinoma (Inv Ca) and a PIN-III lesion are marked. WT, wild type.

(F) Western blots of isolated ventral prostates (VPs) and anterior prostates (APs) from 3- to 4-month-old mice. A macroscopic tumor was included as marked. See also Figure S5.

arrows), demonstrating that they were actively synthesizing DNA during the labeling period (Figure 7A). The ratios of BrdU-positive cells versus BrdU-negative cells were similar between pRbp53DKO MEFs and Skp2KO;pRbp53DKO MEFs (2.0 and 1.7, respectively), but much higher than the ratio of WT MEFs (0.3), consistent with the results shown in Figures 2C and 2D.

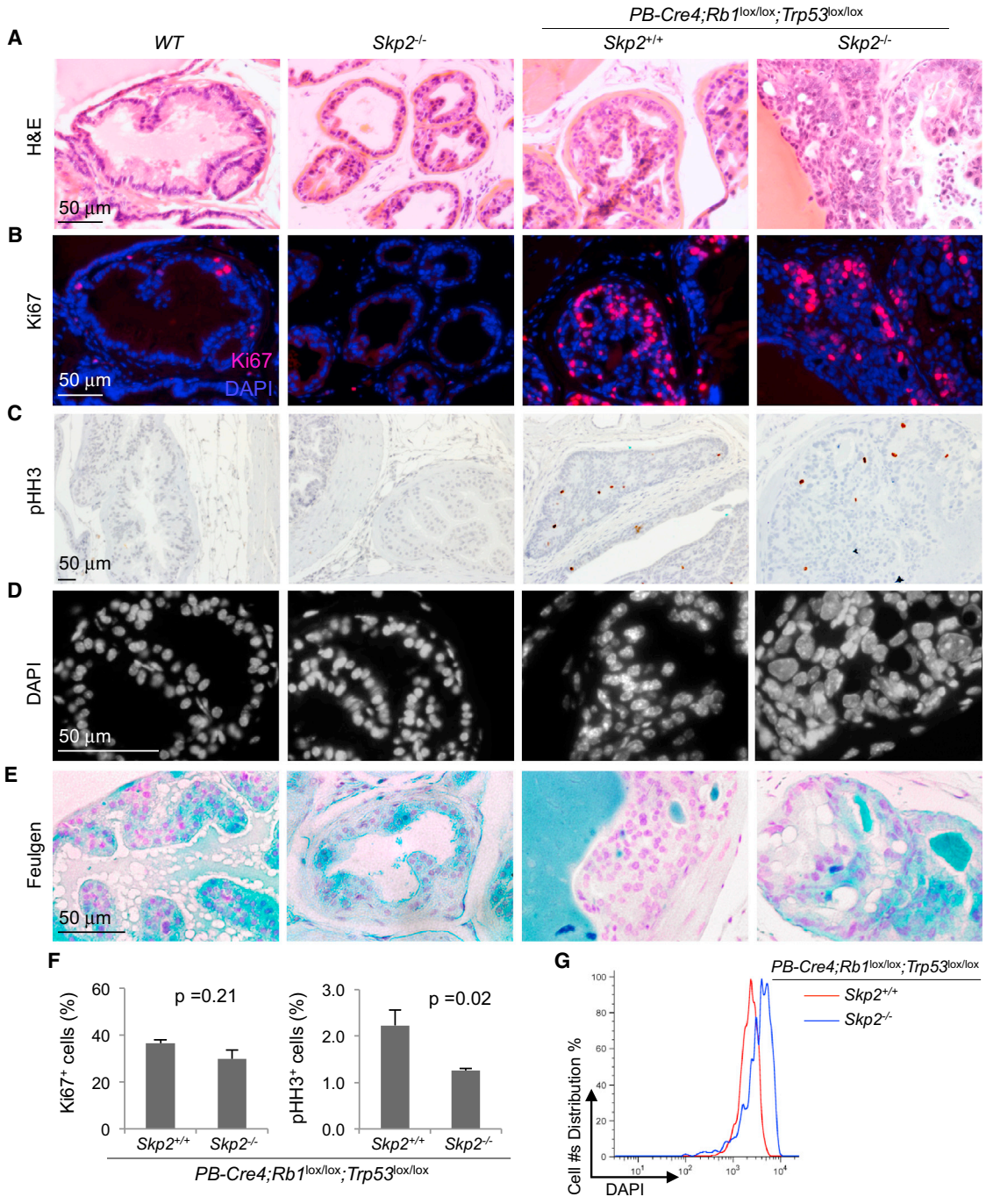

Figure 6. Comparisons of Proliferation Markers and Nuclear Sizes in Prostate of the Indicated Genotypes

(A–E) Sections of prostates from mice with indicated genotypes at same ages as those shown in Figure 5C were stained with hematoxylin and eosin (H&E; A), anti-Ki67 (B), anti-phosphohistone 3 (anti-pHH3) (C), 4′,6-diamidino-2-phenylindole (DAPI; D), and Feulgen (E).

(F) Quantification of Ki67-positive cells and pHH3-positive cells from (B) and (C), respectively.

(G) DAPI-stained slides were quantified using an iCys Research Imaging Cytometer and iCys Cytometric Analysis Software.

Quantitative data are presented as averages ± SEM. Student's t test was used for statistical analysis.

Cells containing more than 4N DNA content were also largely BrdU-positive. The ratios of BrdU-positive cells with more than 4N DNA to BrdU-negative cells with more than 4N DNA were 5.7 for both pRbp53DKO and Skp2KO;pRbp53DKO MEFs, but 1.1 for WT MEFs. Thus, there was no indication of a pRb- and p53-independent inhibitory checkpoint effect on DNA synthesis in response to DNA rereplication.

We labeled mice with BrdU (2 hr) to determine whether prostate PINs were actively synthesizing DNA. We found numerous BrdU-positive cells in PINs of both genotypes, although labeling

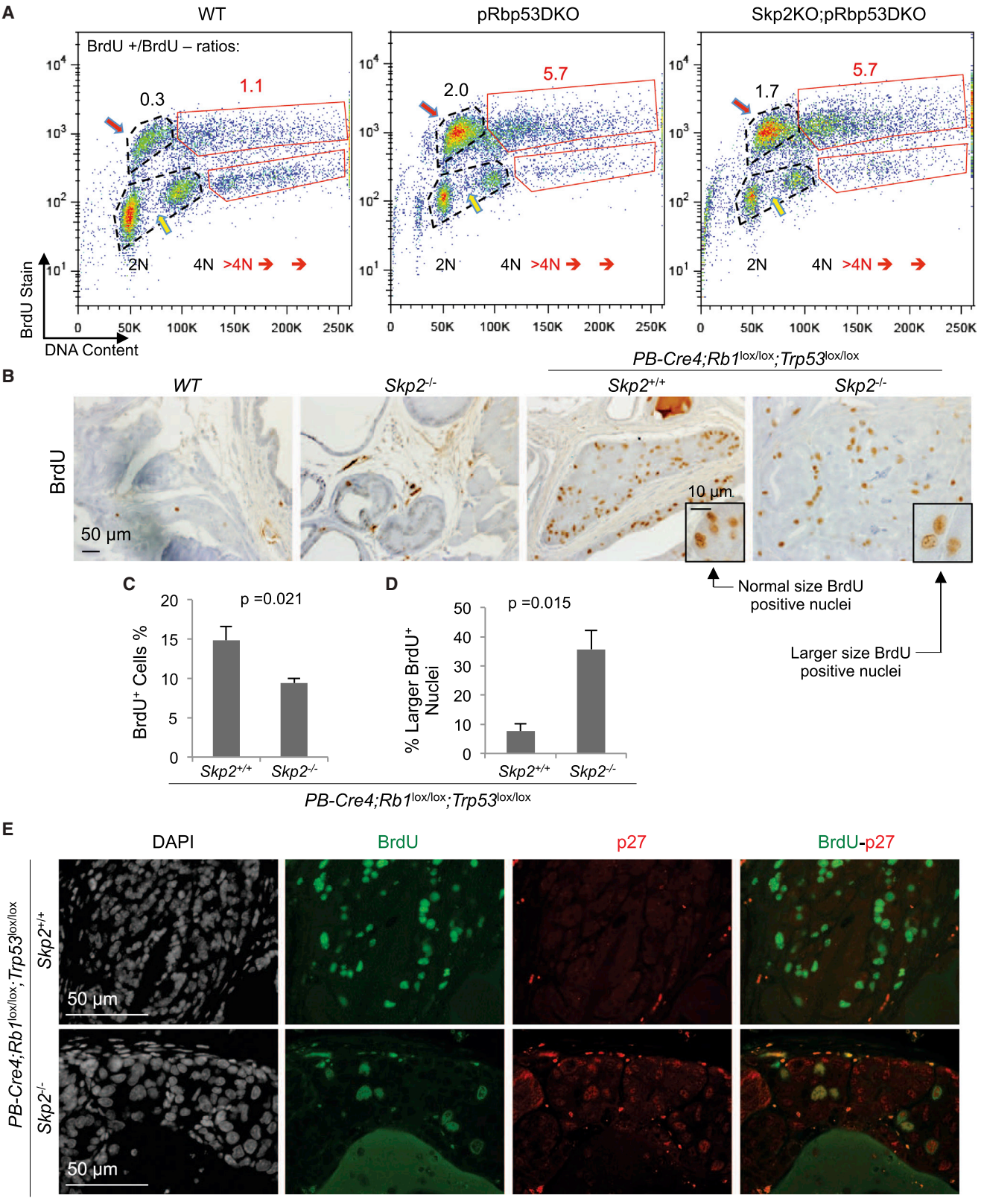

(legend on next page)

frequency was reduced from 14.85% to 9.39% by the deletion of *Skp2* (Figures 7B and 7C). Although this was a statistically significant reduction, it was less than twofold. We noticed that BrdU-positive nuclei in *Skp2*$^{-/-}$;*PB-Cre4*;*Rb1*$^{lox/lox}$;*Trp53*$^{lox/lox}$ PINs were larger than those in *PB-Cre4*;*Rb1*$^{lox/lox}$;*Trp53*$^{lox/lox}$ PINs (compare the two insets in Figure 7B). Figure 7D shows that 35.7% of BrdU-positive cells contained larger nuclei in *Skp2*$^{-/-}$;*PB-Cre4*;*Rb1*$^{lox/lox}$;*Trp53*$^{lox/lox}$ PINs, compared to 7.6% in *PB-Cre4*;*Rb1*$^{lox/lox}$;*Trp53*$^{lox/lox}$ PINs. These findings suggest that DNA synthesis activities in *Skp2*$^{-/-}$;*PB-Cre4*;*Rb1*$^{lox/lox}$;*Trp53*$^{lox/lox}$ PINs derived largely from DNA rereplication, explaining the presence of larger nuclei in them. Furthermore, BrdU-positive and larger nuclei also contained higher p27, as shown by double-staining for BrdU and p27 (Figure 7E).

The results discussed in this section solidify the salient feature of the *Skp2* deletion-mediated block of pRb/p53 doubly deficient tumorigenesis. In the absence of pRb and p53, deregulation of DNA replication in the form of rereplication persists in neoplastic lesions that are apparently blocked for life by higher levels of p27. Figure S6 shows more examples of BrdU-labeling PINs in four *Skp2*$^{-/-}$;*PB-Cre4*;*Rb1*$^{lox/lox}$;*Trp53*$^{lox/lox}$ mice ages 11 to 22 months.

Blocked Skp2KO;pRbp53DKO Prostatic Intraepithelial Neoplasia Cells Succumb to Apoptosis

Although pRb/p53 doubly deficient prostate tumorigenesis did not progress beyond PINs in *Skp2*$^{-/-}$ mice as old as 22 months, the PIN lesions persisted coexistent with active DNA synthesis. Although entry to mitosis was blocked, as indicated by significant reduction in pHH3-positive cells (Figures 6C and 6F; Figure S6), more than half of the pHH3-positive cells were in metaphase. Mitotic figures were also present in hematoxylin and eosin–stained sections of blocked PIN lesions. These features appeared inadequate to explain the lifelong block of pRb/p53 doubly deficient prostate tumorigenesis in *Skp2*$^{-/-}$ mice and would be compatible for selection of resistant cells.

To determine whether this block of tumorigenesis also involved cell elimination, we measured the rates of apoptosis in these PINs. TUNEL stain–positive cells were about 5.3% in pRbp53DKO PINs and increased to 8.4% in Skp2KO;pRbp53DKO PINs, which is not statistically significant (Figures 8A and 8D). Invasive carcinomas showed similar rates of apoptosis as measured by TUNEL staining. Detection of activated caspase 3 (aCasp3) yielded similar results. We next used nuclear condensation and fragmentation morphology (also called apoptotic bodies or pyknosis) to detect apoptosis (Figure 8B, inset a). We unexpectedly found that morphologically apoptotic cells were TUNEL-positive (Figure 8B, inset b) as well as TUNEL-negative (Figure 8B, inset c). Similarly, cells with condensed nuclei (by DAPI staining) were positive or negative for aCasp3 (Figure 8B, insets d and e). After we confirmed the ability of our TUNEL and aCasp3 staining to detect apoptosis by examining intestinal villi (Figure S7), we reevaluated apoptosis by combining TUNEL staining with morphological assessment. The results (Figures 8C and 8D) show that apoptosis rates remained similar with determination by TUNEL alone for DKO PINs, but increased twofold in invasive cancer and triple-knockout (TKO) PINs. Areas with as much as 20% apoptotic cells were frequently observed in TKO PINs. Figure 8C (black arrows in a, b, and c) indicates a typical stepwise process of late apoptosis leading to the elimination of the cell. The block of pRb/p53 doubly deficient prostate tumorigenesis in *Skp2*$^{-/-}$ mice therefore was not solely due to cytostatic mechanisms. Apoptotic elimination of blocked Skp2KO;pRbp53DKO PIN cells could contribute to the lifelong block of tumorigenesis by reducing the possibility for the emergence of resistant cells by, for example, epigenetically silencing p27 expression.

DISCUSSION

Tumorigenesis is a multistep process. Because of the cells' intrinsic antitumor safeguards, the first oncogenic events seldom succeed. pRb and p53 tumor suppressors are major effectors of antitumor safeguards and are therefore frequently inactivated in cancer. To learn how to treat cancers after all the antitumor mechanisms exemplified by pRb and p53 have been exhausted, we conducted the current study. To completely and irreversibly inactivate pRb and p53, we deleted the genes encoding them.

In this context, we discovered that deletion of *Skp2* unmasked a *Trp53* deletion-induced safeguard to elevate p27 protein levels. In the absence of Skp2, loss of activated p53 shrinks the pool of p27 ubiquitin ligases further by reducing expression of the p27 E3 ligases Pirh2 and KPC1 and therefore accumulates p27 protein further. This rise of p27 in Skp2KO;p53KO cells effectively inhibited the S phase to the extreme of cellular senescence. Critically, additional deletion of *Rb1* disabled this senescence antitumor mechanism. Not only DNA replication but also rereplication became uninhibitable, even in the presence of high levels of p27. These findings add a dramatic piece of evidence for the importance of keeping at least one of these two major tumor suppressors for the prevention and treatment of cancer.

Figure 7. Sustained Active DNA Synthesis in Skp2KO;pRbp53DKO Mouse Embryo Fibroblasts and in *Skp2*$^{-/-}$;*PB-Cre4*;*Rb1*$^{lox/lox}$;*Trp53*$^{lox/lox}$ Prostatic Intraepithelial Neoplasias

(A) Representative fluorescence-activated cell sorting analysis plots (from three experiments) of DNA content by propidium iodide staining and bromodeoxyuridine (BrdU) content by anti-BrdU staining. The numbers of BrdU-positive and BrdU-negative cells in the regular cell cycle were determined within the dotted black circles, and the ratios are indicated in black numbers above the circles. Numbers of cells with > 4N DNA contents were similarly analyzed with red boxes and red numbers. DKO, double-knockout; KO, knockout.

(B and C) Prostate sections from BrdU-injected mice with indicated genotypes were stained with BrdU (B), and quantification of BrdU-positive cells is shown in (C). WT, wild type.

(D) Quantification of normal-sized and larger BrdU-positive nuclei as portions of the entire BrdU-positive cell populations is shown.

(E) Prostate sections from BrdU-injected mice with indicated genotypes were stained with 4′,6-diamidino-2-phenylindole (DAPI), anti-BrdU and anti-p27. The *Skp2*$^{-/-}$;*PB-Cre4*;*Rb1*$^{lox/lox}$;*Trp53*$^{lox/lox}$ sample, which was taken from a 21.7-month-old mouse, shows persistence of prostatic intraepithelial neoplasia cells containing enlarged nuclei with high p27 and BrdU incorporation.

Quantitative data in (C) and (D) are presented as averages ± SEM. Student's t test was used for statistical analysis. See also Figure S6.

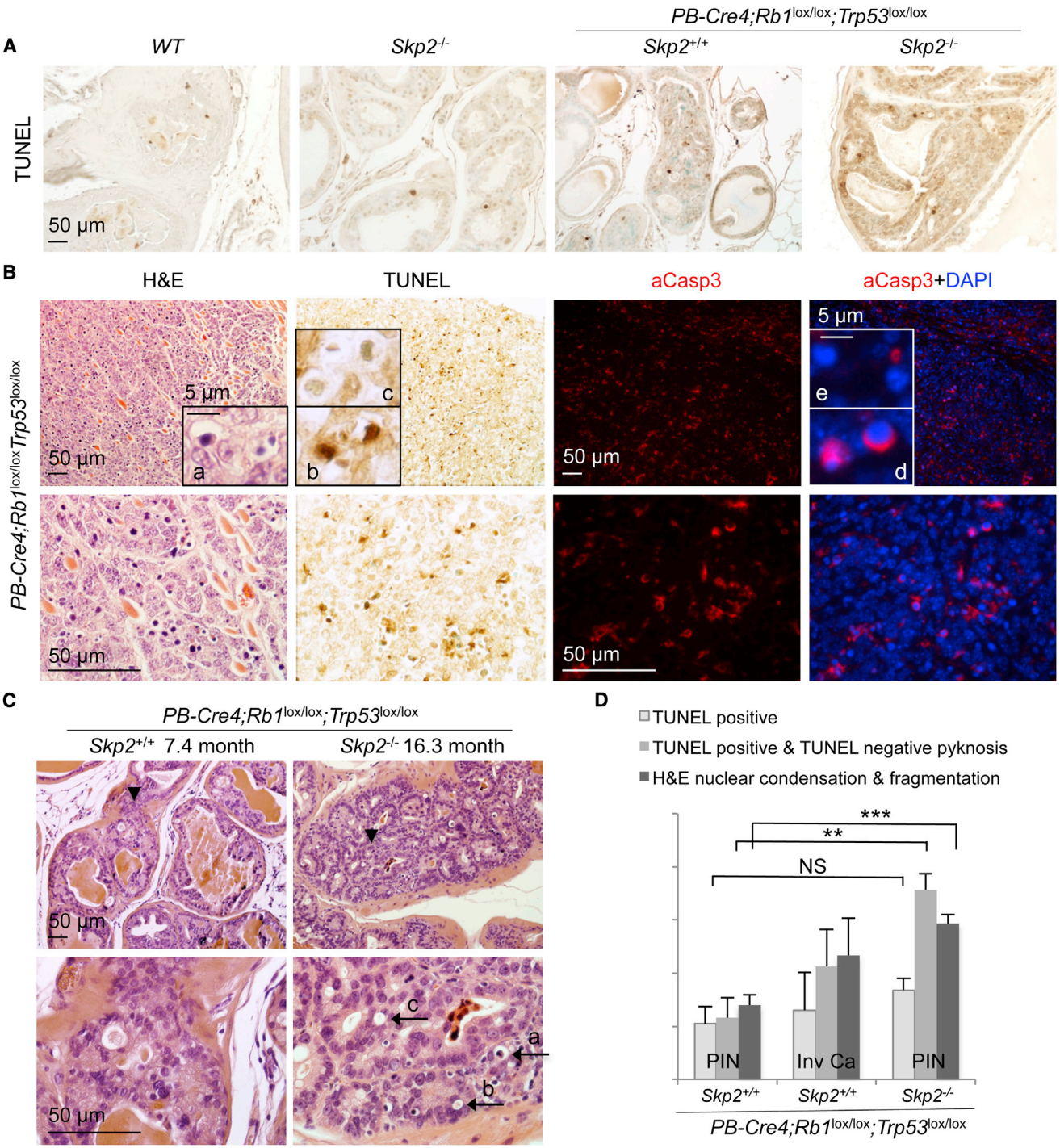

Figure 8. Blocked *Skp2*$^{-/-}$;*PB-Cre4;Rb1*$^{lox/lox}$;*Trp53*$^{lox/lox}$ Prostatic Intraepithelial Neoplastic Cells Succumb to Apoptosis

(A) Terminal deoxynucleotidyl transferase deoxyuridine triphosphate nick-end labeling (TUNEL) staining of prostate sections of the indicated genotypes. WT, wild type.

(B) Comparison of apoptosis detection by nuclear morphology (inset a), TUNEL stain (insets b and c), and activated caspase 3 (aCasp3) and 4′,6-diamidino-2-phenylindole (DAPI) costains (insets d and e) in a microscopic tumor. H&E, hematoxylin and eosin.

(C) Representative H&E-stained prostatic intraepithelial neoplasia (PIN) section of the indicated genotypes. Lower panels show higher-magnification views of areas indicated by black arrowheads in the corresponding upper panels. Black arrows indicate typical apoptotic morphologies as described in the text.

(D) Quantification of apoptosis rates in the indicated lesions by three different methods as marked.

Quantitative data are presented as averages ± SEM. Student's t test was used for statistical analysis. $^{**}p < 0.01$; $^{***}p < 0.002$; NS, $p > 0.05$.

See also Figure S7.

Unexpectedly, however, our study results consistently show that pRb/p53 doubly deficient prostate tumorigenesis in the absence of Skp2 was blocked lastingly. This unique coexistence of BrdU-labeling neoplastic lesions and a tumor-free life generated a counterintuitive preclinical model of complete block of tumorigenesis. In addition to revealing a vulnerability of pRb/p53 doubly deficient tumors, this model suggests an unconventional concept for the diagnosis, treatment, and management of the worst types of cancer. At the surface level, detection of abundant proliferation markers would immediately lead to the diagnosis of a more aggressive cancer carrying a poor prognosis, whereas in fact they could be lastingly blocked neoplastic lesions.

Up to now, tumor block has been associated with dramatic reduction of proliferation markers down to the extremes of cellular senescence. Although ostensibly elevated to block tumorigenesis, cellular senescence, the most studied safeguard, could also secrete cytokines and growth factors to promote tumorigenesis (Coppé et al., 2010; Krtolica et al., 2001; Kuilman and Peeper, 2009). Recent evidence shows that oncogenic Nras induced senescence in hepatocytes to induce liver cancer when the senescence cells were not cleared (Kang et al., 2011) and that DOX treated *Wnt1*-induced mammary tumors more effectively in the absence of p53 induced cellular senescence than in its presence (Jackson et al., 2012).

Persistent DNA rereplication could provide different ways to overcome tumor block and promote tumorigenesis. DNA rereplication is logically a source for gene amplification and genomic instability. On an ongoing basis, these changes can generate new mutations that inhibit p27 expression or promote p27 protein degradation and/or nuclear export to disable the block to pRb/p53 doubly deficient tumorigenesis. This scenario is expected to lead to rapid tumorigenesis because pRb and p53 are already inactivated. The fact that this scenario did not materialize up to the old age of 22 months of mouse life is surprising. It is possible, however, that this blocking mechanism for pRb/p53 doubly deficient tumorigenesis will delay tumor progression to the end stage only within the longer time frames of typical human cancers. On the other hand, our findings may suggest that Skp2 inactivation also stabilizes the genome via mechanisms yet to be identified. Further studies are required to determine the effects of inhibiting Skp2 on established tumors that are caused by inactivation of pRb and p53 but likely have undergone additional mutations during tumorigenesis.

Targeting Skp2 to treat cancer has already been actively pursued. The finding that *Skp2* deletion can induce p53-independent senescence (Lin et al., 2010) broadens its application to p53-deficient cancers, and a recent report has described a Skp2 inhibitor with this ability preclinically (Chan et al., 2013). Our present study broadens its application further to include pRb/p53 doubly deficient cancers and sheds more light on the design of Skp2 inhibitors. Protein degradation in the ubiquitin proteasome system (Ciechanover, 2005) proceeds via a set of hierarchic steps starting with target-specific polyubiquitination and ending in degradation of polyubiquitinated proteins in the proteasomes. For Skp2-mediated p27 ubiquitination and degradation, the most target-specific step is the interaction between $SCF(CRL1)^{Skp2/Cks1}$ with T187 phosphorylated p27, and an inhibitor blocking this interface has recently been identified (Wu et al., 2012). Inhibitors targeting the interaction between Skp2 and Skp1 in SCF E3 (Chan et al., 2013; Chen et al., 2008) blocks ubiquitination of p27 together with other substrates of SCF^{Skp2}, but they might spare substrates of SCF E3s employing other F-box proteins. Further upstream are inhibitors targeting the cullin subunit in all CRL E3 ligases (Soucy et al., 2009). Inhibitors of ubiquitin-conjugating enzymes (E2s) have also been identified. Targeting CDC34, which functions with CRLs, inhibited not only p27 ubiquitination but also a larger group of CRL substrates (Ceccarelli et al., 2011). Although the above-named inhibitors and their designs can all inhibit Skp2-mediated p27 ubiquitination with varying degrees of selectivity, they do not inhibit Pirh2 and KPC1, because they are not CRL-type E3s and do not depend on CDC34 as E2 for the ubiquitination of p27.

Proteasome inhibitors, by definition, do not target specific proteins or specific groups of proteins. Impressively, however, the proteasome inhibitor bortezomib was approved by the U.S. Food and Drug Administration and has demonstrated remarkable efficacy in treating multiple myeloma and mantle cell lymphoma. Stabilization of p27 might be an important mechanism for its therapeutic efficacy, although other effects caused by nonspecific accumulation of proteins might also be responsible, especially for its side effects. In this respect, the proteasome inhibitor argyrin A (Nickeleit et al., 2008) exhibited antitumor activities in a p27-dependent manner. Because argyrin A is a more specific proteasome inhibitor than bortezomib (Nickeleit et al., 2008), its intriguing effects could suggest that truly specific inhibition of proteasomes could indeed effectively treat cancer "specifically" through p27 stabilization. It will be important to determine whether this occurs because inhibiting proteasomes disabled the whole cellular pool of p27 E3s, including Skp2, Pirh2, KPC1, and likely others (Cao et al., 2011). Our study provides a basis for explaining why pan-inhibition of p27 degradation mechanisms would be more effective than specific inhibition of Skp2 for cancer treatment.

EXPERIMENTAL PROCEDURES

Mice

POMC-Cre mice (Balthasar et al., 2004), *PB-Cre4* mice (Wu et al., 2001), $Rb1^{lox/lox}$ mice (Sage et al., 2003), $Trp53^{lox/lox}$ mice (Jonkers et al., 2001), $Skp2^{+/-}$ mice (Nakayama et al., 2000), and $p27^{-/-}$ mice (Fero et al., 1996) have been described. *POMC-Cre* mice (Bradford B. Lowell Laboratory) were obtained on an FVB background, $Rb1^{lox/lox}$ mice (Tyler Jacks Laboratory) on a C57BL6J×129Sv background, $Trp53^{lox/lox}$ mice (National Cancer Institute (NCI) mouse repository) on an FVB×129 background, $Skp2^{-/-}$ mice on a C57BL6J×129Sv background, $p27^{-/-}$ mice (The Jackson Laboratory) on a C57BL6J background, and *PB-Cre4* mice (NCI mouse repository) on a C57BL6J×Cg background. Subsequent breeding did not select for or against any particular strain background. Testing genotypes were studied with control genotypes from littermates. Genotyping details are provided in the Supplemental Information. Animals were housed in the Albert Einstein College of Medicine animal facility. Mouse procedures were reviewed and approved by the Albert Einstein College of Medicine Animal Care Committee, conforming to accepted standards of humane animal care. Mouse pathological studies were conducted together with the Albert Einstein Cancer Center Mouse Pathology Core.

Mouse Embryo Fibroblasts, Human Breast Cancer Cell Lines, and Treatments

MEFs were prepared from embryonic day 13.5 embryos and cultured in Dulbecco's modified Eagle's medium (DMEM) containing 10% fetal bovine serum (FBS). Parallel infection with adeno-Cre or adeno-GFP were used to delete or

mock-delete *Rb1* or/and *Trp53* in MEFs containing floxed *Rb1* or/and floxed *Trp53*. Controls also included infection with adeno-Cre of MEFs without floxed *Rb1* or *Trp53*. Knockdown or overexpression was carried out by lentiviral transduction and drug selection with puromycin (catalog no. BP2956-100; Fisher Scientific) or blasticidin (catalog no. ant-bl-1; InvivoGen). DNA damage response was generated by treatment with 1 μM DOX (catalog no. BP2516-1; Fisher Scientific). Human breast cancer cell lines MDA-MB468, BT549, Hs578T, and HCC1143 (American Type Culture Collection) were cultured in RPMI 1640 medium containing 10% FBS, 1% penicillin/streptomycin, and 1% glutamine. Knockdown of Skp2 by miRNA was achieved by lentiviral transduction at near 100% efficiency. See Supplemental Information for details.

SA-β-gal Staining for Senescence, FACS Analysis for DNA Content and BrdU Labeling, and Cell Number Counting for Proliferation Determination

Standard protocols were used; details are in Supplemental Information.

Western Blot Analysis, RT-qPCR, and ChIP

Antibodies used for western blot analysis are Skp2 (H435), cyclin A (C-19), p21 (C-19), Pirh2 (FL261), PCNA (PC10), and Cdk2 (C-19) (all from Santa Cruz Biotechnology). Mouse anti-p27 antibody was obtained from BD Biosciences (catalog no. 610242), mouse anti-p53 antibody was obtained from Cell Signaling Technology (catalog no. 1C12) and Santa Cruz Biotechnology (SC-126). Antibody to α-tubulin was obtained from Sigma-Aldrich (catalog no. T6074). Antibody to KPC1 was described previously (Kamura et al., 2004). See Supplemental Information for experimental details and sequences of primers.

Cycloheximide Chase and Serum Starvation Release

For protein stability analysis, MEFs were plated into 60-mm dishes at 70%–80% confluence. Cycloheximide (CHX, catalog no. 239764; Calbiochem) was added at 50 μg/ml. At the indicated time points, cell extracts were prepared and western blotted. Quantification of protein levels was performed using ImageJ software (National Institutes of Health). Serum starvation of MEFs was carried out in 100-mm dishes at 80%–90% confluence in DMEM (1% penicillin/streptomycin, 1% glutamine) with 0.2% FBS. After 72 hr, cells were aliquoted into 60-mm dishes and restimulated with DMEM (1% penicillin/streptomycin, 1% glutamine) containing 10% FBS.

Immunohistochemistry, Immunofluorescence, TUNEL, and Bromodeoxyuridine Labeling

Antibodies included PCNA (catalog no. PC10; Santa Cruz Biotechnology), BrdU (catalog no. Ab-2; Calbiochem), pHH3 (Cell Signaling Technology), Ki67 (catalog no. SP6; Vector Laboratories), activated caspase 3 (catalog no. 9664S; Cell Signaling Technology), mouse anti-p27 antibody (catalog no. 610242; BD Biosciences), and rabbit anti-p27 antibody (catalog no. ab92741; Abcam). TUNEL staining was performed with an apoptosis detection kit (catalog no. S7100; EMD Millipore). For BrdU labeling, mice were injected with 0.4% BrdU (B5002; Sigma-Aldrich) at 25 μl/g body weight 2 hr before they were killed. See Supplemental Information for experiment details.

Statistical Analysis

In the survival analysis, differences in Kaplan-Meier survival curves were analyzed using a logrank test with GraphPad Prism 6 software (GraphPad Software). Differences in Ki67-, pHH3-, BrdU-, and TUNEL-positive cells between indicated samples were analyzed by Student's t test. P values < 0.05 were considered statistically significant.

SUPPLEMENTAL INFORMATION

Supplemental Information includes Supplemental Experimental procedures and seven figures and can be found with this article online at http://dx.doi.org/10.1016/j.ccr.2013.09.021.

AUTHOR CONTRIBUTIONS

H.Z. and L.Z. conceived and designed the research; H.Z., F.B., H.F., Z.L., and J.C. performed the research; K.I.N. and K.N. provided Skp2-mutant mice and KPC1 antibody; H.Z., J.L., and L.Z. analyzed the data; H.Z. and L.Z. wrote the manuscript; and all authors reviewed and approved the manuscript for publication.

ACKNOWLEDGMENTS

This work was supported by National Institutes of Health grants R01 CA127901 and R01 CA131421 (to L.Z.). The Albert Einstein Comprehensive Cancer Research Center (grant 5P30CA13330) and the Albert Einstein Comprehensive Liver Research Center (grant 5P30DK061153) provided core facility support. We thank Dr. Sarah Schweber of the Oncology Division for suggestions of human breast cancer cell lines and Dr. Jinghang Zhang of the Flow Cytometry Core Facility of the Albert Einstein Cancer Center for assistance in using iCys Research Imaging Cytometer and iCys Cytometric Analysis Software. H.Z. is a recipient of U.S. Department of Defense Prostate Cancer Research Program Postdoctoral Fellowship (PC121837), and L.Z. is a recipient of the Irma T. Hirschl Career Scientist Award.

Received: May 8, 2013
Revised: August 22, 2013
Accepted: September 30, 2013
Published: November 11, 2013

REFERENCES

Arias, E.E., and Walter, J.C. (2007). Strength in numbers: preventing rereplication via multiple mechanisms in eukaryotic cells. Genes Dev. *21*, 497–518.

Balthasar, N., Coppari, R., McMinn, J., Liu, S.M., Lee, C.E., Tang, V., Kenny, C.D., McGovern, R.A., Chua, S.C., Jr., Elmquist, J.K., and Lowell, B.B. (2004). Leptin receptor signaling in POMC neurons is required for normal body weight homeostasis. Neuron *42*, 983–991.

Berman, S.D., Calo, E., Landman, A.S., Danielian, P.S., Miller, E.S., West, J.C., Fonhoue, B.D., Caron, A., Bronson, R., Bouxsein, M.L., et al. (2008). Metastatic osteosarcoma induced by inactivation of Rb and p53 in the osteoblast lineage. Proc. Natl. Acad. Sci. USA *105*, 11851–11856.

Burkhart, D.L., and Sage, J. (2008). Cellular mechanisms of tumour suppression by the retinoblastoma gene. Nat. Rev. Cancer *8*, 671–682.

Cao, X., Xue, L., Han, L., Ma, L., Chen, T., and Tong, T. (2011). WW domain-containing E3 ubiquitin protein ligase 1 (WWP1) delays cellular senescence by promoting p27(Kip1) degradation in human diploid fibroblasts. J. Biol. Chem. *286*, 33447–33456.

Ceccarelli, D.F., Tang, X., Pelletier, B., Orlicky, S., Xie, W., Plantevin, V., Neculai, D., Chou, Y.C., Ogunjimi, A., Al-Hakim, A., et al. (2011). An allosteric inhibitor of the human Cdc34 ubiquitin-conjugating enzyme. Cell *145*, 1075–1087.

Chan, C.H., Morrow, J.K., Li, C.F., Gao, Y., Jin, G., Moten, A., Stagg, L.J., Ladbury, J.E., Cai, Z., Xu, D., et al. (2013). Pharmacological inactivation of Skp2 SCF ubiquitin ligase restricts cancer stem cell traits and cancer progression. Cell *154*, 556–568.

Chen, Q., Xie, W., Kuhn, D.J., Voorhees, P.M., Lopez-Girona, A., Mendy, D., Corral, L.G., Krenitsky, V.P., Xu, W., Moutouh-de Parseval, L., et al. (2008). Targeting the p27 E3 ligase SCF(Skp2) results in p27- and Skp2-mediated cell-cycle arrest and activation of autophagy. Blood *111*, 4690–4699.

Chicas, A., Wang, X., Zhang, C., McCurrach, M., Zhao, Z., Mert, O., Dickins, R.A., Narita, M., Zhang, M., and Lowe, S.W. (2010). Dissecting the unique role of the retinoblastoma tumor suppressor during cellular senescence. Cancer Cell *17*, 376–387.

Ciechanover, A. (2005). Proteolysis: from the lysosome to ubiquitin and the proteasome. Nat. Rev. Mol. Cell Biol. *6*, 79–87.

Coppé, J.P., Desprez, P.Y., Krtolica, A., and Campisi, J. (2010). The senescence-associated secretory phenotype: the dark side of tumor suppression. Annu. Rev. Pathol. *5*, 99–118.

el-Deiry, W.S., Kern, S.E., Pietenpol, J.A., Kinzler, K.W., and Vogelstein, B. (1992). Definition of a consensus binding site for p53. Nat. Genet. *1*, 45–49.

Fero, M.L., Rivkin, M., Tasch, M., Porter, P., Carow, C.E., Firpo, E., Polyak, K., Tsai, L.-H., Broudy, V., Perlmutter, R.M., et al. (1996). A syndrome of multiorgan hyperplasia with features of gigantism, tumorigenesis, and female sterility in p27(Kip1)-deficient mice. Cell *85*, 733–744.

Flesken-Nikitin, A., Choi, K.C., Eng, J.P., Shmidt, E.N., and Nikitin, A.Y. (2003). Induction of carcinogenesis by concurrent inactivation of *p53* and *Rb1* in the mouse ovarian surface epithelium. Cancer Res. *63*, 3459–3463.

Hattori, T., Isobe, T., Abe, K., Kikuchi, H., Kitagawa, K., Oda, T., Uchida, C., and Kitagawa, M. (2007). Pirh2 promotes ubiquitin-dependent degradation of the cyclin-dependent kinase inhibitor p27Kip1. Cancer Res. *67*, 10789–10795.

Jackson, J.G., Pant, V., Li, Q., Chang, L.L., Quintás-Cardama, A., Garza, D., Tavana, O., Yang, P., Manshouri, T., Li, Y., et al. (2012). p53-mediated senescence impairs the apoptotic response to chemotherapy and clinical outcome in breast cancer. Cancer Cell *21*, 793–806.

Jiang, Z., Deng, T., Jones, R., Li, H., Herschkowitz, J.I., Liu, J.C., Weigman, V.J., Tsao, M.S., Lane, T.F., Perou, C.M., and Zacksenhaus, E. (2010). Rb deletion in mouse mammary progenitors induces luminal-B or basal-like/EMT tumor subtypes depending on p53 status. J. Clin. Invest. *120*, 3296–3309.

Jonkers, J., Meuwissen, R., van der Gulden, H., Peterse, H., van der Valk, M., and Berns, A. (2001). Synergistic tumor suppressor activity of BRCA2 and p53 in a conditional mouse model for breast cancer. Nat. Genet. *29*, 418–425.

Kamura, T., Hara, T., Matsumoto, M., Ishida, N., Okumura, F., Hatakeyama, S., Yoshida, M., Nakayama, K., and Nakayama, K.I. (2004). Cytoplasmic ubiquitin ligase KPC regulates proteolysis of p27(Kip1) at G1 phase. Nat. Cell Biol. *6*, 1229–1235.

Kang, T.W., Yevsa, T., Woller, N., Hoenicke, L., Wuestefeld, T., Dauch, D., Hohmeyer, A., Gereke, M., Rudalska, R., Potapova, A., et al. (2011). Senescence surveillance of pre-malignant hepatocytes limits liver cancer development. Nature *479*, 547–551.

Kiyokawa, H., Kineman, R.D., Manova-Todorova, K.O., Soares, V.C., Hoffman, E.S., Ono, M., Khanam, D., Hayday, A.C., Frohman, L.A., and Koff, A. (1996). Enhanced growth of mice lacking the cyclin-dependent kinase inhibitor function of p27(Kip1). Cell *85*, 721–732.

Krtolica, A., Parrinello, S., Lockett, S., Desprez, P.Y., and Campisi, J. (2001). Senescent fibroblasts promote epithelial cell growth and tumorigenesis: a link between cancer and aging. Proc. Natl. Acad. Sci. USA *98*, 12072–12077.

Kuilman, T., and Peeper, D.S. (2009). Senescence-messaging secretome: SMS-ing cellular stress. Nat. Rev. Cancer *9*, 81–94.

Leng, R.P., Lin, Y., Ma, W., Wu, H., Lemmers, B., Chung, S., Parant, J.M., Lozano, G., Hakem, R., and Benchimol, S. (2003). Pirh2, a p53-induced ubiquitin-protein ligase, promotes p53 degradation. Cell *112*, 779–791.

Lin, H.K., Chen, Z., Wang, G., Nardella, C., Lee, S.W., Chan, C.H., Yang, W.L., Wang, J., Egia, A., Nakayama, K.I., et al. (2010). Skp2 targeting suppresses tumorigenesis by Arf-p53-independent cellular senescence. Nature *464*, 374–379.

Marino, S., Vooijs, M., van Der Gulden, H., Jonkers, J., and Berns, A. (2000). Induction of medulloblastomas in p53-null mutant mice by somatic inactivation of Rb in the external granular layer cells of the cerebellum. Genes Dev. *14*, 994–1004.

McClendon, A.K., Dean, J.L., Ertel, A., Fu, Z., Rivadeneira, D.B., Reed, C.A., Bourgo, R.J., Witkiewicz, A., Addya, S., Mayhew, C.N., et al. (2011). RB and p53 cooperate to prevent liver tumorigenesis in response to tissue damage. Gastroenterology *141*, 1439–1450.

Meuwissen, R., Linn, S.C., Linnoila, R.I., Zevenhoven, J., Mooi, W.J., and Berns, A. (2003). Induction of small cell lung cancer by somatic inactivation of both Trp53 and Rb1 in a conditional mouse model. Cancer Cell *4*, 181–189.

Nakayama, K., Ishida, N., Shirane, M., Inomata, A., Inoue, T., Shishido, N., Horii, I., Loh, D.Y., and Nakayama, K.-i. (1996). Mice lacking p27(Kip1) display increased body size, multiple organ hyperplasia, retinal dysplasia, and pituitary tumors. Cell *85*, 707–720.

Nakayama, K., Nagahama, H., Minamishima, Y.A., Matsumoto, M., Nakamichi, I., Kitagawa, K., Shirane, M., Tsunematsu, R., Tsukiyama, T.I., Ishida, N., et al. (2000). Targeted disruption of Skp2 results in accumulation of cyclin E and p27(Kip1), polyploidy and centrosome overduplication. EMBO J. *19*, 2069–2081.

Nakayama, K., Nagahama, H., Minamishima, Y.A., Miyake, S., Ishida, N., Hatakeyama, S., Kitagawa, M., Iemura, S., Natsume, T., and Nakayama, K.I. (2004). Skp2-mediated degradation of p27 regulates progression into mitosis. Dev. Cell *6*, 661–672.

Nickeleit, I., Zender, S., Sasse, F., Geffers, R., Brandes, G., Sörensen, I., Steinmetz, H., Kubicka, S., Carlomagno, T., Menche, D., et al. (2008). Argyrin a reveals a critical role for the tumor suppressor protein p27(kip1) in mediating antitumor activities in response to proteasome inhibition. Cancer Cell *14*, 23–35.

Old, J.B., Kratzat, S., Hoellein, A., Graf, S., Nilsson, J.A., Nilsson, L., Nakayama, K.I., Peschel, C., Cleveland, J.L., and Keller, U.B. (2010). Skp2 directs Myc-mediated suppression of p27Kip1 yet has modest effects on Myc-driven lymphomagenesis. Mol. Cancer Res. *8*, 353–362.

Park, J.H., Walls, J.E., Galvez, J.J., Kim, M., Abate-Shen, C., Shen, M.M., and Cardiff, R.D. (2002). Prostatic intraepithelial neoplasia in genetically engineered mice. Am. J. Pathol. *161*, 727–735.

Sage, J., Miller, A.L., Pérez-Mancera, P.A., Wysocki, J.M., and Jacks, T. (2003). Acute mutation of retinoblastoma gene function is sufficient for cell cycle re-entry. Nature *424*, 223–228.

Sherr, C.J. (2012). Ink4-Arf locus in cancer and aging. Wiley interdisciplinary reviews. Dev. Biol. *1*, 731–741.

Soucy, T.A., Smith, P.G., Milhollen, M.A., Berger, A.J., Gavin, J.M., Adhikari, S., Brownell, J.E., Burke, K.E., Cardin, D.P., Critchley, S., et al. (2009). An inhibitor of NEDD8-activating enzyme as a new approach to treat cancer. Nature *458*, 732–736.

Sun, D., Melegari, M., Sridhar, S., Rogler, C.E., and Zhu, L. (2006). Multi-miRNA hairpin method that improves gene knockdown efficiency and provides linked multi-gene knockdown. Biotechniques *41*, 59–63.

Walkley, C.R., Qudsi, R., Sankaran, V.G., Perry, J.A., Gostissa, M., Roth, S.I., Rodda, S.J., Snay, E., Dunning, P., Fahey, F.H., et al. (2008). Conditional mouse osteosarcoma, dependent on p53 loss and potentiated by loss of Rb, mimics the human disease. Genes Dev. *22*, 1662–1676.

Wang, H., Bauzon, F., Ji, P., Xu, X., Sun, D., Locker, J., Sellers, R.S., Nakayama, K., Nakayama, K.I., Cobrinik, D., and Zhu, L. (2010). Skp2 is required for survival of aberrantly proliferating Rb1-deficient cells and for tumorigenesis in Rb1+/- mice. Nat. Genet. *42*, 83–88.

Wei, C.L., Wu, Q., Vega, V.B., Chiu, K.P., Ng, P., Zhang, T., Shahab, A., Yong, H.C., Fu, Y., Weng, Z., et al. (2006). A global map of p53 transcription-factor binding sites in the human genome. Cell *124*, 207–219.

Wu, X., Wu, J., Huang, J., Powell, W.C., Zhang, J., Matusik, R.J., Sangiorgi, F.O., Maxson, R.E., Sucov, H.M., and Roy-Burman, P. (2001). Generation of a prostate epithelial cell-specific Cre transgenic mouse model for tissue-specific gene ablation. Mech. Dev. *101*, 61–69.

Wu, L., Grigoryan, A.V., Li, Y., Hao, B., Pagano, M., and Cardozo, T.J. (2012). Specific small molecule inhibitors of Skp2-mediated p27 degradation. Chem. Biol. *19*, 1515–1524.

Xuan, Z., Zhao, F., Wang, J., Chen, G., and Zhang, M.Q. (2005). Genome-wide promoter extraction and analysis in human, mouse, and rat. Genome Biol. *6*, R72.

Zhou, Z., Flesken-Nikitin, A., Corney, D.C., Wang, W., Goodrich, D.W., Roy-Burman, P., and Nikitin, A.Y. (2006). Synergy of p53 and Rb deficiency in a conditional mouse model for metastatic prostate cancer. Cancer Res. *66*, 7889–7898.

Zhu, W., Chen, Y., and Dutta, A. (2004). Rereplication by depletion of geminin is seen regardless of p53 status and activates a G2/M checkpoint. Mol. Cell. Biol. *24*, 7140–7150.

Cancer Cell, Volume *24*

Supplemental Information

Skp2 Deletion Unmasks a p27 Safeguard that Blocks Tumorigenesis in the Absence of pRb and p53 Tumor Suppressors

Hongling Zhao, Frederick Bauzon, Hao Fu, Zhonglei Lu, Jinhua Cui, Keiko Nakayama, Keiich I. Nakayama, Joseph Locker, and Liang Zhu

Supplemental Data

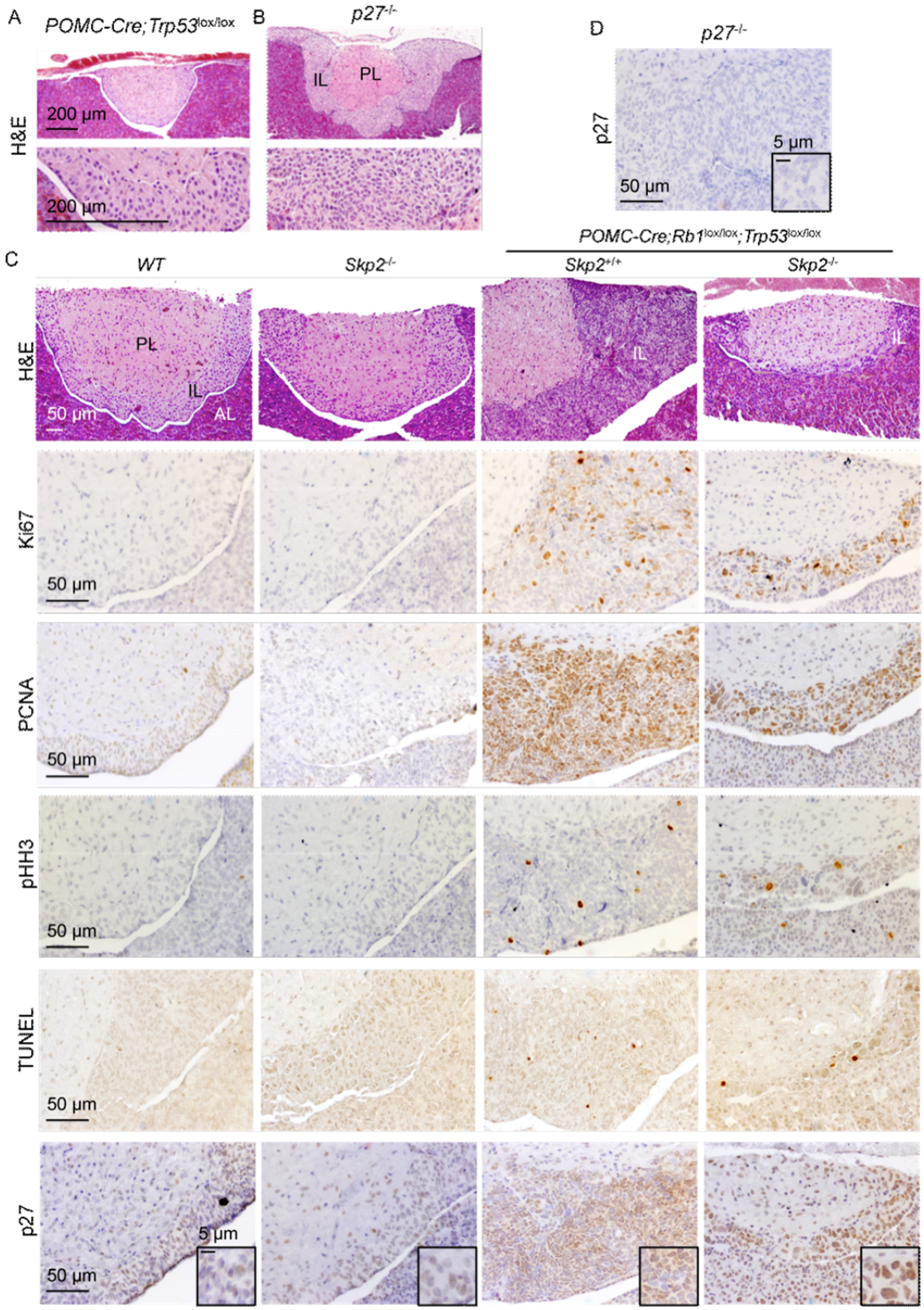

Figure S1. Related to Figure 1. (A and B) H&E staining of pituitary sections of 7 weeks old *POMC-Cre;Trp53*$^{lox/lox}$ (A) or *p27*$^{-/-}$ (B) mice. (C) Pituitary sections of the indicated genotypes were stained as indicated. (D) Pituitary sections of *p27*$^{-/-}$ mice stained with anti-p27.

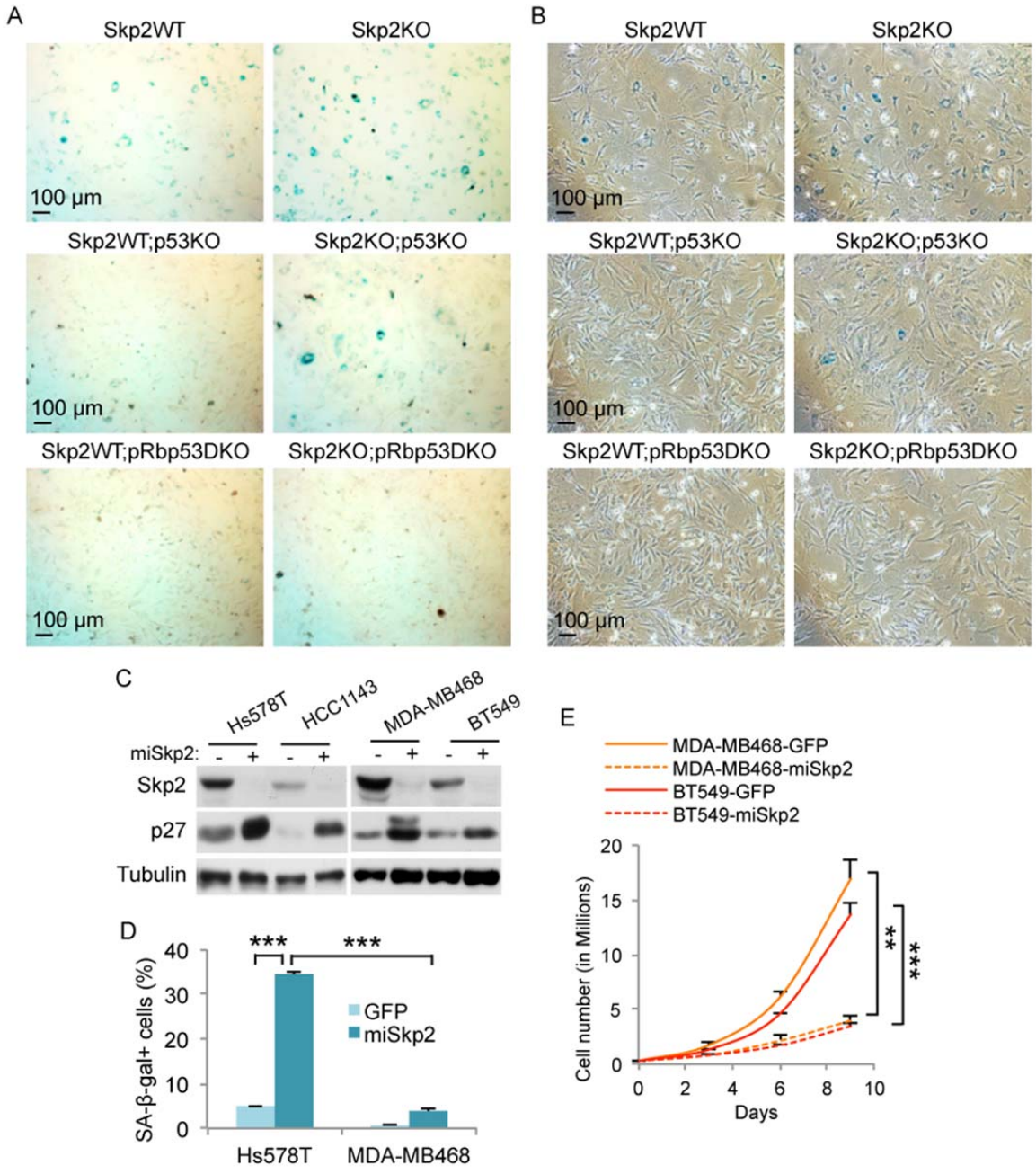

Figure S2. Related to Figure 2. (A and B) MEFs of the indicated genotypes were stained with SA-β-gal and photographed in bright field (A) or in phase contrast (B). (C) Indicated human breast cancer cell lines, with or without Skp2 knockdown (miSkp2) were subjected to Western blot. (D) Quantification of SA-β-gal stain in photographs shown in Figure 2B. (E) Actual cell proliferations for the indicated human breast cancer cells expressing GFP or miSkp2. Quantitative data are presented as average +/- SEM. Student's *t* test was used for statistical analysis. **, $p < 0.01$; ***, $p < 0.002$.

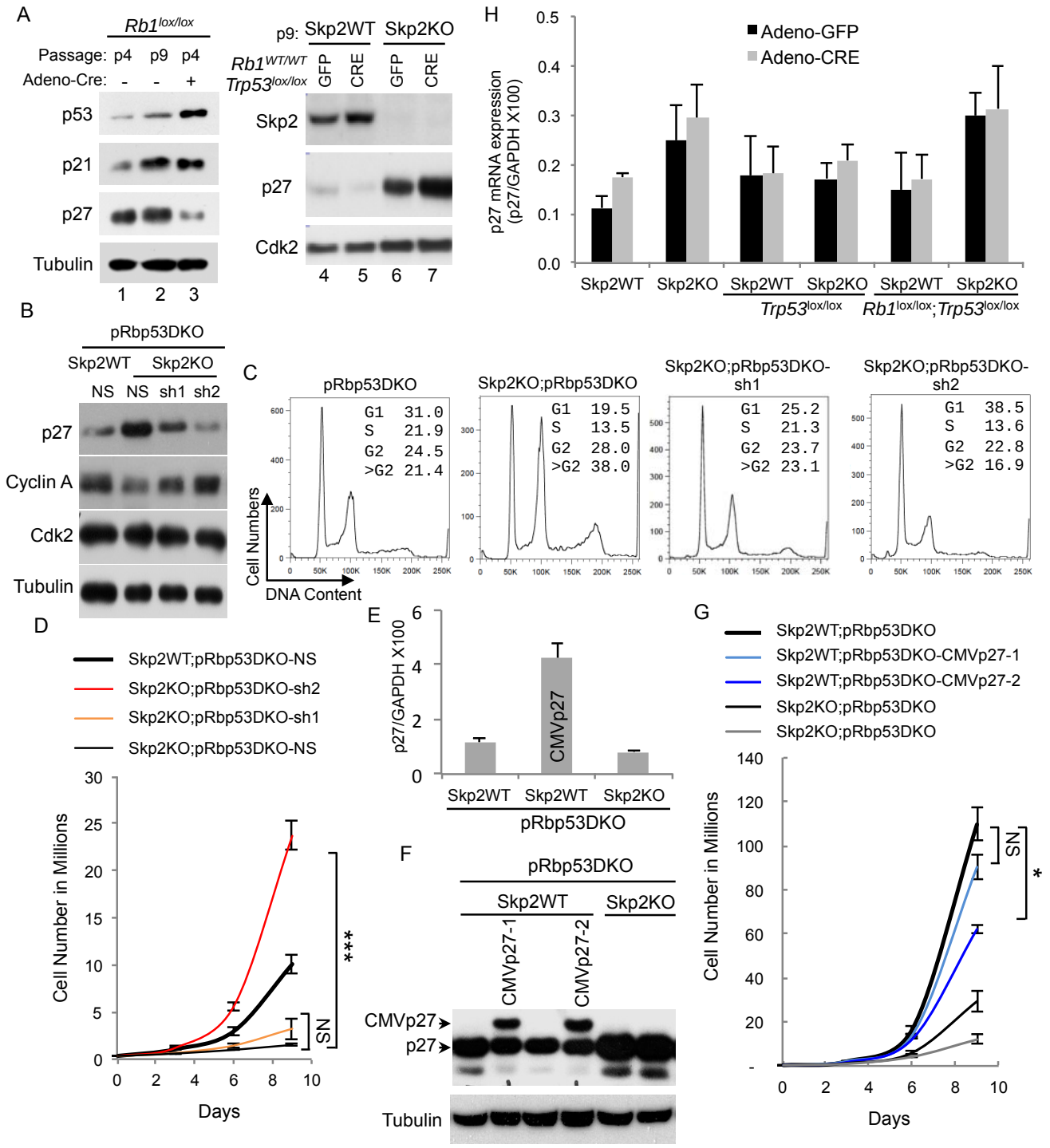

Figure S3. Related to Figure 3. (A) Western blots of indicated MEFs. MEF cultures established from dissected embryos on previous days are "Passage" 1 (p1). (B) Western blots of indicated MEFs transduced with indicated knockdown hairpins. NS, non-specific random sequence hairpins. (C) DNA content FACS. (D) Same cells as in (C) were counted to determine actual cell proliferation. (E) RT-qPCR of p27 mRNA from indicated MEFs. (F) Western blot of cell in (E). (G) Proliferation curves of the indicated cells. (H) RT-qPCR of p27 mRNA. Quantitative data are presented as average +/- SEM. Student's *t* test was used for statistical analysis. *, $p < 0.05$; ***, $p < 0.002$; NS, $p > 0.05$.

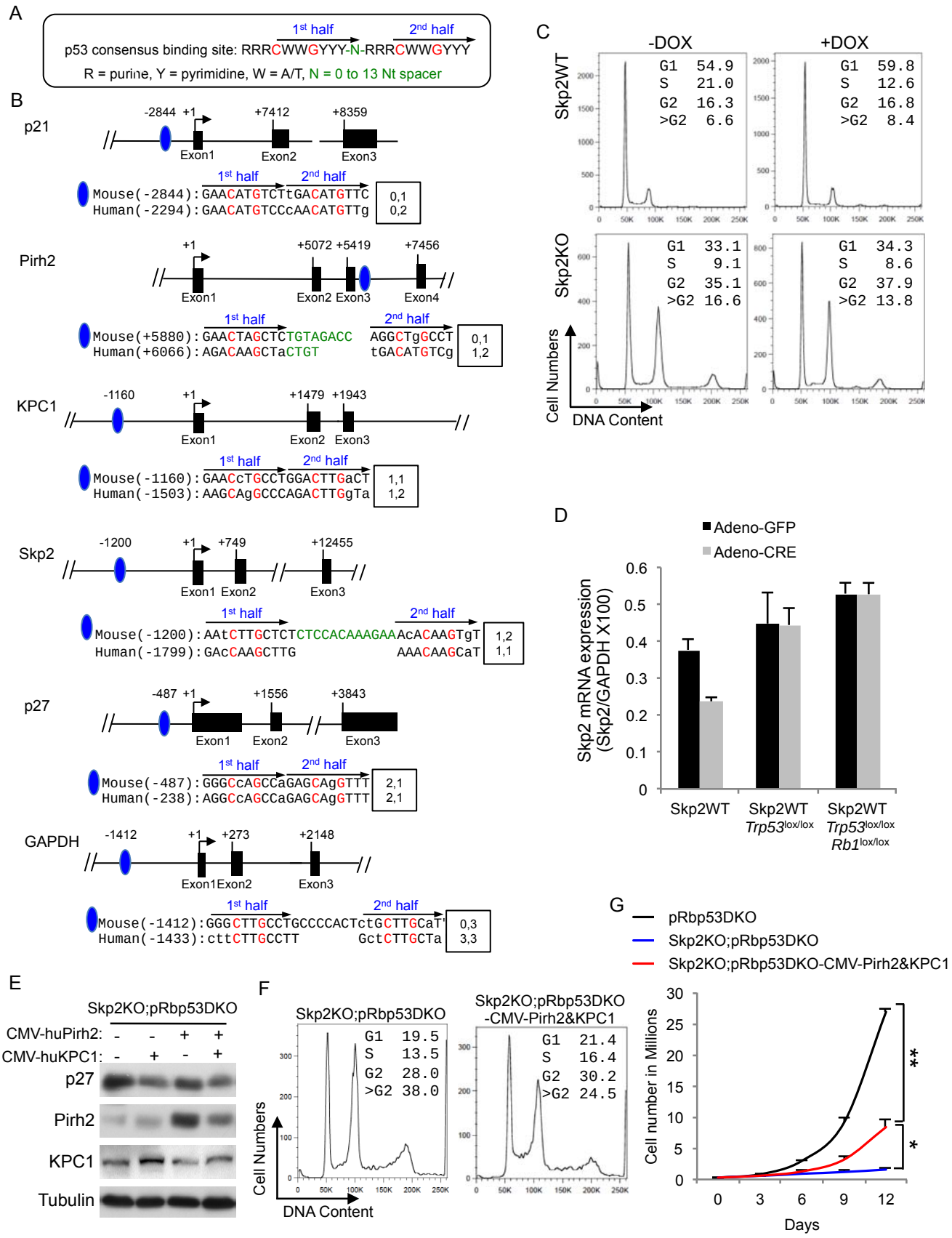

<< Continued on the next page >>

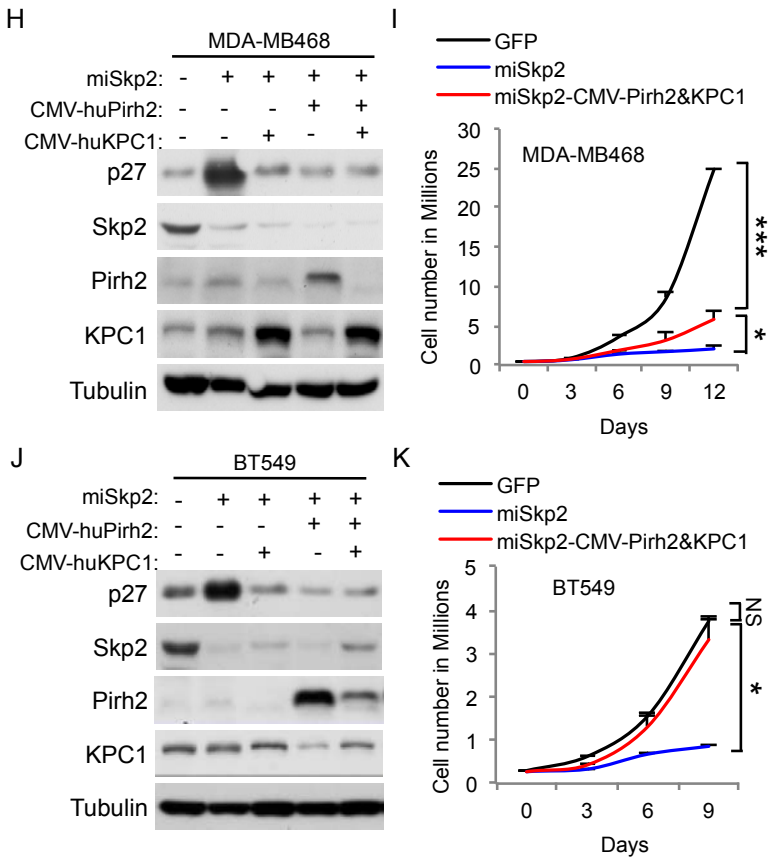

Figure S4. Related to Figure 4. (A) The consensus p53 binding site. (B) The best matching sequence to the consensus p53 binding site for each genes. Conservations between mouse and human are indicated. (C) DNA content FACS showing cell cycle profiles of WT and Skp2KO MEFs before and after DOX treatment, as in Figure 4A to 4C. (D) Effects of deleting *Trp53* alone or together with *Rb1* on mRNA levels of Skp2 is measured by RT-qPCR. (E to G) Expression of human Pirh2 and KPC1 from a CMV promoter was examined by western blots (E), their effects on cell cycle profiles were determined by DNA content FACS (F), and their effects on actual cell proliferation by cell number counts for 12 days (G). (H to K) Expression of CMV-huPirh2 and CMV-huKPC1 in human breast cancer cell lines were examined by Western blots (H and J) and their effects on cell proliferation by cell number counts (I and K). Quantitative data are presented as average +/- SEM. Student's *t* test was used for statistical analysis. *, $p < 0.05$; **, $p < 0.01$; ***, $p < 0.002$; NS, $p > 0.05$.

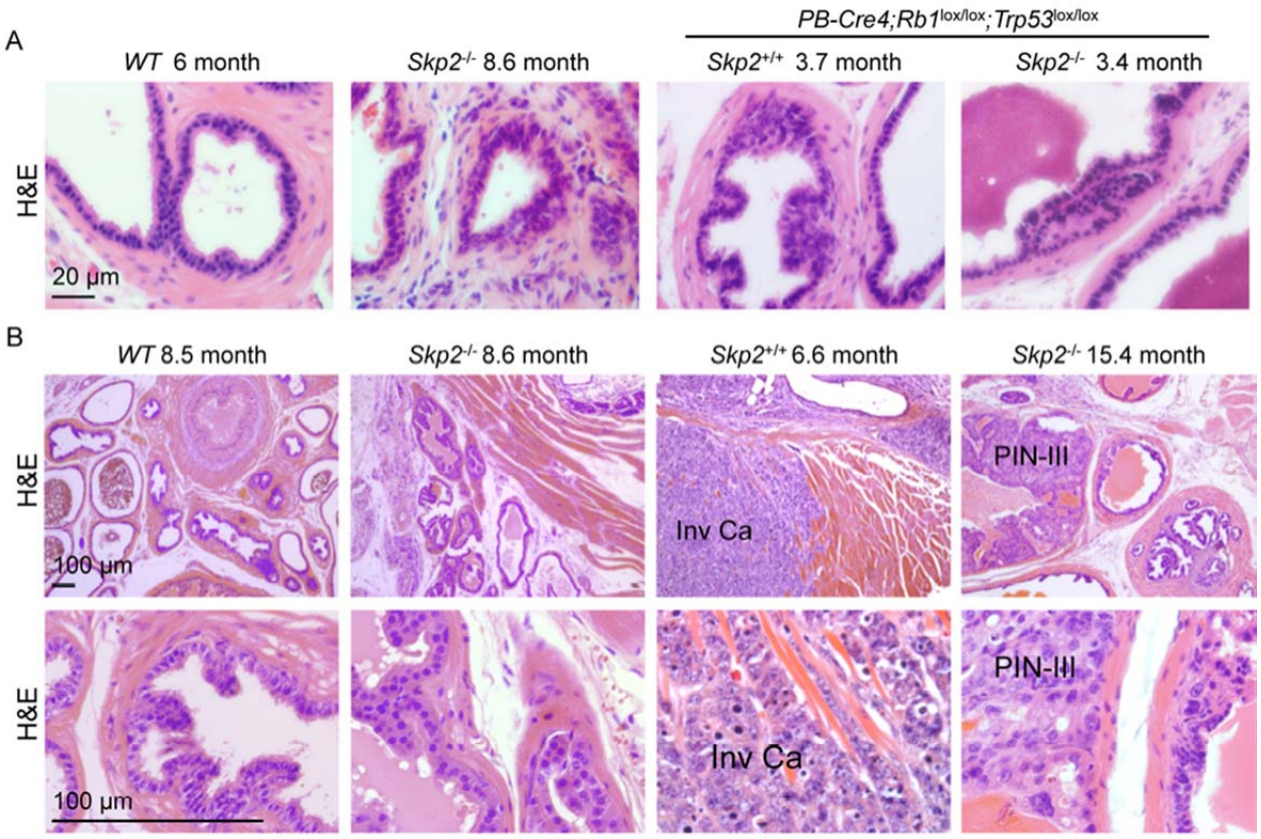

Figure S5. Related to Figure 5. (A) PINs at 3 months. (B) Invasive carcinoma in the presence of Skp2 at 6.6 month, and PIN-III in the absence of Skp2 at 15.4 month. Two magnifications are shown.

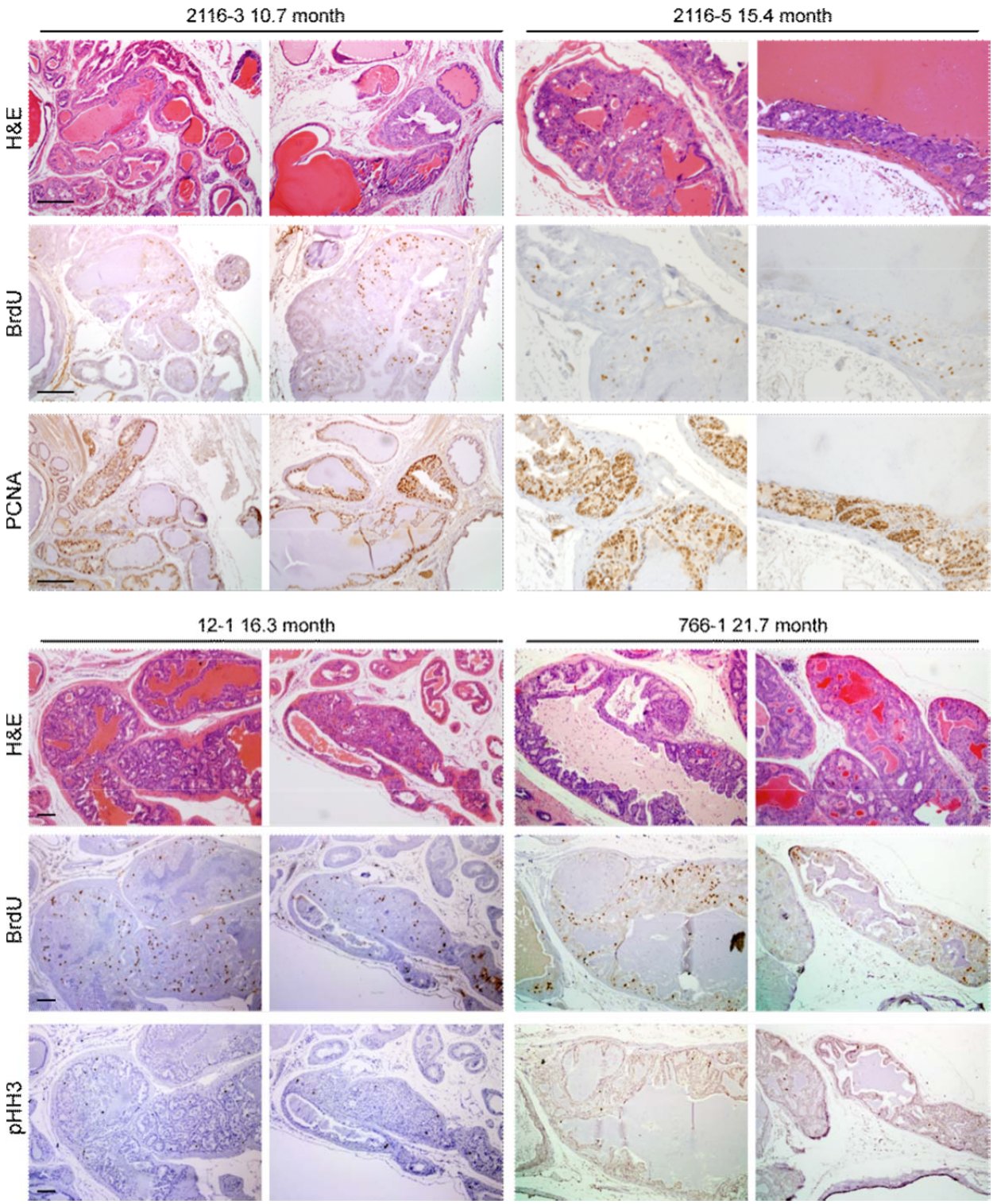

Figure S6. Related to Figure 7. Prostate sections from *Skp2*$^{-/-}$;*PB-Cre4;Rb1*$^{lox/lox}$;*Trp53*$^{lox/lox}$ mice in the 10-22 months age group (with their IDs) were analyzed with H&E, BrdU (2 hr labeling), PCNA, and pHH3 staining, as indicated. Scale bars = 100 μm.

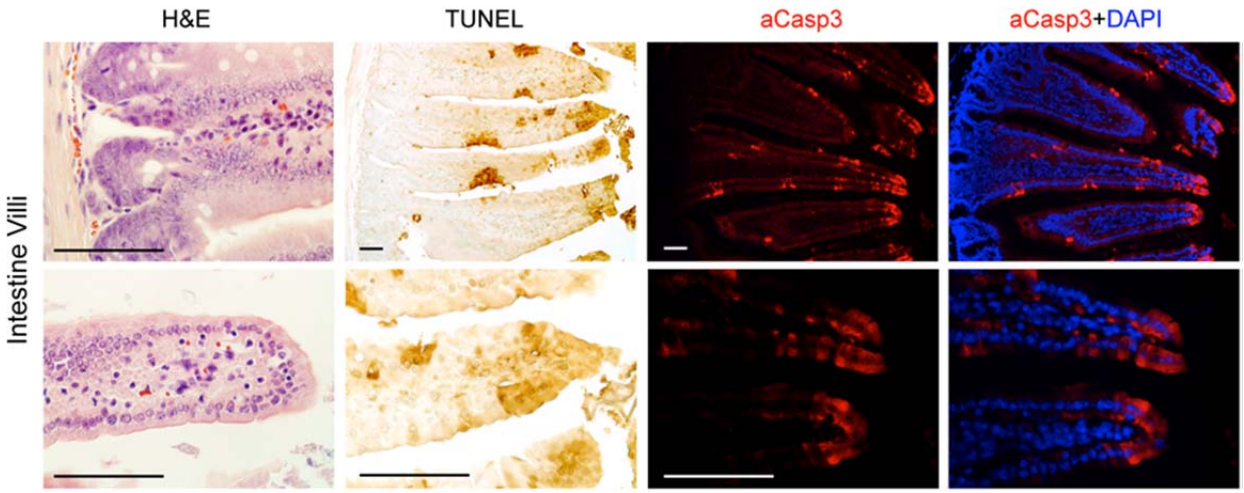

Figure S7. Related to Figure 8. Validation of TUNEL and aCasp3 staining for apoptosis with the characteristic distribution of apoptotic cells in intestine villi. Scale bars = 50 μm.

Supplemental Experimental Procedures

Mouse genotyping. For *POMC-Cre* transgenic mice: POMC-Cre-F: 5'-TGGCTCAATGTCCTTCCTGG-3' and POMC-Cre-R: 5'-GAAATCAGTGCGTTCGAACGCTAGA-3'. The transgene yields a PCR product of 400bp. For $Rb1^{lox/lox}$ mice: Rblox-F: 5'-CTCTAGATCCTCTCATTCTTC-3' and Rblox-R: 5'-CCTTGACCATAGCCCAGCAC-3'. The Rblox allele yields a PCR product of 310bp while the wild type allele a 250bp PCR product. For $Trp53^{lox/lox}$ mice: p53lox-F: 5'-CACAAAAACAGGTTAAACCCAG-3' and p53lox-R: 5'-AGCACATAGGAGGCAGAGAC-3'. The p53lox allele yields a PCR product of 370bp while the wild type allele a 288bp PCR product. For $Skp2^{+/-}$ mice: wild type allele, KN3: 5'-AGAGTGGAAGAACCCAGGCAGGAC-3' and KN4: 5'-CCCGTGGAGGGAAAAAGAGGGACG-3', yielding a 430bp PCR product, and KO allele: KN13: 5'- GCATCGCCTTCTATCGCCTTCTTG-3' and KN38: 5'-TTCCCACCCCCACATCCAGTCATT-3' yielding a PCR product of 500bp. For *PB-Cre4* mice: PB-CRE4-F: 5'-CTGAAGAATGGGACAGGCATTG-3' and PB-CRE4-R: 5'-CATCACTCGTTGCATCGACC-3'. The PB-Cre4 transgene yields a PCR product of 393bp. For $p27^{+/-}$ mice: WT-F: 5'-GATGGACGCCAGACAAGC-3' and WT-R: 5'-AGGGGCTTATGATTCTGAAAGTCG-3', p27KO-F: 5'-CCTTCTATCGCCTTCTTG-3' and p27KO-R: 5'-TGGAACCCTGTGCCATCTCTAT-3'. WT allele yields a PCR product of 166bp, KO allele a 500bp PCR product.

MEF preparation and infection. Embryos from timed pregnancies were harvested between E12.5-E14.5. Heads, livers, and blood clots were removed and the rest of tissues were minced and put into 1 ml Trypsin (25300-054, Gibco) for 10 min at 37°C. The tissue and Trypsin mixture was pipetted up and down several times and the dissociated cells were cultured in DMEM (11965-092, Giboco) containing 10% FBS (S11550, Atlanta Biologicals) and 1% Pen/Strep (15140-122, Giboco). Cells were split every 3-4 days during early passages, and MEFs at passage 2 or 3 were used for infection to delete, knockdown or overexpress specific proteins. Adeno-GFP and Adeno-CRE viruses were from Einstein Gene therapy Core, lentivirus vectors expressing p27, p53, or shRNAs from Einstein shRNA Core facility. Lentiviral helper constructs were from L. Naldini and A. Follenzi (Follenzi et al., 2000) and Xia Wang of Einstein Gene therapy Core. Lentivirus stocks were generated and concentrated as described previously (Sun et al., 2006).

SA-β-gal stain. To determine cellular senescence, MEFs and human breast cancer cell lines were plated in triplicate 6 cm plates for 3 days, and were fixed with 0.2% glutaraldehyde (G5882, Sigma-Aldrich) for 15 minutes at room temperature. SA-β-gal activity was determined by staining cells with SA-β-gal staining solution (5 mM Potassium Ferrocyanide, 5 mM Potassium Ferricyanide, 2 mM $MgCl_2$, 150

mM NaCl, 40 mM citric acid/sodium phosphate buffer pH6.0, and 1 mg/ml X-gal) for 16 hr (MEFs) and 5 hr (human cancer cell lines) at 37°C. Results were quantified under microscope.

FACS. Cells were washed and fixed by adding 6 ml ice-cold 80% EtOH (~70% EtOH final) while vortexing. Cells were then washed with 5 ml PBS and resuspended in 0.5 ml of 0.25 mg/ml RNase A and 10 µg/ml propidium iodide in PBS for FACS analysis. BrdU labeling was for 30 min in 10 µM BrdU. After EtOH fixation for 30 minutes in 4˚C, cells were incubated in 1 ml 2 M HCl, 0.5% Triton X-100 for 30 min at room temperature, neutralized in 1 ml 0.1 M Sodium Borate pH9.0, and resuspended in 100-200 µl 0.2% BSA/0.5% Tween 20/PBS for 5 min. We used 20 µl anti-BrdU-FITC per 10^6 cells and incubated for 30-60 min at room temperature. Staining for pHH3 was performed with the same steps as anti-BrdU. FACS and data analysis were performed together with the Einstein FACS Core.

Cell proliferation assay. $3X10^5$ cells were plated in 6 cm plates in triplicate, and cell numbers were counted every 2 or 3 days under the microscope with hemocytometers for indicated days.

Western blot. MEF lysates were prepared with RIPA buffer (50 mM Tris-HCl pH7.4, 1% NP40, 0.5% sodium deoxycholate, 0.1% SDS, 1 mM EDTA, 150 mM NaCl, and standard protease inhibitors). Prostate tissues or tumors were snap-frozen in dry ice and stored in −80 °C. Frozen tissues were homogenized with Dounce glass homogenizer in tissue lysis buffer (50 mM HEPES, pH 7.2, 150 mM NaCl, 1 mM EDTA, 0.1% Tween-20, 1 mM dithiothreitol and standard protease inhibitors). Debris was removed by centrifugation for 10 min at 14,000 r.p.m. in an Eppendorf Centrifuge 5415C at 4 °C. Protein concentrations of the extracts were determined by Bio-Rad protein assay kit, and equal amounts of protein samples were loaded on 10% SDS gels and blotted onto polyvinylidene fluoride membrane.

RT-qPCR. RNA was extracted by Trizol reagent (Invitrogen). Oligo-dT and SuperScript II (Invitrogen) were used for the synthesis of the first-strand cDNA at 42 °C for 60 min. The qPCR primers for mouse Skp2, p21, p27, KPC1, Pirh2 and GAPDH are listed below. SYBR Green PCR Master Mix (4309155, ABI) and the standard program of ABI 7500 Fast real-time PCR were used.

ChIP and qPCR. MEFs were cross-linked with 1% formaldehyde (#252549, Sigma-Aldrich) in culture medium for 10 min at room temperature. Cross-link was stopped by addition of glycine to a final concentration of 0.125 M for 5 min at room temperature. Fixed cells were scraped off the plates, washed twice with PBS, pelleted and stored. Cell pellets were re-suspended in 1 ml of cell lysis buffer containing PMSF (5 mM HEPES pH8.0, 85 mM KCl, 0.5% Triton X-100,) and put on ice for 20 min before being pelleted again by centrifugation at 2500g for 5 minutes. Pellets were re-suspended with 600 µl nuclear lysis buffer containing PMSF (50 mMTris-HCl pH8.0, 10 mM EDTA, 1% SDS). DNA was sheared by sonication for 15 s x 4 in a 60 Sonic Dismembrator (Fisher), at a power setting of 10. The resultant genomic DNA fragments with a bulk size of 100–1000 bp were precleared by addition of 20 µl of blocked protein A-Agrose beads (P9269, Sigma). The beads were blocked with tRNA and Salmon sperm DNA. The precleared chromatin were incubated overnight at 4°C with 2 µg antibody (for p53, SC-71817X, Santa Cruz Biotechnology). The chromatin and antibody mixture were then incubated with blocked protein A-Agrose beads at 4°C for 4 hr with rotation and followed by successive 10-minute washes in 1 ml of IP dilution buffer (16.7 mM Tris-HCl pH 8.0, 167 mM NaCl, 1.2 mM EDTA, 1% Triton X-100, and 0.01% SDS), dialysis buffer (2 mM EDTA, 50 mM Tris-HCl pH 8.0, 0.2% Sarkosyl), TSE-500 buffer (2 mM EDTA, 20 mM Tris-HCl pH 8.0, 500 mM NaCl, 1% Triton X-100, and 0.1% SDS), LiCl detergent buffer (100 mM Tris-HCl pH 8.0, 1% deoxycholic acid, 1% Triton X-100, 500 mM LiCl), and TE buffer. After washing, the samples were eluted with elution buffer (50 mM $NaHCO_3$, 1% SDS). The eluted material was purified by Qiagen PCR purification kit for qPCR.

Tissue preparation and staining. Tissues were fixed in 10% Formalin (SF 100-4, Fisher Scientific), embedded in paraffin wax and sectioned. Paraffin sections were processed according to protocols for the SuperPicture™ kit (879263 and 879163, Invitrogen). Secondary antibodies for IHC were HRP polymer conjugated anti-rabbit or anti-mouse IgG. Color development was by DAB chromogen supplied in the SuperPicture™ kit. Sections were counterstained by Harris Hematoxylin (S212, Poly Scientific). Immunofluorescence detection was by Rhodamine conjugated goat anti-rabbit-IgG (SC-2091, Santa Cruz Biotechnology) or Fluorescein conjugated horse-anti-mouse-IgG (FI-2000, Vector laboratory).

TSA™PLUS Fluorescence Kit (NEL741001KT, PerkinElmer) was used to amplify signals when indicated. DNA was stained with DAPI. Feulgen staining was done with Schiff's reagent (s272, Poly Scientific R&D Corp.), and counter stained with fast green (s2114, Poly Scientific R&D Corp.).

DNA content analysis with tissue sections. DAPI stained prostate sections were scanned and analyzed by the iCys® Research Imaging Cytometer and iCys® Cytometric Analysis Software (CompuCyte Corporation). At least 500 prostate epithelial cells were analyzed for each genotype.

Primer sequences

qPCR primers	
GAPDH	
GAPDH-F	5'-AATGTGTCCGTCGTGGATCT-3'
GAPDH-R	5'-GGTCCTCAGTGTAGCCCAAG-3'
p27	
p27-F	5'-GCGGTGCCTTTAATTGGGTCT-3'
p27-R	5'-GGCTTCTTGGGCGTCTGC T-3'
p21	
p21-F	5'-CCCGAGAACGGTGGAACTT-3'
p21-R	5'-TGCAGCAGGGCAGAGGAA-3'
Skp2	
Skp2-F	5'-CCAGCAAGACTTCTGAACTGC-3'
Skp2-R	5'-GAGGCACAGACAGGAAAAGA-3'
KPC1	
KPC1-F	5'-GAAGTCCAGGGTCACAGGCA-3'
KPC1-R	5'-GGTTATGGAAGTTTAGCGGTT T-3'
Pirh2	
Pirh2-F	5'-GCCTTAGACATGACTCGGTAC-3'
Pirh2-R	5'-CTGCTGATCCACTGGCACTCT-3'
ChIP primers	
GAPDH	
GAPDH-F	5'-GAGTTCTGGGAGTCTCGTGG-3'
GAPDH-R	5'-CTCTTCGGGTGGTGGTTCA-3'
p21	
p21-F	5'- TTCAGTGCAGGGTGGTGGA-3'
p21-R	5'- ATTCTGCTGGCAAAGTGG G-3'
Pirh2	
Pirh2-F	5'- CATTTCTTCCCTCCGAACCCT-3'
Pirh2-R	5'- CTAGTTCCAGGACAGCCAAAG C-3'
KPC1	
KPC1-F	5'-GTAGGCAGGACTTAGGAGGGT-3'
KPC1-R	5'-GGATAGATGGTGGCAGGAAG-3'
Skp2	
Skp2-F	5'-TCTCCCCTGTTGCACAGTTT-3'
Skp2-R	5'-TGATGAGTCTCCCAAATACCA-3'
p27	
p27-F	5'-ACCGCCATATTGGGCAACTAAA-3'
p27-R	5'-GTGGCAAACAGTCGGAGCGTA-3'

Knockdown and overexpression vectors

Constructs	Packaging plasmids	Mammalian selection	Sequences
pGIP2-shp27-1	pCMV-dR8.91; pMD2-VSVG	Puromycin (10ug/ml)	5'-AGAAGATTCTTCTTCGCAA-3'
pGIP2-shp27-2	pCMV-dR8.91; pMD2-VSVG	Puromycin (10ug/ml)	5'-ACAATAACACTAAAATTTT-3'
Lenti-CMV-miSkp2	pMDLg/pRRE, pRSV-REV, and pMD2-VSVG	N/A	5′-CCTTAGACCTCACAGGTAA-3′
pLOC-p27	pCMV-dR8.91; pMD2-VSVG	Blasticidin (10ug/ml)	Human p27 ORF
pLX304-p53	pMDLg/pRRE,	Blasticidin	Human p53 ORF

	pRSV-REV, and pMD2-VSVG	(10ug/ml)	
pLOC-RNF123	pCMV-dR8.91; pMD2-VSVG	Blasticidin (10ug/ml)	Human KPC1 ORF
pLOC-RCHY1	pCMV-dR8.91; pMD2-VSVG	Blasticidin (10ug/ml)	Human Pirh2 ORF

Supplemental Reference

Follenzi, A., Ailles, L.E., Bakovic, S., Geuna, M., and Naldini, L. (2000). Gene transfer by lentiviral vectors is limited by nuclear translocation and rescued by HIV-1 pol sequences. Nat Genet *25*, 217-222.

THE JOURNAL OF BIOLOGICAL CHEMISTRY VOL. 290, NO. 9, pp. 5797–5809, February 27, 2015

Substituting Threonine 187 with Alanine in p27Kip1 Prevents Pituitary Tumorigenesis by Two-Hit Loss of *Rb1* and Enhances Humoral Immunity in Old Age*

Received for publication, November 10, 2014, and in revised form, January 11, 2015 Published, JBC Papers in Press, January 12, 2015, DOI 10.1074/jbc.M114.625350

Hongling Zhao[‡], Frederick Bauzon[‡], Enguang Bi[§], J. Jessica Yu[§], Hao Fu[‡], Zhonglei Lu[‡], Jinhua Cui[‡], Hyungjun Jeon[¶], Xingxing Zang[¶], B. Hilda Ye[§], and Liang Zhu[‡1]

From the [‡]Department of Developmental and Molecular Biology, and Medicine, and [§]Cell Biology, and [¶]Microbiology and Immunology, The Albert Einstein Comprehensive Cancer Center and Liver Research Center, Albert Einstein College of Medicine, Bronx, New York 10461

Background: p27T187A knockin mice facilitate studying p27Kip1 protein in physiology.
Results: p27T187A knockin prevented pituitary tumorigenesis in $Rb1^{+/-}$ mice and enhanced humoral response to immunization in older age.
Conclusion: Phosphorylation of p27T187 is important in *Rb1*-deficient tumorigenesis and immunity in aging.
Significance: Specific cancer is identified for treatment by inhibiting Skp2/Cks1-p27T187p interaction and new directions are revealed in understanding immunity decline in elderly.

p27Kip1 (p27) is an inhibitor of cyclin-dependent kinases. Inhibiting p27 protein degradation is an actively developing cancer therapy strategy. One focus has been to identify small molecule inhibitors to block recruitment of Thr-187-phosphorylated p27 (p27T187p) to $SCF^{Skp2/Cks1}$ ubiquitin ligase. Since phosphorylation of Thr-187 is required for this recruitment, p27T187A knockin (KI) mice were generated to determine the effects of systemically blocking interaction between p27 and Skp2/Cks1 on tumor susceptibility and other proliferation related mouse physiology. $Rb1^{+/-}$ mice develop pituitary tumors with full penetrance and the tumors are invariably $Rb1^{-/-}$, modeling tumorigenesis by two-hit loss of *RB1* in humans. Immunization induced humoral immunity depends on rapid B cell proliferation and clonal selection in germinal centers (GCs) and declines with age in mice and humans. Here, we show that p27T187A KI prevented pituitary tumorigenesis in $Rb1^{+/-}$ mice and corrected decline in humoral immunity in older mice following immunization with sheep red blood cells (SRBC). These findings reveal physiological contexts that depend on p27 ubiquitination by $SCF^{Skp2\text{-}Cks1}$ ubiquitin ligase and therefore help forecast clinical potentials of Skp2/Cks1-p27T187p interaction inhibitors. We further show that GC B cells and T cells use different mechanisms to regulate their p27 protein levels, and propose a T helper cell exhaustion model resembling that of stem cell exhaustion to understand decline in T cell-dependent humoral immunity in older age.

Cyclin-dependent kinase (Cdk)[2] inhibitor p27Kip1 (p27) binds cyclin/Cdk and inhibits their kinase activity. Since cyclin/Cdk drives the cell cycle engine, p27 and its family members p21 and p57 are best known as negative regulators of cell proliferation. p27 knock-out (KO) mice are larger and heavier by about 20% over wild type (WT) mice and develop pituitary intermediate lobe (IL) tumors, providing *in vivo* evidence for the anti-proliferative functions of p27 (1–3). p27 ck-mice [RxL32 to AxA32 knockin (KI) to disrupt p27 binding to cyclins, and FDF64 to ADA64 KI to disrupt p27 binding to Cdks] phenocopied p27 KO mice in larger body size and pituitary tumorigenesis, confirming the biochemical mechanisms of p27 function *in vivo* (4).

The best known mechanism for regulating p27 expression is its polyubiquitination leading to degradation in the proteasome, and the best known regulator of p27 ubiquitination is Skp2, which is the substrate recruiting subunit of the SCF^{Skp2} ubiquitin ligase (5). SCF^{Skp2} has a growing list of substrates. For recruiting p27, threonine 187 of p27 (p27T187) must be phosphorylated (6, 7) and an accessory protein, Cks1, must be present (8, 9). The phosphorylated threonine 187 fits into a pocket formed by Skp2 and Cks1 to enable stable interaction between p27 and Skp2/Cks1 (10); p27 is therefore ubiquitinated in the $SCF^{Skp2/Cks1}$-p27T187p complex.

p27T187A mutation (substitution of threonine with alanine) renders p27T187 unphosphorylable and, therefore, cannot be ubiquitinated by $SCF^{Skp2/Cks1}$. To test the biological significance of ubiquitination of p27T187p by $SCF^{Skp2/Cks1}$, p27T187A KI mice were generated (11).

Studies of cultured $p27^{T187A/T187A}$ mouse embryonic fibroblasts (MEFs) in serum starvation (to maintain MEFs in G0) and re-stimulation (to stimulate MEFs to proliferate) revealed re-

* This work was supported by NIH Grants R01CA127901and R01CA131421 (to L. Z.), and R01 CA85573 (to B. H. Y.). This work was also supported by a Department of Defense PCRP Postdoctoral Fellowship (PC121837) (to H. Z.), and the Irma T. Hirschl Career Scientist Award (to B. H. Y. and L. Z.).
[1] To whom correspondence should be addressed: Dept. of Developmental and Molecular Biology, Albert Einstein College of Medicine, 1300 Morris Park Ave., Room U-521, Bronx, NY 10461. Tel.: 718-430-3320; Fax: 718-430-8975; E-mail: liang.zhu@einstein.yu.edu.

[2] The abbreviations used are: Cdk, cyclin-dependent kinase; GC, germinal center; SRBC, sheep red blood cell; KI, knockin; KO, knock-out; MEF, mouse embryonic fibroblast; FACS, fluorescence-activated cell sorting; PNA, peanut agglutinin; IHC, immunohistochemistry; IF, immunofluorescence.

accumulation of p27 protein when cells entered S phase to levels seen in G0 phase, demonstrating that ubiquitination of p27T187p by $SCF^{Skp2/Cks1}$ is responsible for p27 protein degradation in S-G2 phases of the cell cycle (11). The biological effects of p27T187A KI varied with cell types. In MEFs stimulated by serum refeeding, p27T187A KI reduced S phase cell fraction by 20%. When splenic CD4+ T cells were activated by anti-TCR (T cell receptor), S phase cell reduction reached 80% (11). We will discuss the latter result further below.

At organismal level, since cells in adult tissues are mostly in quiescence, no abnormal p27 protein accumulation was detected in various tissues in $p27^{T187A/T187A}$ mice (11). $p27^{T187A/T187A}$ mice provide a gain-of-protein stability tool to study the effects of p27 protein accumulation in S-G2 of proliferating cells in physiological settings. For examples, Malek *et al.* (11) reported that healing of circular skin punch wounds was delayed by about 2-fold in $p27^{T187A/T187A}$ mice compared with WT mice when sizes of wounds were measured at 4.5 days after wounding. Proliferation of dermal keratinocytes around the wounds was reduced by 2.5 fold as measured by BrdU labeling. However, $p27^{T187A/T187A}$ mice grew larger than WT mice by about 20% in body weight at 80 days of age. Thus, p27T187A mutation produced proliferation-inhibitory as well as proliferation-stimulatory phenotypes. Mechanisms underlying the large body size phenotype of $p27^{T187A/T187A}$ mice remains to be determined.

Later studies examined $p27^{T187A/T187A}$ mice in other physiological processes involving cell proliferation, such as liver regeneration after partial hepatectomy (12), atherosclerosis and atheroma formation in ApoE KO mice on fat feeding (13), lung tumorigenesis following spontaneous activation of endogenous *Kras* (14), and multi-organ tumorigenesis following administration of carcinogen ENU to 15-day-old mice (14). Interestingly, in none of these experimental systems was p27T187A KI found to alter the main pathological/physiological outcomes. Only the ratios of histopathologically diagnosed carcinomas over adenomas were reduced in intestines of ENU-treated $p27^{T187A/T187A}$ mice compared with WT mice at necropsy (14).

At the same time, inhibitors of the Skp2/Cks1-p27T187p interaction are being actively developed as therapeutics for cancer (15–17) with the rationale that inhibiting this interaction would specifically stabilize p27 protein without affecting other substrates of SCF^{Skp2}, thereby minimizing side effects. $p27^{T187A/T187A}$ mice could model inhibitor treatment to block Skp2/Cks1-p27T187p interaction. Altogether, it is highly desirable and timely to define the type of cancers and normal physiological processes affected in $p27^{T187A/T187A}$ mice.

In this study, we examined the role of p27T187A KI in two experimental models. In the first, we crossed $p27^{T187A/T187A}$ mice with $Rb1^{+/-}$ mice to determine the effects of p27T187A KI on pituitary tumorigenesis in $Rb1^{+/-}$ mice, which models two hit loss of *RB1* in humans and is fully penetrant. Next, we tested $p27^{T187A/T187A}$ mice for T cell-dependent immunization response, which depends on B cell clonal expansion, diversification, and affinity selection within the germinal centers (GCs, (18)) in secondary lymphoid organs such as the spleen. We will describe these two experimental models in more details in relevant Results sections below.

EXPERIMENTAL PROCEDURES

Mice—$p27^{T187A/T187A}$ mice were described previously (11). Wild type and $p27^{T187A/T187A}$ mice were on mixed FVB and C57BL6J background. Mice were maintained under pathogen-free conditions in the Albert Einstein College of Medicine animal facility, and genotyped as previously described (19). Mouse experiments protocols were reviewed and approved by Einstein Animal Care and Use Committee, conforming to accepted standards of humane animal care.

Sheep Red Blood Cells (SRBC) Immunization—10–12-week-old mice (young mice) and 15–20-month-old mice (older mice) were immunized with 2×10^8 SRBC (Remel, R54012) by intraperitoneal injection. Spleens and sera were collected on day 10 for analyses.

Isolation of Splenocytes—Pieces of spleens were minced and passed through 70 μm cell strainers using the rod of 1 ml syringe into a 6-well plate in PBS. The strainers were washed with 1–2 ml of PBS. Cells were collected into a 15 ml tube and centrifuged at 1300 rpm for 5 min. Cell pellets were resuspended with 3–5 ml of red blood cell lysis buffer (155 mM NH_4Cl, 12 mM $NaHCO_3$, and 0.1 mM EDTA) and incubated at room temperature for 5 min. Then 10 ml of PBS+10%FCS was added to stop lysis, and splenocytes were collected by centrifugation.

Flow Cytometry (FACS)—5×10^6 to 1×10^7 isolated splenocytes were stained with fluorochrome-labeled antibodies at 4 °C for 30 min followed by washing with PBS/1% BSA, using our previously published protocol (20). Five-color flow cytometry was performed using an LSR II instrument (BD Biosciences) and the data were analyzed using FlowJo software (Tree Star, Inc.). At least 10,000 gated events were analyzed per mouse. For germinal center B cell analysis, isolated splenocytes were stained with DAPI (Sigma, D9564), Alexa 700-anti-B220 (BioLegend, 103231), FITC-PNA (Vector Labs, FL-1071), and PE anti-CD95 (Fas) (eBioscience, 12–0951-81). For T cell and B cell ratios analyses and CD4 and CD8 T cell ratios analyses, isolated splenocytes were stained with PE-anti-CD3 (BioLegend, 100205), Alexa 700-anti-B220 (BioLegend, 103231), Alexa 488-anti-CD4 (BioLegend,100425), and Alexa 647-anti-CD8a (BioLegend, 100727). Splenocytes were also stained with single fluorochrome-labeled antibody and used for compensation analyses.

Serum Anti-SRBC IgG ELISA—96 well EIA/RIA plates (Corning Inc., 9018) were coated for 1 h at 37 °C with either 100 μg/ml of SRBC ghosts prepared from sheep red blood cells (Thermo Fisher Scientific, R54012) for detecting antibodies in sera or mouse anti-goat IgG (H+L) (Southern Biotech, 1031-01) was used as plate coat to generate standard curve. The coated wells were blocked with 100 μl/well of 2% BSA/TBS for 1 h at 37 °C. Sera from unimmunized or immunized mice were serially diluted into 96 well plates in triplicate, and incubated overnight at 4 °C. After washed four times with TBST and bang dried, 96-well plates were added with 50 μl/well of alkaline phosphatase-labeled secondary antibody, goat anti-mouse IgG-AP (Southern Biotech, 1030-04), for 1 h at 37 °C. Alkaline

phosphatase substrate (0.5 mg/ml PNPP (Sigma, S0942)) in diethenolamine buffer (Fisher Scientific, 50-255-870) was then added to each well, and the plates were incubated 1 h at 25 °C before absorbance at 405 nm was measured in an ELISA reader. Serial dilutions and standard curves were performed to calculate antibody concentrations using Excel. Log transformation of concentrations was performed to obtain linear correlation between OD value and $\log_{10}$[concentration]. Purified isotype controls for mouse IgG1, IgG2a, IgG2b, and IgG3 (Southern Biotech) served as standards. Column scatter plots were generated by GraphPad Prism 6 software.

GC Number and Size Measurement—Overlapping images of entire spleen cross sections were reconstructed using "photomerge" (Adobe Photoshop CS3). Areas of entire spleen cross sections were used to determine GC numbers per mm^2. Sizes of individual GCs and spleen cross sections were measured in Image J. Column scatter plot of GC size was generated by GraphPad Prism 6 software; bar graph of GC numbers by Excel.

Tissue Sections and Staining—Pituitary glands and spleens were fixed in 10% formalin (Fisher Scientific, SF 100-4), embedded in paraffin wax and sectioned. For immunohistochemistry (IHC) and immunofluorescence (IF) staining, slides were deparaffinized, hydrated, and incubated in a steamer for 20 min in sodium citrate buffer (Vector Labs, H3301) for antigen retrieval. The following antibodies were used: anti-p27 (Abcam, ab92741), anti-CD3 (Santa Cruz Biotechnology, SC-20047), anti-B220 (BD Pharmingen, 550286), Ki67 (Vector Labs, SP6), anti-phosphorylated-Histon H3 (Cell Signaling Technology, #9701L), FITC-PNA (Vector labs, FL-1071), and Biotinylated PNA (Vector Labs, B-1075). SuperPicture™ kit (Invitrogen, 879263) and DAB kit with or without addition of nickel (Vector Labs, SK-4100) was used to detect p27 and Ki67 signals. Biotinylated anti-mouse (Vector Labs, BA-2000) and anti-rat (Vector Labs, BA-4000) antibodies were used as secondary antibodies for IHC CD3 and B220 staining, respectively, which were followed by Vectastain ABC kit (Vector Labs, PK-4004), and Red substrate kit (Vector Labs, SK-5100) for further red signal development. Biotinylated PNA was detected by Red substrate kit (Vector Labs, SK-5100). IF detection of pHH3, B220, CD3, and p27 was done by TSA™PLUS Fluorescence Kit (NEL741001KT, PerkinElmer), and PNA was by FITC-conjugated horse-anti-mouse-IgG (Vector Labs, FI-2000). DNA was stained with DAPI (Sigma, D9564). TUNEL staining was performed with an Apoptosis Detection Kit (Millipore, S7100).

Statistical Analysis—Four groups (young mice and older mice, each separated into WT and p27T187A KI genotypes) of data from ELISA and GC B cell FACS (Figs. 2 and 3, respectively) were analyzed by two-way (ages and genotypes) ANOVA (GraphPad Prism 6 Software), followed by unpaired two-tailed Student's *t* test (GraphPad Prism 6 Software) for pairs of WT and p27T187A in each age groups and pairs of young and older mice for each genotypes. Two groups (older WT and older p27T187A KI) of data from GC numbers and sizes measurements and pHH3 positive cell frequency in GC, and ratios of T/B cells and CD4+/CD8+ T cells (Figs. 4 and 7, respectively) were analyzed by unpaired two-tailed Student's *t* test (GraphPad Prism 6 Software). $p < 0.05$ is considered statistically significant.

RESULTS

p27T187A KI Prevents $Rb1^{+/-}$ Mice from Developing Pituitary Tumors—Study of retinoblastomas led to the identification of the prototype tumor suppressor pRb. Typical retinoblastoma patients inherit one null allele of *RB1* from one parent and therefore are $RB1^{+/-}$, they develop retinoblastoma with full penetrance and the tumors invariably are $RB1^{-/-}$. These characteristics led to the two-hit hypothesis for tumorigenesis by inactivation of a tumor suppressor. pRb is highly conserved in mouse (*Rb1* in mouse) and $Rb1^{+/-}$ mice develop melanotroph tumors in pituitary IL with full penetrance and the tumors are invariably $Rb1^{-/-}$ (21). We used this physiological setting to test $p27^{T187A/T187A}$ mice in oncogenic proliferation.

As expected, all ($n = 5$) $Rb1^{+/-}$ mice contained pituitary IL tumors when examined at 6 months of age. In comparison, all $Rb1^{+/-}$;$p27^{T187A/T187A}$ mice ($n = 5$) contained microscopically normal pituitary glands at 9 months of age, indistinguishable from pituitaries in wild type and $p27^{T187A/T187A}$ mice (Fig. 1*A*).

When measured by p27 IHC, expression of p27 in IL is low in WT, *Skp2* KO, and *POMC-Cre;*$Rb1^{lox/lox}$ (which deletes *Rb1* in all melanotrophs in IL) mice. Only when *Skp2* and *Trp53* were co-deleted in IL did p27 protein levels rise to produce robust staining, since co-deletion of *Skp2* and *Trp53* reduced the cellular pool of p27 ubiquitin ligases including Skp2, Pirh2, and KPC1 (22). Fig. 1*B* shows that p27 IHC produced similarly low staining in WT and $p27^{T187A/T187A}$ IL; tumors in $Rb1^{+/-}$ IL showed higher nuclear density but individual nuclei showed similar staining intensity with those in areas of normal IL; and $Rb1^{+/-}$;$p27^{T187A/T187A}$ IL was not different from $p27^{T187A/T187A}$ IL. In the same experiment, the IL of *POMC-Cre;*$Rb1^{lox/lox}$;*Trp53*$^{lox/lox}$;$Skp2^{-/-}$ mice showed robust staining (Fig. 1*C*).

These results document that blocking phosphorylation of p27T187 and, by extension, preventing p27 ubiquitination by $SCF^{Skp2/Cks1}$ does not result in overt accumulation of p27 protein in pituitary IL in adult mice, but can prevent pituitary IL tumorigenesis by two hit loss of *Rb1*.

$p27^{T187A/T187A}$ Mice Develop Normal T Cell-dependent Antibody Response that Does Not Decline with Age—Immunization with T cell dependent antigens, such as SRBC, induces robust antibody response that is largely dependent upon the formation of GCs in secondary lymphoid tissues (humoral immunity). The GC reaction is characterized by dramatic clonal expansion of GC B cells and selection of affinity matured subclones into either plasma cell or memory B cell pools. These dynamic changes in the GC B cell population are orchestrated by CD4+ follicular helper T cells (Tfh) in GC (23, 24). The GC response provides a physiological setting of robust but non-oncogenic proliferation to study cell cycle regulation (20, 25). In addition, both the magnitude and functional output of GC reaction decline in old age, a phenomenon contributing to increased incidence of vaccine-preventable diseases in the elderly population (26). We hypothesized that $p27^{T187A/T187A}$ mice, especially in older age, wound show impaired T cell-dependent antibody response, and set out to test our hypothesis.

In unimmunized mice, serum anti-SRBC IgG levels were at base levels in all test groups (Fig. 2*A*). We immunized 12-week-old WT and $p27^{T187A/T187A}$ mice (10–12-week-old mice will be

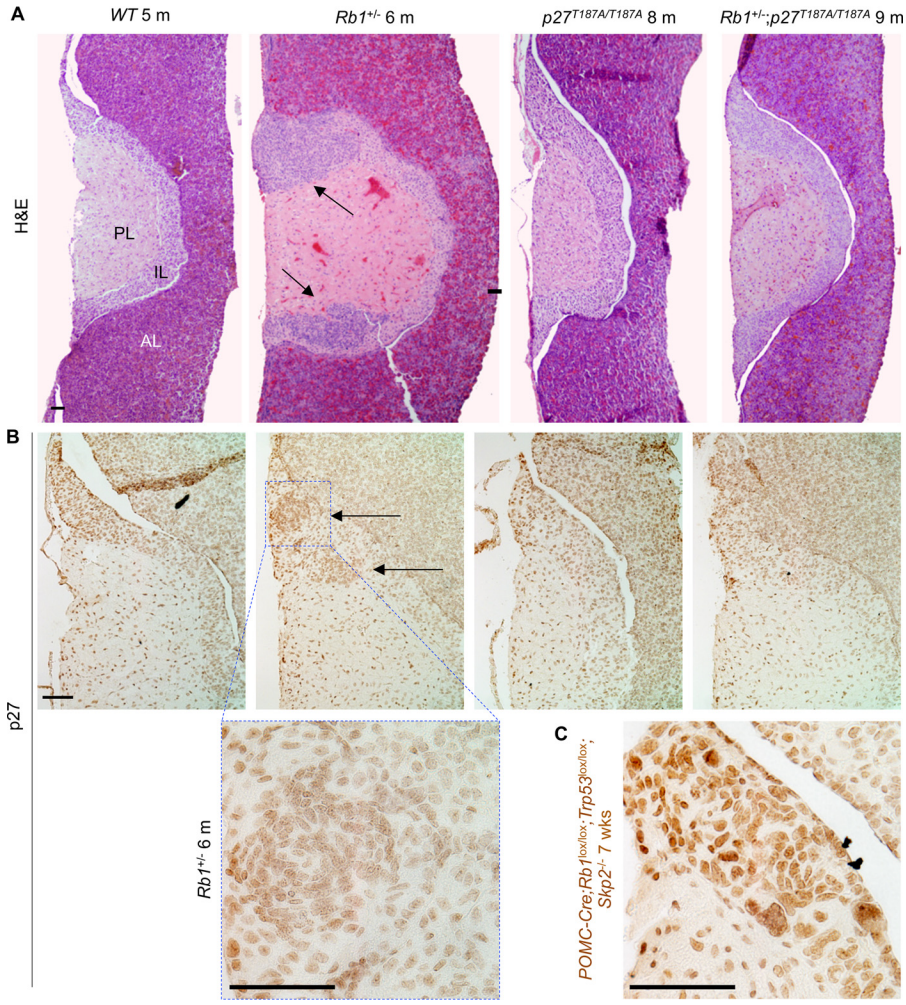

FIGURE 1. **Rb1$^{+/-}$;p27$^{T187A/T187A}$ mice do not develop pituitary tumors.** *A*, representative coronal sections of mouse pituitaries were stained with H&E. The three pituitary lobes are marked. *PL*, posterior lobe; *IL*, intermediate lobe; *AL*, anterior lobe. *Rb1*$^{+/-}$ mice at 6 months of age ($n = 5$) contained one to two IL tumors as marked by *black arrows*, while *Rb1*$^{+/-}$,*p27*$^{T187A/T187A}$ mice at 9 months of age ($n = 5$) contained pituitaries identical to those in WT and *p27*$^{T187A/T187A}$ mice. *B*, representative p27 IHC sections showing low level staining in WT, *Rb1*$^{+/-}$, *p27*$^{T187A/T187A}$, and *Rb1*$^{+/-}$;*p27*$^{T187A/T187A}$ IL, under the H&E images of the same genotypes. *C*, in the same experiment, *POMC-Cre;Rb1*$^{lox/lox}$;*Trp53*$^{lox/lox}$;*Skp2*$^{-/-}$ IL showed robust p27 staining. Scale bars, 100 μm.

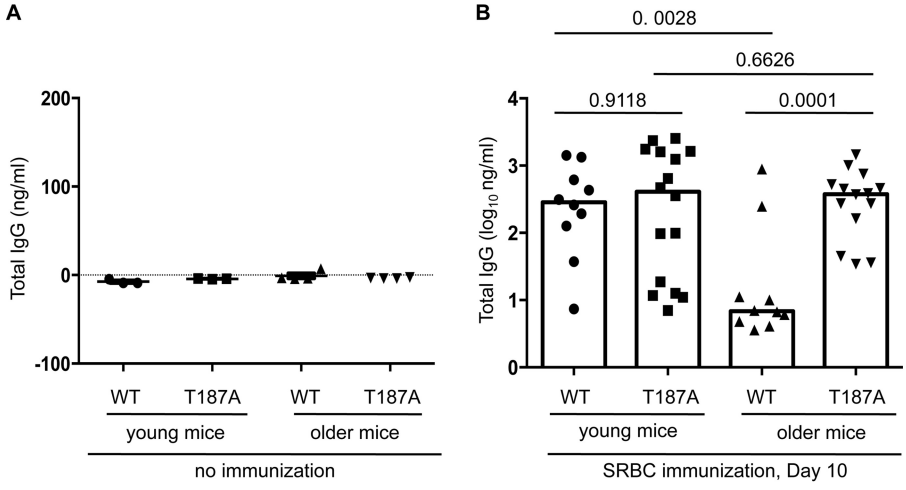

FIGURE 2. **Serum anti-SRBC IgG titers following SRBC immunization decline with age in WT but not *p27*$^{T187A/T187A}$ mice.** *A*, unimmunized WT or *p27*$^{T187A/T187A}$, young or older mice show similar base level serum anti-SRBC IgG titer. *B*, serum anti-SRBC IgG was measured 10 days after SRBC immunization. *WT* represents *p27*$^{+/+}$, *T187A* for *p27*$^{T187A/T187A}$. *young mice* were between 10 and 12 weeks old; *older mice* between 15 and 20 months old. Each data point represents one individual, and column heights show medians. Statistical analysis by two-way ANOVA with these four groups of data showed $p = 0.0129$ for differences between young and older, and $p = 0.0036$ for differences between WT and T187A. Unpaired two-tailed Student's *t* tests were used to determine *p* values between various pairs of samples as marked in the plot.

called "young mice") with SRBC and, on day 10, measured serum titers of anti-SRBC IgG. We found no significant differences between serum titers of anti-SRBC IgG in young WT and young $p27^{T187A/T187A}$ mice (Fig. 2*B*, *young mice*). Thus, p27T187A KI does not change the outcomes of SRBC immunization in young mice.

We went on to determine whether decline in humoral immunity would be greater in aging $p27^{T187A/T187A}$ mice than in aging WT mice. We found that anti-SRBC IgG titers reduced significantly in 15–20-month-old WT mice (15–20-month-old mice will be called "older mice") compared with young WT mice, but anti-SRBC titers in older $p27^{T187A/T187A}$ mice were not different from those in young $p27^{T187A/T187A}$ mice (Fig. 1*B*). As such, older $p27^{T187A/T187A}$ mice produced significantly higher titers of anti-SRBC IgG than older WT mice. Both two-way (ages and genotypes) ANOVA and Student's *t* test were performed for these analyses (see Fig. 2 legend). These findings proved opposite to our hypothesis, but phenotypically reveal that phosphorylation of p27T187 and, by extension, ubiquitination of p27 by $SCF^{Skp2/Cks1}$ promotes decline in humoral immunity in older mice.

Spleen GC Reactions Decline in Older WT, but Not Older $p27^{T187A/T187A}$, Mice—Antigen-specific antibody titers reflect the magnitude and quality of the GC response, in which naïve resting B cells convert to highly proliferating GC B cells. To determine the bases for the higher antibody titer in immunized older $p27^{T187A/T187A}$ mice, we determined how much B cell in total B cell population had converted to GC B cells at day 10 following SRBC immunization of four test groups of mice (as plotted in Fig. 3*D*). B cells are identified by B cell marker B220. GC B cells have additionally become positive for peanut agglutinin (PNA) affinity-staining and anti-Fas immune-staining. Spleen cell suspensions prepared on day 10 following SRBC injection were first gated on side and forward scatter to exclude aggregates and then for high B220 staining (for total B cells) and low DAPI staining (for total live B cells) (Fig. 3*A*). Within the total live B cell populations, GC B cell populations were identified as positive for both PNA and Fas. As shown in Fig. 3, *B* and *C*, and quantified in Fig. 3*D*, GC B cell populations ranged from 0.1% to 0.8% of the total B cell populations in non-immunized young and older, WT, and $p27^{T187A/T187A}$ mice. Following SRBC immunization GC B cell populations within total B cell populations increased in young WT and young $p27^{T187A/T187A}$ mice to 4.6% and 6.1%, respectively. With aging, GC B cell populations within total B cell populations declined in older WT mice (from 4.6% to 2.1%), but not in older $p27^{T187A/T187A}$ mice (from 6.1% to 6.3%). When older mice are compared, total B cell populations of older $p27^{T187A/T187A}$ mice contained significantly more GC B cells than older WT mice's total B cell populations. Both two-way (ages and genotypes) ANOVA and Student's *t* test were performed for the four groups of data (see Fig. 3*D* and its legend).

To directly visualize the GC structure, we stained spleen sections from immunized animals with PNA, and defined the PNA positive regions within the primary B cell follicles as GCs. p27T187A KI did not alter the spleen red pulp or white pulp morphology, nor did it cause spontaneous GCs in unimmunized animals of all age groups (not shown). After SRBC immunization, however, older $p27^{T187A/T187A}$ spleens developed many large GCs and often contained several GCs in each primary follicle compared with small to medium sized GCs each located within one follicle in the WT spleens (Fig. 4*A*). We quantified the GC density and size for individual spleen sections among the four experimental groups, and the results show that older $p27^{T187A/T187A}$ mice contained more numerous and larger GCs than older WT mice (Fig. 4, *B* and *C*). These results support the findings by FACS that GC B cell population sizes were larger in older $p27^{T187A/T187A}$ mice than in older WT mice (Fig. 3). A more robust GC reaction in older $p27^{T187A/T187A}$ mice could explain their improved anti-SRBC IgG titers relative to their WT counterparts.

We next examined the proliferation status of GC B cells using immune-staining for Ki67. Ki67 staining appeared similarly intense between older WT and young WT mice and between older WT and older $p27^{T187A/T187A}$ mice (Fig. 4*D* and data not shown). Although GCs in older WT mice are smaller than GCs in older $p27^{T187A/T187A}$ mice, nearly all PNA positive cells stained positive for Ki67 in both types of older mice (Fig. 4*D*). When GC B cells were stained with the mitotic marker phosphorylated histone H3 (pHH3), we found more pHH3 positive cells in GCs in older $p27^{T187A/T187A}$ mice than in older WT mice (Fig. 4, *E* and *F*), suggesting that more cell division could explain the larger GC B cell population sizes in older $p27^{T187A/T187A}$ mice. However, the increases did not reach statistical significance (Fig. 4*F*). TUNEL staining was similarly intense in older WT mice, young WT mice, and older $p27^{T187A/T187A}$ mice (data not shown). Thus, both the decline in older WT mice and the maintenance in older $p27^{T187A/T187A}$ mice of GC B cell population sizes were not correlated with dramatic decreases (in the decline in older WT mice) or increases (in the maintenance in older $p27^{T187A/T187A}$ mice) in Ki67 or pHH3 labeling of GC B cells.

In aggregate, by showing more robust production of GC B cells in older $p27^{T187A/T187A}$ mice than in older WT mice, results in this section explained improved serum titers of anti-SRBC IgG in older $p27^{T187A/T187A}$ mice. These findings however do not explain how p27T187A KI induced more robust GC B cell production.

p27 Expression Decreases When Naïve B Cells Are Recruited into GC in Both Older WT and Older $p27^{T187A/T187A}$ Mice—We next compared p27 expression in the spleens of older WT and older $p27^{T187A/T187A}$ mice at day 10 following SRBC injection, when the GC reactions were more robust in older $p27^{T187A/T187A}$ mice than in older WT mice.

In post-immunization spleens from both older WT and older $p27^{T187A/T187A}$ mice, the B220+ B cell area and CD3+ T cell zone occupy discrete areas in the white pulp (Fig. 5, *A*, *a*,*e* and *B*, *a*,*e*). The PNA+B220weak GCs were embraced by the PNA-B220+ primary B cell follicles from one side (Fig. 5*A*, *a*–*h*) with its other side likely facing the more discrete T cell zone (27, 28) (Fig. 5*B*, *a*–*h*).

Interestingly, the pattern of p27 staining is much broader than either the B220- or CD3-marked areas alone, suggesting that p27 is expressed in the majority of B and T cells outside of the GCs (also see below), and similar in older WT and older $p27^{T187A/T187A}$ spleen sections, suggesting that T187A KI did

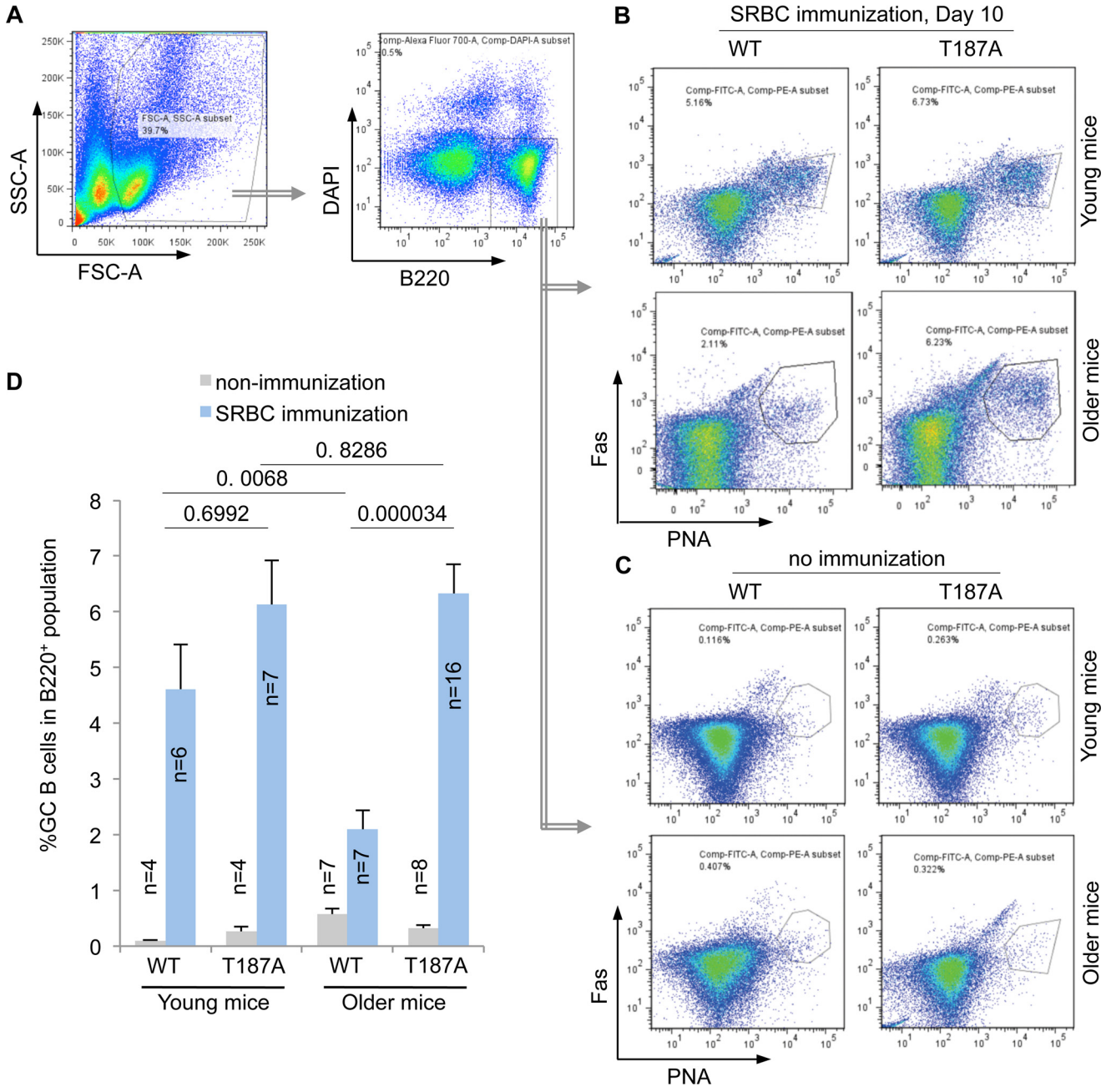

FIGURE 3. **Production of spleen GC B cells following SRBC immunization decline with age in WT but not *p27*$^{T187A/T187A}$ mice.** *A*, FACS of total spleen cell suspension, showing the first FSC-SSC gate, followed by the B220 and DAPI gate. DAPI^{low},B220^{high} cells then underwent FACS on PNA and Fas to determine population sizes of GC B cells (PNA^{high} and Fas^{high}) in total B cell population at day 10 following SRBC immunization (*B*) or from unimmunized mice (*C*). Quantifications of *B* and *C* are shown in *D*. Error bars represent S.E. Two-way ANOVA with these four groups of data from immunized mice showed $p = 0.0850$ for differences between young and older, and $p = 0.0001$ for differences between WT and T187A. Unpaired two-tailed Student's *t* tests were used to determine *p* values between various sample pairs as shown in *D*.

not induce notable p27 accumulation in *p27*$^{T187A/T187A}$ spleens (Fig. 5*C*, *a* and *e*). Notable however are round punctuates where p27 staining was dramatically reduced (*black arrows* in Fig. 5*C*, *a* and *e*) inside the broad and otherwise evenly stained p27+ areas in both WT and *p27*$^{T187A/T187A}$ spleens. Double immunofluorescence (IF) staining with PNA and anti-p27 demonstrate that the p27 low areas are populated by PNA+ GC B cells (*white arrows* in Fig. 5, *c*,*d* and *g*,*h*). High magnification images confirmed that the vast majority of PNA+ GC B cells are p27 negative irrespective of the p27 genotype (Fig. 6*A*). Thus, in the B cell lineage, p27 protein levels were dramatically down regulated when the naïve resting B cells (which populate the more intensely stained B220+ area) are recruited into the highly proliferative GCs regardless of the *p27*$^{T187A/T187A}$ mutation status.

Since GC B cells were actively proliferating in both older WT and older *p27*$^{T187A/T187A}$ mice (Fig. 4, *D* and *E*), the dramatic down-regulation of p27 in GC correlated with highly active proliferation of GC B cells. To identify mechanisms for this down-regulation in GC B cells, we determined whether p27 mRNA levels were down regulated in GC B cells. For this purpose, we searched NCBI databases for gene expression profile datasets that compared naïve resting B cells with GC B cells. We

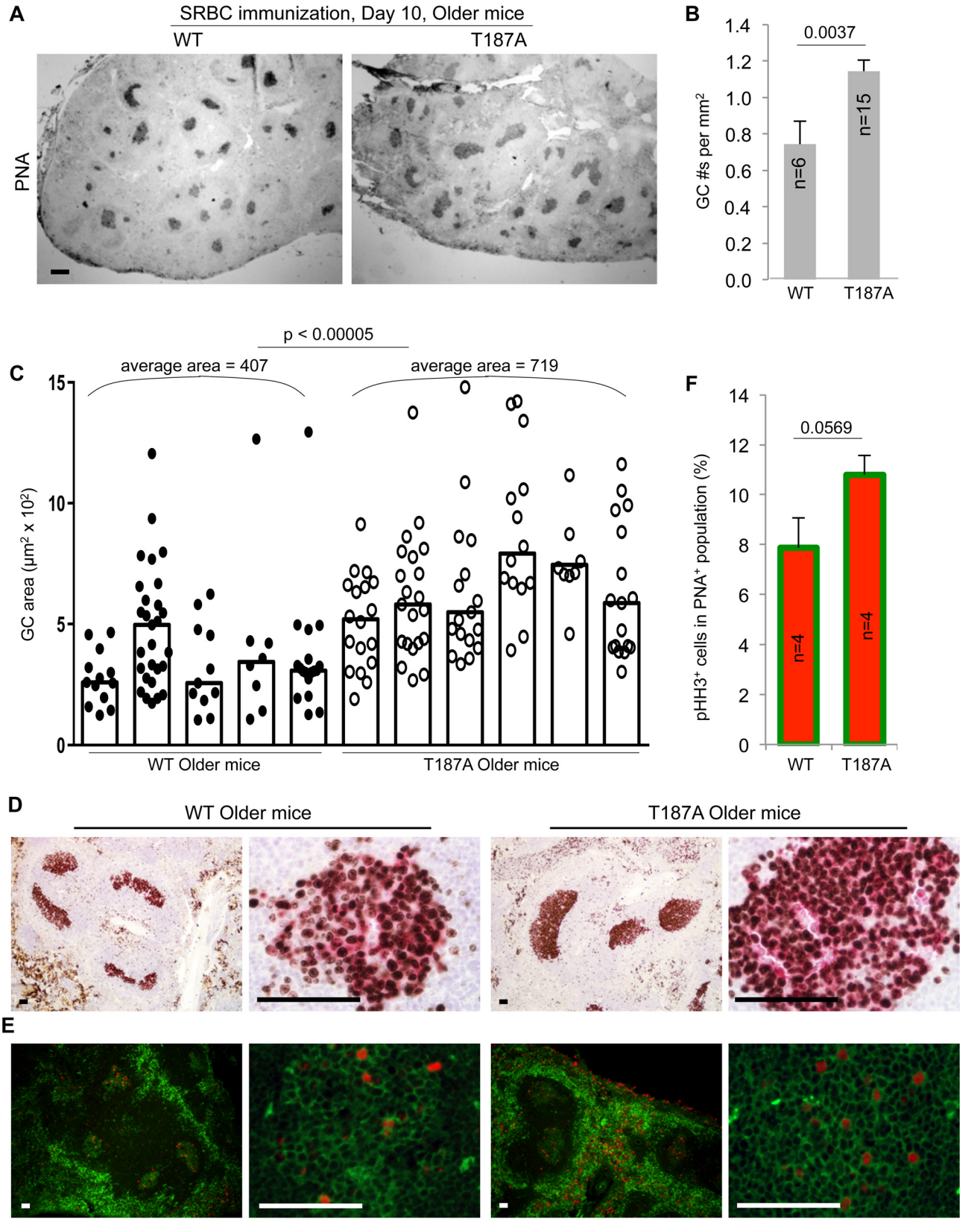

FIGURE 4. **Spleen GC numbers and sizes are higher and larger in older *p27*$^{T187A/T187A}$ mice than in older WT mice at 10 days following SRBC immunization.** *A*, representative images of spleen sections stained with PNA to visualize GC. Scale bars, 200 μm. *B*, quantifications of GC numbers on spleen sections, error bars are S.E. *C*, quantifications of GC sizes. Each column represents one individual, and each point is an individual GC. Column heights represent medians. Co-staining of Ki67 (*black*) and PNA (*red*) (*D*), and pHH3 (*red*) and PNA (*green*) (*E*), of GC were performed on spleen sections as marked. Scale bars, 50 μm. *F*, quantification of data in *E*. *p* values are from two-tailed Student's *t* tests.

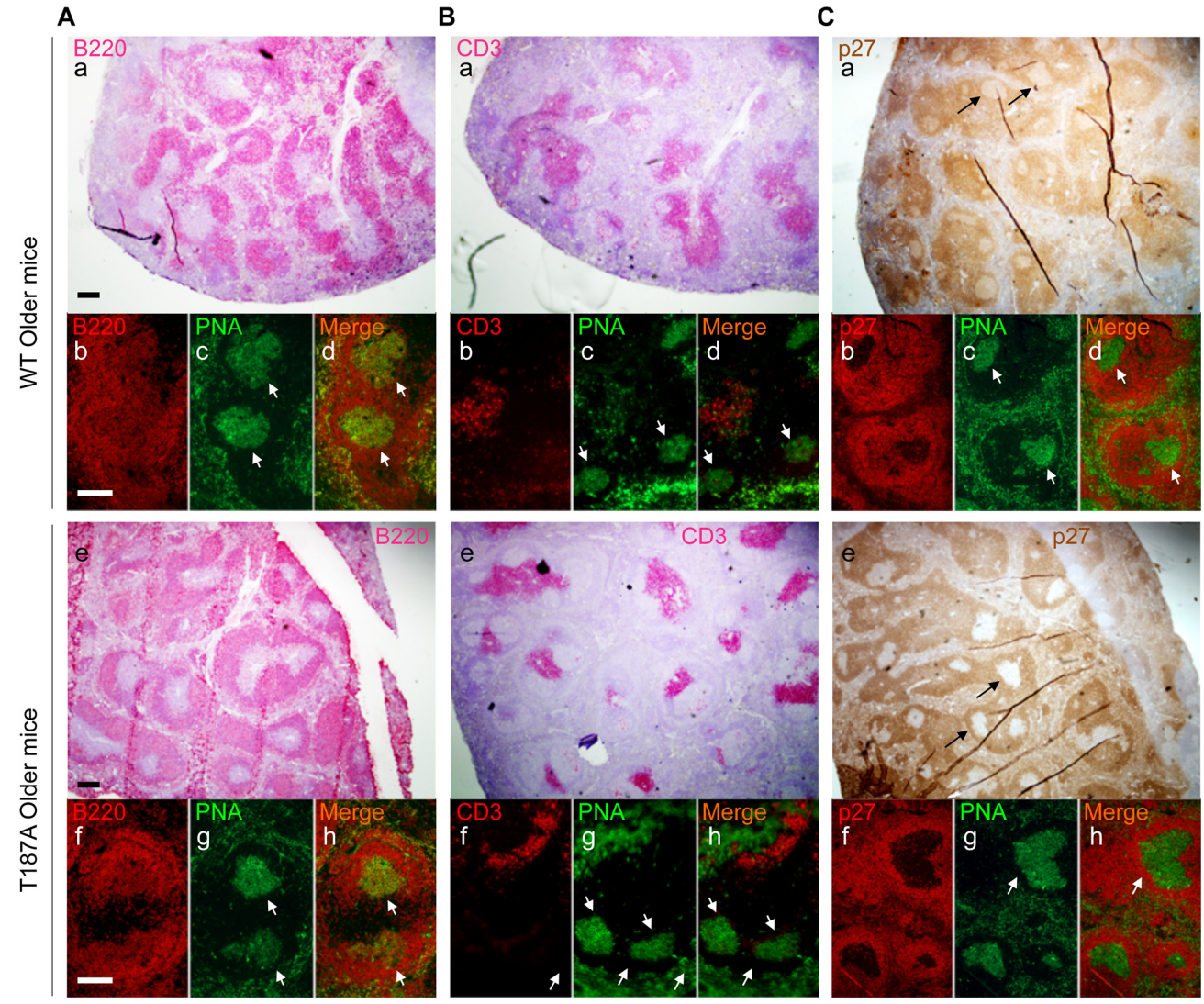
A
B
C
WT Older mice
T187A Older mice
B220
CD3
p27
PNA
Merge
a
b
c
d
e
f
g
h

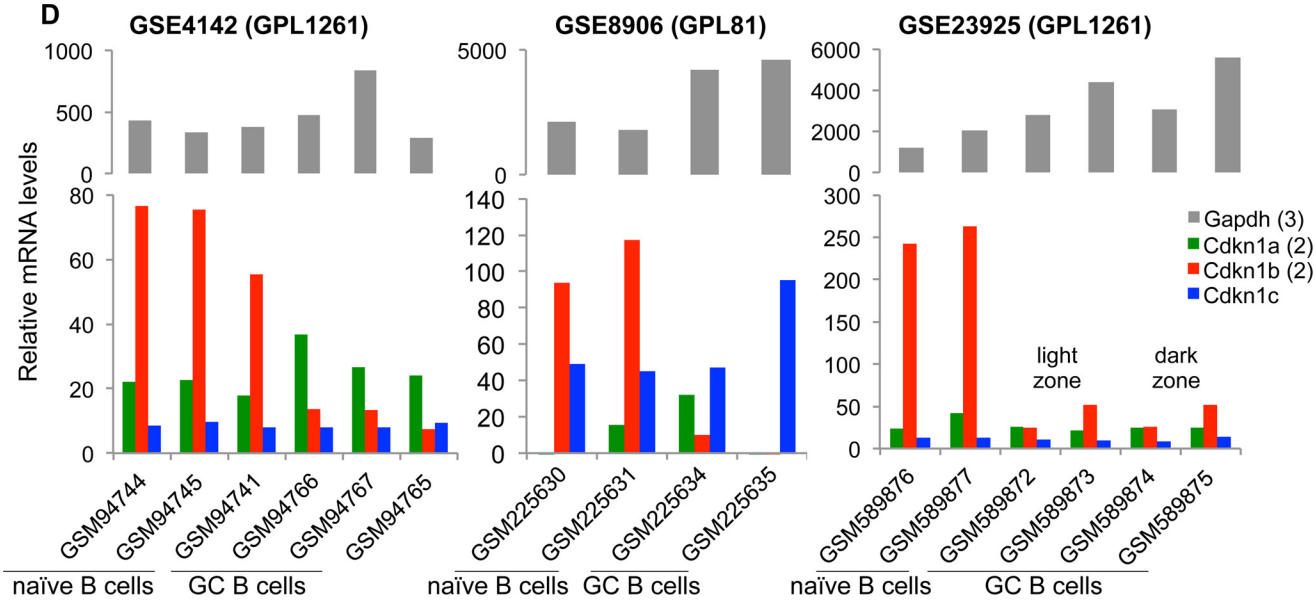
D
GSE4142 (GPL1261)
GSE8906 (GPL81)
GSE23925 (GPL1261)
Relative mRNA levels
Gapdh (3)
Cdkn1a (2)
Cdkn1b (2)
Cdkn1c
light zone
dark zone
GSM94744
GSM94745
GSM94741
GSM94766
GSM94767
GSM94765
GSM225630
GSM225631
GSM225634
GSM225635
GSM589876
GSM589877
GSM589872
GSM589873
GSM589874
GSM589875
naïve B cells
GC B cells

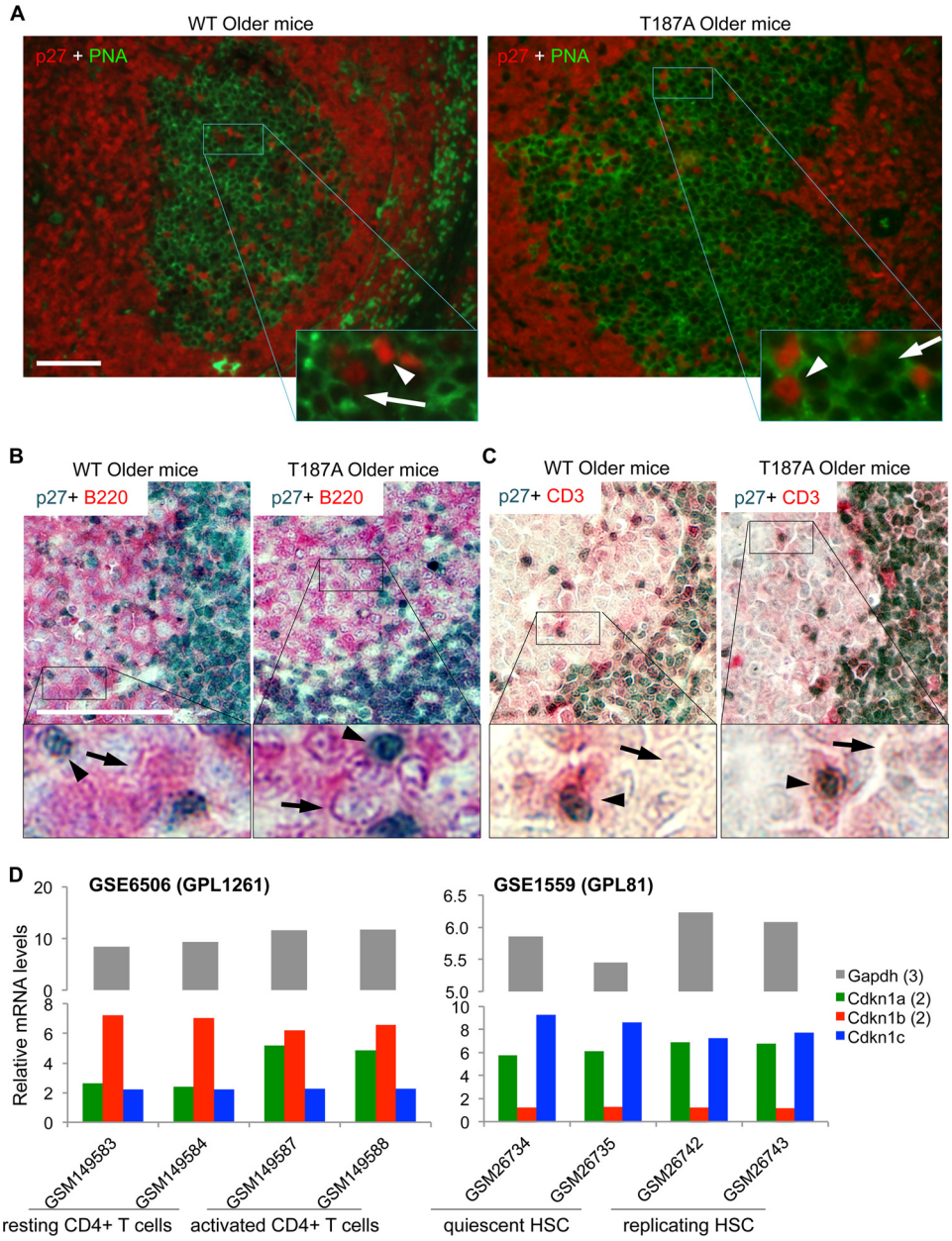

FIGURE 6. **p27 expression is dramatically reduced in GC B cells but maintained in GC T cells in older WT and older *p27*$^{T187A/T187A}$ mice at 10 days following SRBC immunization.** *A*, high magnification and red-green channel merge images of co-IF for p27 and PNA, as indicated, of representative GC, as marked. In enlarged areas, *white arrows* point to cells with membrane staining by PNA but negative for p27, while *white arrowheads* point to cells with positive staining for p27 without membrane PNA staining. *B*, two-color co-IHC for p27 (*dark blue*) and B cell marker B220 (*pink*), as marked, showing approximately one-quarter of a GC. *Black arrows* point to cells with positive membrane staining for B220 but negative for p27, while *black arrowheads* point to cells with positive p27 staining but negative for B220 membrane staining. *C*, same experiments as in *B*, except B220 antibody was replaced with CD3 antibody. *D*, in NCBI GEO database, gene expression profiles for naïve and activated CD4+ T cells (GSE6506) and quiescent and replicating HSC (GSE1559) were queried for expression of p21 (Cdkn1a, average of 2 probe sets), p27 (Cdkn1b, average of 2 probe sets), and p57 (Cdkn1c), as well as a housekeeping gene Gapdh (average of 3 probe sets). Sample records (GSMxxx) and experimental platforms (GPLxxx) are shown. Data in both datasets were normalized by GC-RMA, and two biological replicates were analyzed.

found three such datasets and queried them for expression of the three p27 family members including p21 (Cdkn1a), p27 (Cdkn1b), and p57 (Cdkn1c) together with a housekeeping gene *Gapdh*. As shown in Fig. 5*D*, p27 mRNA levels were reduced by 5.5 to 10.5-fold in GSE4142, 117 to 9.5-fold in GSE8906, or 4.7 to 10.6-fold in GSE23925 when naïve B cells

FIGURE 5. **p27 expression is reduced in GC in both older WT and older *p27*$^{T187A/T187A}$ mice.** Spleen samples were collected 10 days following SRBC immunization, and stained by IHC with anti-B220 (*A, a* and *e*), anti-CD3 (*B, a* and *e*), or anti-p27 (*C, a* and *e*). Co-IF was then performed with PNA and each of these three antibodies to identify areas of GC, pointed by *white arrows*, in stains by each of these three antibodies (*b,c,d* and *f,g,h panels*). Scale bars, 200 μm. *D*, three gene expression profile databases (NCBI GEO accession numbers, GSExxx, are as marked) were queried for expression of p27 family members p21 (Cdkn1a, average of 2 probe sets), p27 (Cdkn1b, average of 2 probe sets), and p57 (Cdkn1c), as well as a housekeeping gene Gapdh (average of 3 probe sets). Sample records (GSMxxx) obtained from purified naïve B cells and GC B cells are as marked. Accession numbers GPLxxx contain information on experimental platforms (Affymatrix microarrays). Data in GSE4142 were RMA (Robust Multi-array Average) normalized unlogged, and GSE23925 was normalized by RMA. GSE8906 contained raw data. Two to three biological replicates were analyzed.

were compared with GC B cells. In the same samples, p21 and p57, as well as Gapdh, mRNA levels showed no such reduction patterns.

These findings suggest the activation of a robust mechanism that inhibited p27 mRNA expression when naïve B cells are stimulated to enter GC to proliferate. The dramatic p27 mRNA down-regulation might have overridden any reduction in p27 protein degradation caused by p27T187A KI, resulting in dramatic p27 protein level reductions in GC B cells in both WT and $p27^{T187A/T187A}$ mice, as shown in Fig. 5*C*. With this line of reasoning, we conclude that the enhanced GC reaction in older T187A mice is not caused by p27T187A KI cell-autonomously in GC B cells.

GC T Cells Maintain p27 Protein Levels—Because GC B cells dramatically down-regulate both p27 mRNA and protein expression, any effects of the p27T187A KI on p27 protein degradation might be inconsequential in GC B cells. We reasoned that cells in GC that maintain p27 protein levels are more likely to be affected by p27T187A KI. Although B cells outnumber T cells within GC, the CD4+ helper T cells in GC play a critical role in all aspects of the GC response including its initiation, expansion, and termination (24). As such, we next focused our p27 protein expression study on GC T cells. High magnification images of p27 and PNA co-IF indeed revealed a number of p27-positive cells in GC (Fig. 6*A*), with the vast majority of the p27-positive cells stained negative for PNA (*white arrowheads*), indicating that they are not B cells.

To determine the lineage status of the p27 expressing cells in GC, we concurrently stained p27 with either B220 or CD3 in double IHC. Consistent with co-IF for p27 and PNA in Fig. 6*A*, p27 positive cells in GC are negative for B220 in co-IHC (Fig. 6*B*, *black arrowheads*), while most cells in GC show positive B220 membrane staining with negative p27 staining (*black arrows*). In contrast, p27 positive cells in GC are positive for CD3 in co-IHC while most cells in GC are negative for both p27 and CD3 (Fig. 6*C*, *black arrowheads* and *black arrows*, respectively). These findings demonstrate that, while GC B cells dramatically down regulate p27 protein expression, GC T cells maintain p27 protein expression. Based on the IHC technique, we could not demonstrate any difference in p27 protein levels between the WT and $p27^{T187A/T187A}$ GC T cells.

Rapid proliferation of GC B cells leading to the generation of GC in response to immunization by T cell dependent antigen is completely dependent on CD4+ T helper cells (29). Inhibition of T cell proliferation by transgenic expression of p27 in T cells (from the mouse *Lck* promoter) blocked spleen GC reactions (30). Decline in CD4+ T cell population with aging has been suggested as a cause for the decline in GC response to T cell-dependent antigen immunization in older WT mice (31, 32). And it is known that proliferation of splenic CD4+ T helper cells in response to stimulation by anti-TCR was significantly (80%) reduced by p27T187A KI (11).

Combining these previous knowledge with our current findings that GC B cells do not express p27 mRNA and protein but GC T cells maintain p27 protein expression led us to hypothesize that CD4+ T cells in young $p27^{T187A/T187A}$ mice might be more difficult to activate and therefore have undergone less accumulative proliferation to have conserved a larger proliferative reservoir to maintain robust GC responses in older $p27^{T187A/T187A}$ mice. This principle is well known in stem cell studies (33, 34). In adult mice, hematopoietic stem cells (HSCs) remain proliferative quiescence until stimulated to proliferate to replenish the lost cell population. In resemblance, naïve CD4+ T cells are resting until activated by antigen binding to TCR to expand and migrate to GC to play essential roles in establishing humoral immunity (35, 36). In fact, it was shown in 2007 that CD4+ T cell activation and HSC activation shared both up-regulated and down-regulated gene expression programs (37). To determine whether regulation of p27 mRNA expression is also similar between CD4+ T cell activation and HSC activation, we queried NCBI GEO databases as shown in Fig. 6*D*. In GSE6506 (37) mouse splenic CD4+ T cells were activated by Concanavalin A and, in GSE1559 (38), mouse HSCs were activated by administering 5-fluorouracil. We found that p27 mRNA levels were not reduced when naïve CD4+ T cells were activated, consistent with the presence of p27 positive T cells in GC (Fig. 6*C*). Interestingly, p27 mRNA levels were also not reduced when HSCs were activated to replicate. These findings add a further relatedness between the activation programs in naïve CD4+ T cells and adult HSCs. Lack of p27 mRNA down-regulation could provide an opportunity for p27 down-regulation by p27 protein degradation.

Spleen CD4+/CD8+ T Cell Ratios following SRBC Immunization Is Higher in Older $p27^{T187A/T187A}$ Mice than in Older WT Mice—Altered cell proliferation control may lead to changes in clonal expansion, differentiation, and cell death. As an indirect measurement of the impact of p27 T187A KI on lymphocyte population maintenance, we assessed the population size of total T and B cells (as T/B cell ratios), and CD4+ and CD8+ T cell subsets (as CD4+/CD8+ T cell ratios) in older mice. As shown in Fig. 7*A*, the T/B cell ratios were comparable between WT and $p27^{T187A/T187A}$ mice. Interestingly, the ratio of CD4+ helper T cells over CD8+ killer T was significantly higher in older $p27^{T187A/T187A}$ mice compared with older WT mice (Fig. 7*B*). This finding suggests that a more difficult-to-activate CD4+ T cell population in $p27^{T187A/T187A}$ mice (11) might have better maintained its population size in older age, and could explain how older $p27^{T187A/T187A}$ mice responded more robustly than older WT mice to SRBC immunization. To strengthen this finding, we further determined the CD4+/CD8+ T cell ratios inside CD3+ gate, and obtained similar results (Fig. 7*C*). We conclude that older $p27^{T187A/T187A}$ mice contained larger populations of CD4+ T cells during SRBC immunization, which, at least in part, enhanced GC B cell reaction.

DISCUSSION

Modeling Effects of Skp2/Cks1-p27T187p Interaction Inhibitors—Roles of p27 in proliferation related physiology have been well studied with loss-of-function approaches using p27 KO mice and p27 ck- mice. Since increasing p27 is an actively developing cancer therapy strategy, studying effects of p27 gain-of-function in proliferation related physiology would more directly facilitate cancer therapy development. In this regard, $p27^{T187A/T187A}$ mice are especially important since they model actions of an actively developing type of inhibitors that block p27T187p interaction with Skp2/Cks1 (see Introduction). Fur-

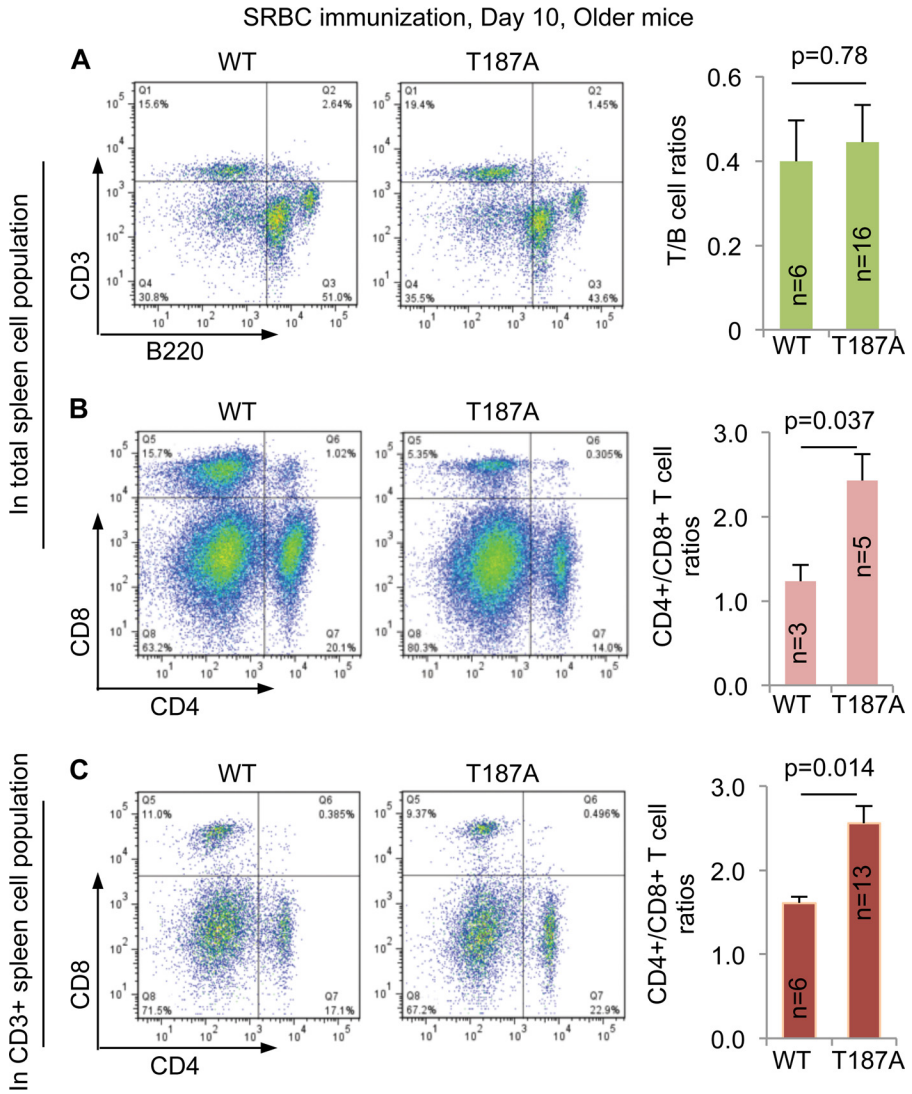

FIGURE 7. **CD4+/CD8+ T cell ratios are higher in older $p27^{T187A/T187A}$ mice than in older WT mice at 10 days following SRBC immunization.** *A*, representative FACS profiles of spleen cell suspensions following CD3 and B220 double staining and quantifications. *B*, FACS profiles following CD4 and CD8 double staining of total spleen cell suspension and quantifications. *C*, FACS profiles following CD4 and CD8 double staining of CD3+ cells in spleen cell suspension and quantifications. *p* values are from two-tailed Student's *t* tests, and error bars represent S.E.

ther, $p27^{T187A/T187A}$ mice do not accumulate p27 protein in quiescent tissues and their lack of overt defects already demonstrated that inhibitors of p27T187p interaction with Skp2/Cks1 should be harmless to normal physiology. Remarkably, since its generation and first characterization in 2001 (11), studies of $p27^{T187A/T187A}$ mice have revealed few physiological phenotypes including tumorigenesis (see Introduction). Our study now reveal that fully penetrant pituitary tumorigenesis in $Rb1^{+/-}$ mice is fully blocked in $Rb1^{+/-}$;$p27^{T187A/T187A}$ mice, identifying $Rb1^{+/-}$ mice as the preclinical tumor model against which inhibitors of p27T187p interaction with Skp2/Cks1 can be definitively compared.

p27T187A KI models the most potent inhibitors of p27T187p-Skp2/Cks1 interaction and, therefore, can be an impossible match for inhibitor candidates. On the other hand, inhibitors of p27T187p-Skp2/Cks1 interaction may also block interaction of Skp2-Cks1 to p27 family members p21 and any unknown substrates of $SCF^{Skp2/Cks1}$, potentially inhibiting pituitary tumorigenesis in $Rb1^{+/-}$ mice through mechanisms other than stabilizing p27. More sophisticated preclinical mouse tumor models may be desired to improve on these aspects of inhibitor testing using $Rb1^{+/-}$ mice.

Mechanisms of Tumor Blocking in $Rb1^{+/-}$;$p27^{T187A/T187A}$ Mice—In our previous studies, we induced mouse pituitary IL tumors by artificial deletion of *Rb1* in all melanotrophs and POMC-Cre;$Rb1^{lox/lox}$ mice developed pituitary tumors across the entire IL. POMC-Cre;$Rb1^{lox/lox}$;$p27^{T187A/T187A}$ mice produced greatly thinned pituitary IL with apoptosis (19). In this artificial setting, p27T187A KI resulted in synthetic lethality with *Rb1* deletion by further activating E2F1 (39). Our current finding documents a tumor suppressive role of p27T187A KI in a physiological "two hit" setting. Whether this block was achieved by promoting apoptosis or inhibiting proliferation is difficult to determine in the "two hit" setting. It is however likely that the observed blocking to pituitary tumorigenesis by two hit *Rb1* loss does not require significant accumulation of p27, since p27 IHC showed similarly low levels of p27 in WT, $p27^{T187A/T187A}$, and $Rb1^{+/-}$;$p27^{T187A/T187A}$ IL (Fig. 1*B*).

It is notable that, p27T187A KI showed little antitumor effects in lung tumorigenesis by oncogenic activation of endogenous *Kras* (14), another tumor model in a physiological setting. Since p27 mRNA levels were significantly reduced in this lung tumor model (14), the lack of an antitumor phenotype demonstrates that the inhibitory effects of p27T187A KI on p27 protein degradation might only be relevant when p27 protein levels were reduced primarily by enhanced protein degradation. Differences in oncogenic mechanisms by two hit loss of *Rb1* in melanotrophs and by activation of endogenous *Kras* in lung may also determine whether p27T187A KI is effective. Now that the "positive control" is available (that $Rb1^{+/-}$; $p27^{T187A/T187A}$ mice do not develop pituitary tumors), testing antitumor effects of p27T187A KI in other physiological mouse tumor models will be more informative.

How Does p27T187A KI Maintain Robust Antibody Response to SRBC Immunization?—While blocking pituitary tumorigenesis by "two hit" loss of *Rb1* identifies a sought-after role for an anticipated effect, enhancing GC B cell expansion leading to improved antigen specific humoral immunity in older mice is opposite to our anticipation. This unexpected finding has the potential to address another important medical issue: improve vaccination efficacy in the elderly. Vaccination efficacy depends on long lived plasma cells and memory B cells, both of them produced by the GC reaction following immunization. Both B and T cell repertoires experience age-associated impairment in mice and humans. In co-transfer experiments testing different combination of old and young B and T cells, it was observed that the age-related GC impairment mainly engrafts with old T cells instead of old B cells (32, 40). More recent studies have revealed multiple, age-associated molecular changes in the follicular T helper cell lineage (Tfh cells, which are CD4+ T cells in GC) (26). Our findings have now implicated the regulation of p27 protein stability in these aspects.

We suggest that ubiquitination of p27T187p by $SCF^{Skp2/Cks1}$ in CD4+ T cells may have set a threshold for their activation at a level that could lead these cells to proliferate in young age to the extent that compromises their proliferation in older age. Indeed, there were more GCs in a given area of the spleen section in older $p27^{T187A/T187A}$ mice than older WT mice (Fig. 4*B*), suggesting increased availability of cognitive T cells to SRBC-reactive B cells to initiate the GC response in the mutant mice. In other words, the efficiency of T cell priming, which is normally reduced with aging (26, 29), was maintained by the expression of the p27T187A protein. In humans, reduced antibody response to vaccination correlates with reduced frequency of naïve T cells (41). Thus, it is possible that a stabilized p27 protein and the consequent reduced cell cycle activity upon antigen stimulation (11) preserved more proliferation potential of the naïve CD4+ T cell pool, while this pool is diminished with aging in WT mice. This notion is supported by our observation that older $p27^{T187A/T187A}$ mice had a higher CD4+/CD8+ T cell ratio relative to older WT mice (Fig. 7).

The second aspect of the observed enhanced GC phenotype is that individual GCs formed in older $p27^{T187A/T187A}$ mice was 77% larger on average than those in older WT mice (Fig. 4*C*), indicating that more mitogenic signals were provided by Tfh in GC to the GC B cells, which is another aspect of T cell function known to deteriorate with aging (26, 29). While detailed molecular mechanisms linking a stabilized p27 protein to enhanced B cell help function of GC T cells await future studies, it is worth noting that a recent study has correlated reduced proliferation of Tfh cells to their enhanced B cell help function (42).

In summary, our study have provided evidence that targeting p27T187 phosphorylation-dependent ubiquitination by $SCF^{Skp2/Cks1}$ could be very effective against specific types of cancer (43) and have suggested strategies to better understand, and potentially leading to methods to prevent, the decline of humoral immunity in the elderly (26).

Acknowledgments—We thank Dr. James Roberts for providing the p27T187A KI mice, Hong Zhang and Drs. Yong Chen and Giorgio Cattoretti for valuable suggestions in spleen IF and IHC, and Dr. Herbert Morse III for assistance with histopathological evaluation of the spleen sections. Albert Einstein Comprehensive Cancer Research Center (5P30CA13330) and Liver Research Center (5P30DK061153) provided core facility support.

REFERENCES

1. Nakayama, K., Ishida, N., Shirane, M., Inomata, A., Inoue, T., Shishido, N., Horii, I., Loh, D. Y., and Nakayama, K.-i. (1996) Mice lacking p27Kip1 display increased body size, multiple organ hyperplasia, retinal dysplasia, and pituitary tumors. *Cell* **85,** 707–720
2. Fero, M. L., Rivkin, M., Tasch, M., Porter, P., Carow, C. E., Firpo, E., Polyak, K., Tsai, L.-H., Broudy, V., Perlmutter, R. M., Kaushansky, K., and Roberts, J. M. (1996) A syndrome of multiorgan hyperplasia with features of gigantism, tumorigenesis, and female sterility in p27Kip1-deficient mice. *Cell* **85,** 733–744
3. Kiyokawa, H., Kineman, R. D., Manova-Todorova, K., Soares, V. C., Hoffman, E. S., Ono, M., Khanam, D., Hayday, A. C., Frohman, L. A., and Koff, A. (1996) Enhanced growth of mice lacking the cyclin-dependent kinase inhibitor function of p27Kip1. *Cell* **85,** 721–732
4. Besson, A., Gurian-West, M., Chen, X., Kelly-Spratt, K. S., Kemp, C. J., and Roberts, J. M. (2006) A pathway in quiescent cells that controls p27Kip1 stability, subcellular localization, and tumor suppression. *Genes Dev.* **20,** 47–64
5. Bassermann, F., Eichner, R., and Pagano, M. (2014) The ubiquitin proteasome system - implications for cell cycle control and the targeted treatment of cancer. *Biochim. Biophys. Acta* **1843,** 150–162
6. Vlach, J., Hennecke, S., and Amati, B. (1997) Phosphorylation-dependent degradation of the cyclin-dependent kinase inhibitor p27. *EMBO J.* **16,** 5334–5344
7. Montagnoli, A., Fiore, F., Eytan, E., Carrano, A. C., Draetta, G. F., Hershko, A., and Pagano, M. (1999) Ubiquitination of p27 is regulated by Cdk-dependent phosphorylation and trimeric complex formation. *Genes Dev.* **13,** 1181–1189
8. Ganoth, D., Bornstein, G., Ko, T. K., Larsen, B., Tyers, M., Pagano, M., and Hershko, A. (2001) The cell-cycle regulatory protein Cks1 is required for SCF(Skp2)-mediated ubiquitinylation of p27. *Nat. Cell Biol.* **3,** 321–324
9. Spruck, C., Strohmaier, H., Watson, M., Smith, A. P. L., Ryan, A., Krek, W., and Reed, S. I. (2001) A CDK-independent function of mammalian Cks1: targeting of SCF^{Skp2} to the CDK inhibitor $p27^{Kip1}$. *Mol. Cell* **7,** 639–650
10. Hao, B., Zheng, N., Schulman, B. A., Wu, G., Miller, J. J., Pagano, M., and Pavletich, N. P. (2005) Structural basis of the Cks1-dependent recognition of p27(Kip1) by the SCF(Skp2) ubiquitin ligase. *Mol. Cell* **20,** 9–19
11. Malek, N. P., Sundberg, H., McGrew, S., Nakayama, K., Kyriakides, T. R., and Roberts, J. M. (2001) A mouse knock-in model exposes sequential proteolytic pathways that regulate p27Kip1 in G1 and S phase. *Nature* **413,** 323–327
12. Kossatz, U., Dietrich, N., Zender, L., Buer, J., Manns, M. P., and Malek, N. P. (2004) Skp2-dependent degradation of p27kip1 is essential for cell cycle progression. *Genes Dev.* **18,** 2602–2607

13. Sanz-González, S. M., Melero-Fernández de Mera, R., Malek, N. P., and Andrés, V. (2006) Atheroma development in apolipoprotein E-null mice is not regulated by phosphorylation of p27(Kip1) on threonine 187. *J. Cell. Biochem.* **97,** 735–743
14. Timmerbeul, I., Garrett-Engele, C. M., Kossatz, U., Chen, X., Firpo, E., Grünwald, V., Kamino, K., Wilkens, L., Lehmann, U., Buer, J., Geffers, R., Kubicka, S., Manns, M. P., Porter, P. L., Roberts, J. M., and Malek, N. P. (2006) Testing the importance of p27 degradation by the SCFskp2 pathway in murine models of lung and colon cancer. *Proc. Natl. Acad. Sci. U.S.A.* **103,** 14009–14014
15. Wu, L., Grigoryan, A. V., Li, Y., Hao, B., Pagano, M., and Cardozo, T. J. (2012) Specific small molecule inhibitors of Skp2-mediated p27 degradation. *Chem. Biol.* **19,** 1515–1524
16. Ungermannova, D., Lee, J., Zhang, G., Dallmann, H. G., McHenry, C. S., and Liu, X. (2013) High-throughput screening AlphaScreen assay for identification of small-molecule inhibitors of ubiquitin E3 ligase SCF-Skp2-Cks1. *J. Biomol. Screen.* **18,** 910–920
17. Ooi, L. C., Watanabe, N., Futamura, Y., Sulaiman, S. F., Darah, I., and Osada, H. (2013) Identification of small molecule inhibitors of p27(Kip1) ubiquitination by high-throughput screening. *Cancer Science* **104,** 1461–1467
18. Victora, G. D. (2014) SnapShot: The Germinal Center Reaction. *Cell* **159,** 700–700.e701
19. Wang, H., Bauzon, F., Ji, P., Xu, X., Sun, D., Locker, J., Sellers, R. S., Nakayama, K., Nakayama, K. I., Cobrinik, D., and Zhu, L. (2010) Skp2 is required for survival of aberrantly proliferating Rb1-deficient cells and for tumorigenesis in Rb1+/- mice. *Nat. Genet.* **42,** 83–88
20. Peled, J. U., Yu, J. J., Venkatesh, J., Bi, E., Ding, B. B., Krupski-Downs, M., Shaknovich, R., Sicinski, P., Diamond, B., Scharff, M. D., and Ye, B. H. (2010) Requirement for cyclin D3 in germinal center formation and function. *Cell Res.* **20,** 631–646
21. Jacks, T., Fazeli, A., Schmitt, E. M., Bronson, R. T., Goodell, M. A., and Weinberg, R. A. (1992) Effects of an Rb mutation in the mouse. *Nature* **359,** 295–300
22. Zhao, H., Bauzon, F., Fu, H., Lu, Z., Cui, J., Nakayama, K., Nakayama, K. I., Locker, J., and Zhu, L. (2013) Skp2 Deletion Unmasks a p27 Safeguard that Blocks Tumorigenesis in the Absence of pRb and p53 Tumor Suppressors. *Cancer Cell* **24,** 645–659
23. MacLennan, I. C. (1994) Germinal centers. *Annu. Rev. Immunol.* **12,** 117–139
24. Crotty, S. (2011) Follicular helper CD4 T cells (TFH). *Annu. Rev. Immunol.* **29,** 621–663
25. Béguelin, W., Popovic, R., Teater, M., Jiang, Y., Bunting, K. L., Rosen, M., Shen, H., Yang, S. N., Wang, L., Ezponda, T., Martinez-Garcia, E., Zhang, H., Zheng, Y., Verma, S. K., McCabe, M. T., Ott, H. M., Van Aller, G. S., Kruger, R. G., Liu, Y., McHugh, C. F., Scott, D. W., Chung, Y. R., Kelleher, N., Shaknovich, R., Creasy, C. L., Gascoyne, R. D., Wong, K. K., Cerchietti, L., Levine, R. L., Abdel-Wahab, O., Licht, J. D., Elemento, O., and Melnick, A. M. (2013) EZH2 is required for germinal center formation and somatic EZH2 mutations promote lymphoid transformation. *Cancer Cell* **23,** 677–692
26. Linterman, M. A. (2014) How T follicular helper cells and the germinal centre response change with age. *Immunol. Cell Biol.* **92,** 72–79
27. Mountz, J. D., Wang, J. H., Xie, S., and Hsu, H. C. (2011) Cytokine regulation of B-cell migratory behavior favors formation of germinal centers in autoimmune disease. *Discovery Medicine* **11,** 76–85
28. Bronte, V., and Pittet, M. J. (2013) The spleen in local and systemic regulation of immunity. *Immunity* **39,** 806–818
29. Foy, T. M., Aruffo, A., Bajorath, J., Buhlmann, J. E., and Noelle, R. J. (1996) Immune regulation by CD40 and its ligand GP39. *Annu. Rev. Immunol.* **14,** 591–617
30. Tsukiyama, T., Ishida, N., Shirane, M., Minamishima, Y. A., Hatakeyama, S., Kitagawa, M., Nakayama, K., and Nakayama, K. (2001) Down-regulation of p27Kip1 expression is required for development and function of T cells. *J. Immunol.* **166,** 304–312
31. Callahan, J. E., Kappler, J. W., and Marrack, P. (1993) Unexpected expansions of CD8-bearing cells in old mice. *J. Immunol.* **151,** 6657–6669
32. Eaton, S. M., Burns, E. M., Kusser, K., Randall, T. D., and Haynes, L. (2004) Age-related defects in CD4 T cell cognate helper function lead to reductions in humoral responses. *J. Exp. Med.* **200,** 1613–1622
33. Liu, L., Cheung, T. H., Charville, G. W., Hurgo, B. M., Leavitt, T., Shih, J., Brunet, A., and Rando, T. A. (2013) Chromatin modifications as determinants of muscle stem cell quiescence and chronological aging. *Cell Reports* **4,** 189–204
34. Cheung, T. H., and Rando, T. A. (2013) Molecular regulation of stem cell quiescence. *Nat. Rev. Mol. Cell Biol.* **14,** 329–340
35. Shulman, Z., Gitlin, A. D., Targ, S., Jankovic, M., Pasqual, G., Nussenzweig, M. C., and Victora, G. D. (2013) T follicular helper cell dynamics in germinal centers. *Science* **341,** 673–677
36. Gitlin, A. D., Shulman, Z., and Nussenzweig, M. C. (2014) Clonal selection in the germinal centre by regulated proliferation and hypermutation. *Nature* **509,** 637–640
37. Chambers, S. M., Boles, N. C., Lin, K. Y., Tierney, M. P., Bowman, T. V., Bradfute, S. B., Chen, A. J., Merchant, A. A., Sirin, O., Weksberg, D. C., Merchant, M. G., Fisk, C. J., Shaw, C. A., and Goodell, M. A. (2007) Hematopoietic fingerprints: an expression database of stem cells and their progeny. *Cell Stem Cell* **1,** 578–591
38. Venezia, T. A., Merchant, A. A., Ramos, C. A., Whitehouse, N. L., Young, A. S., Shaw, C. A., and Goodell, M. A. (2004) Molecular signatures of proliferation and quiescence in hematopoietic stem cells. *PLoS Biology* **2,** e301
39. Lu, Z., Bauzon, F., Fu, H., Cui, J., Zhao, H., Nakayama, K., Nakayama, K. I., and Zhu, L. (2014) Skp2 suppresses apoptosis in Rb1-deficient tumours by limiting E2F1 activity. *Nat. Commun.* **5,** 3463
40. Yang, X., Stedra, J., and Cerny, J. (1996) Relative contribution of T and B cells to hypermutation and selection of the antibody repertoire in germinal centers of aged mice. *J. Exp. Med.* **183,** 959–970
41. Looney, R. J., Hasan, M. S., Coffin, D., Campbell, D., Falsey, A. R., Kolassa, J., Agosti, J. M., Abraham, G. N., and Evans, T. G. (2001) Hepatitis B immunization of healthy elderly adults: relationship between naïve CD4+ T cells and primary immune response and evaluation of GM-CSF as an adjuvant. *J. Clin. Immunol.* **21,** 30–36
42. Good-Jacobson, K. L., Szumilas, C. G., Chen, L., Sharpe, A. H., Tomayko, M. M., and Shlomchik, M. J. (2010) PD-1 regulates germinal center B cell survival and the formation and affinity of long-lived plasma cells. *Nat. Immunol.* **11,** 535–542
43. Zhu, L., Lu, Z., and Zhao, H. (2014) Antitumor mechanisms when pRb and p53 are genetically inactivated. *Oncogene* 10.1038/onc.2014.399

Biological Sciences – Medical Sciences

p27T187A knockin mutation identifies Skp2/Cks1 pocket inhibitors for advanced prostate cancer

Hongling Zhao [1], Zhonglei Lu [1], Frederick Bauzon [1], Hao Fu [1], Jinhua Cui [1], Joseph Locker[2], and

Liang Zhu[1]

[1]Department of Developmental and Molecular Biology, and Ophthalmology & Visual Sciences, and Medicine, The Albert Einstein Comprehensive Cancer Center and Liver Research Center, Albert Einstein College of Medicine, Bronx, NY 10461, USA. [2]Department of Pathology, University of Pittsburgh School of Medicine, Pittsburgh, PA 15261, USA

Corresponding author:
Dr. Liang Zhu
Department of Developmental and Molecular Biology
Albert Einstein College of Medicine
1300 Morris Park Avenue, Room U-521
Bronx, NY 10461
USA
Phone: 718-430-3320
Fax: 718-430-8975
Email: liang.zhu@einstein.yu.edu

Running Title
Skp2/Cks1 inhibitors for advanced prostate cancer

Keywords
p27 phosphorylation and accumulation, specific Skp2/Cks1 inhibitors, advanced prostate cancer, tumor organoids

Total characters (with spaces): 35,547

Abstract

Over-expression of Skp2 coupled with under-expression of p27 are frequent characteristics of cancer cells. Ubiquitination of p27 by SCF^{Skp2} requires Cks1 and depends on the interaction between the Skp2/Cks1 pocket and the phosphorylated Thr187 of p27. p27 Thr187-to-Ala knockin (p27T187A KI) mice do not accumulate p27 protein nor show abnormal phenotypes. When p27 knockout (KO) accelerated lethality by ENU or $Kras^{G12D}$ induced tumorigenesis, p27T187A KI also did not improve survival. Here we identify pRb and p53 deficient (DKO) tumorigenesis in prostate as a context in which p27 ubiquitination by $SCF^{Skp2/Cks1}$ becomes rate-limiting. Thus, p27 protein accumulated in prostate when p27T187A KI mice underwent DKO prostate tumorigenesis. p27T187A KI or Skp2 knockdown (KD) induced similar degrees of p27 protein accumulation in DKO prostate cells, and Skp2 KD did not increase p27 protein in DKO prostate cells that contained p27T187A KI (AADKO prostate cells). p27T187A KI activated an E2F1-p73-apoptosis axis in DKO prostate tumorigenesis, slowed disease progression, and significantly extended survival. A Skp2/Cks1 pocket inhibitor preferentially collapsed DKO prostate tumor organoids over AADKO organoids, which spontaneously disintegrated over time when DKO prostate tumor organoids grew larger. Querying TCGA of prostate cancer for the genetic status of five prostate cancer drivers revealed statistically significant co-occurrences of *TP53* inactivation and *MYC* activation in primary prostate cancer. With disease progression to metastatic castration resistant prostate cancer (mCRPC), co-inactivation of *RB1* and *TP53* became the only statistically significant co-occurrences. Our findings identify targeting the Skp2/Cks1 pocket as a potential therapy strategy for mCRPC.

Significance

Ubiquitination of p27 by $SCF^{Skp2/Cks1}$ is an established biochemical mechanism that allow the SCF^{Skp2} ubiquitin ligase to specifically target p27. The Skp2/Cks1 pocket is amenable to inhibition by small molecules and the normal p27T187A KI mice forecast these inhibitors to be non-toxic (since p27T187A KI genetically disrupts p27 binding to the Skp2/Cks1 pocket). Critically however, p27T187A KI did not extend survival of mice undergoing ENU or $Kras^{G12D}$ induced tumorigenesis. Our findings identify Skp2/Cks1 pocket inhibitors as potentially effective therapeutics against mCRPC, for which there is no effective and durable treatment at the present time.

Introduction

Expression of p27, a cyclin-dependent kinase inhibitor, is regulated by mRNA expression, protein synthesis, and protein degradation. One negative regulatory mechanism is its ubiquitination by $SCF^{Skp2/Cks1}$ ubiquitin ligases, which prepares p27 for degradation in the proteasomes (1). $SCF^{Skp2/Cks1}$-mediated p27 ubiquitination requires its phosphorylation on Thr187 (to become p27T187p). Replacing Thr187 with alanine (p27T187A) to render this position unphosphorylable prevents p27 binding to and ubiquitination by $SCF^{Skp2/Cks1}$ (2, 3). This is because T187p and a conserved E185 together mediate p27 binding to a pocket formed jointly by Skp2 and the accessory protein Cks1 (4-6). To test the physiological significance of this biochemical mechanism, $p27^{T187A/T187A}$ (p27T187A KI) mice were generated (7). p27T187A KI mice do not show p27 protein accumulation and are without undesirable phenotypes, demonstrating that p27 ubiquitination by $SCF^{Skp2/Cks1}$ is dispensable for p27 degradation in normal physiology.

p27 is a haplo-insufficient tumor suppressor (8), whose reduced expression is frequently associated with aggressive cancers (9). Knockout of p27 induces spontaneous pituitary tumorigenesis and can accelerate tumorigenesis induced by a large number of oncogenic events in numerous tissues, suggesting that stabilizing p27 can be therapeutic for many types of cancer. Critically, however, when p27 KO accelerated lung tumorigenesis in $Kras^{G12D/+}$ mice, p27T187A KI did not have a protective effect (10), suggesting that $SCF^{Skp2/Cks1}$ is dispensable for p27 degradation in lung tumorigenesis by oncogenic Kras. On the other hand, p27 KO accelerated pituitary melanotroph tumorigenesis in $Rb1^{+/-}$ mice (11) and p27T187A KI blocked it (12). Thus, the role of $SCF^{Skp2/Cks1}$ in mediating p27 degradation can be highly critical in promoting tumorigenesis but only in specific contexts.

Finding additional tumorigenic contexts in which $SCF^{Skp2/Cks1}$ plays a critical role in promoting tumorigenesis is a challenging goal. Mouse pituitary melanotroph tumorigenesis is

exceptional since it can be induced by deleting *Rb1* or p27 alone, while tumorigenesis in most other tissues requires inactivation of additional tumor suppressors and activation of oncoproteins. On the other hand, it is evident that, once the susceptible contexts are identified, inhibition of $SCF^{Skp2/Cks1}$ is technically feasible (13, 14), affects a highly select sub-group of SCF^{Skp2} substrates, and is forecasted by the p27T187A KI mice to be non-toxic. Here we demonstrate that pRb and p53 deficient prostate tumorigenesis is an additional susceptible context, and make the case for testing a specific $SCF^{Skp2/Cks1}$ inhibitor on metastatic castration resistant prostate cancer, an incurable and highly lethal malignancy.

Results and Discussion

Thr187 phosphorylation becomes rate-limiting for Skp2-mediated p27 degradation in DKO prostate tumorigenesis

p27 can be ubiquitinated by several ubiquitin ligases, including $SCF^{Skp2/Cks1}$, Pirh2 (15), KPC1 (16), Cul4 (17), and WWP1 (18). Combined activities of these ligases likely determine the stability of p27 protein in a context dependent manner. pRb inhibits Skp2 binding to p27T187p (19), represses Skp2 expression (20, 21), and promotes Skp2 protein degradation (22); pRb loss may thereby enhance Skp2 activity to promote p27 degradation in *Rb1* deficient pituitary tumorigenesis (12, 23). DNA damage-activated p53 stimulates expression of Pirh2 and KPC1 as typical p53 target genes to degrade p27 in mouse embryonic fibroblasts (24) but p53 deletion in prostate did not induce p27 protein accumulation, likely because p53 is not activated in quiescent prostate and small reduction in Pirh2 and KPC1 can be compensated by other p27 ubiquitin ligases. Addition of *Rb1* deletion reduced p27 protein (Fig. 1Ae,f), likely because the other p27 ubiquitin ligases now included an activated Skp2 due to pRb loss. When DKO prostate was generated in Skp2 KO mice, p27 protein accumulated (24).

We hypothesized that the DKO prostate provides a context in which p27 ubiquitination by $SCF^{Skp2/Cks1}$ becomes rate-limiting for p27 protein degradation. To test this hypothesis, we

generated mice of *p27*$^{+/+}$, *p27*$^{T187A/T187A}$, and *PB-Cre4;Rb1*$^{lox/lox}$*;Trp53*$^{lox/lox}$ on *p27*$^{+/+}$ or *p27*$^{T187A/T187A}$ background to determine p27 expression in their prostates by IHC. We found similar p27 staining in *p27*$^{+/+}$ and *p27*$^{T187A/T187A}$ prostates (Fig. 1Ab,d). When *Rb1* and *Trp53* were co-deleted, p27 staining reduced in *p27*$^{+/+}$ prostate (Fig. 1Af), but increased in *p27*$^{T187A/T187A}$ prostates (Fig. 1Ah). At 5-6 months of age, co-deletion of *Rb1* and *Trp53* induced neoplastic lesions only in proximal prostate acini. We show p27 staining in distal prostate acini to compare the four genotypes in normal appearing tissues (see the corresponding consecutive sections, Fig. 1Aa,c,e,g). p27 Western blot of the prostate ventral and anterior lobes provided similar findings (Fig. 1B). Thus, ubiquitination of p27T187p by SCF$^{Skp2/Cks1}$ became rate-limiting in preventing p27 accumulation in prostate when *Rb1* and *Trp53* were co-deleted in it.

To learn the molecular basis for this requirement for p27 Thr187 phosphorylation, we established early passage prostate cells from DKO prostate in *p27*$^{+/+}$ mice (called DKO cells) and in *p27*$^{T187A/T187A}$ mice (AADKO cells). We found that Skp2 knockdown in DKO cells increased p27 protein levels while AADKO cells intrinsically contained similarly increased levels of p27 (Fig. 1C). RT-qPCR and CHX experiments suggest that p27 accumulation in AADKO prostate cells was not due to increased expression of p27 mRNA (Fig. 1D) but was due to increased protein stability (Fig. 1E). If p27T187A KI prevented p27 ubiquitination by SCF$^{Skp2/Cks1}$ to accumulate p27, knockdown of Skp2 in p27T187A KI cells would not further increase p27, and this proved true (Fig. 1C). These genetic and molecular findings suggest that this requirement for p27 Thr187 phosphorylation reflects a critical role for SCF$^{Skp2/Cks1}$ ubiquitination of p27T187p to prevent p27 accumulation in DKO prostate tumorigenesis.

p27T187A KI activates a p27-E2F1-p73-apoptosis axis in DKO prostate tumorigenesis

Skp2 KO or p27T187A KI inhibited pRb deficient pituitary melanotroph tumorigenesis by increasing apoptosis (23). In mouse embryonic fibroblasts, Skp2 KO protected E2F1 from binding to and repression by cyclin A following deletion of *Rb1*; the further activated E2F1

induced apoptosis (25). E2F1 can induce p53-dependent and -independent apoptosis; the relative contributions of these two apoptotic mechanisms are not known (Fig. S1A). To explore the possibility that this E2F1-dependent apoptosis in *Rb1* deficient MEFs could remain effective when *Trp53* is additionally deleted, we determined the contribution of p73, an E2F1 target gene and a p53 family member, to this apoptosis. As shown in Fig. S1B. *Rb1* deletion did not increase apoptosis, measured as sub-G1 cells, in Skp2 WT MEFs, but increased them to 19% of the population in Skp2 KO MEFs. Combined knockdown of p73 reduced sub-G1 cells to 7-8% of the population (Fig. S1C), demonstrating that p73 contributed about half of the E2F1 induced apoptosis in this context.

We next investigated whether p27T187A KI activated this p27-E2F1-p73 axis in AADKO prostate tumor cells. We found that Skp2 knockdown in DKO cells increased p73 protein. AADKO cells intrinsically contained a similarly increased level of p73 protein, which Skp2 knockdown did not further increase (Fig. 2A). Thus, effects of Skp2 knockdown and p27T187A KI on p73 protein mirrored their effects on p27 protein. In contrast to p27 however, p27T187A KI increased expression of p73 mRNA in AADKO cells compared to DKO cells (Fig. 2B), accompanied by increased occupancy of E2F1 and p73 promoters (both are typical E2F target genes) but not GAPDH promoter (a housekeeping gene) by E2F1 in AADKO cells compared to DKO cells (Fig. 2C, upper), and ChIP with normal IgG did not enrich E2F1 or p73 promoter sequences (Fig. 2C, lower). Occupancy on E2F1 and p73 promoters by E2F4, which does not bind cyclin A, did not increase in AADKO cells (Fig. S2). We next determined p73 protein expression in prostate tissues. Of the four genotypes examined ($p27^{+/+}$, $p27^{T187A/T187A}$, *PB-Cre4;*$Rb1^{lox/lox}$;$Trp53^{lox/lox}$, and $p27^{T187A/T187A}$;*PB-Cre4;*$Rb1^{lox/lox}$;$Trp53^{lox/lox}$), we found robust anti-p73 staining only in $p27^{T187A/T187A}$;*PB-Cre4;*$Rb1^{lox/lox}$;$Trp53^{lox/lox}$ prostate by IHC (Fig. 2D). p73 protein similarly increased in $Skp2^{-/-}$;*PB-Cre4;*$Rb1^{lox/lox}$;$Trp53^{lox/lox}$ prostate (Fig. S3). Western blot of prostate tissues confirmed the staining findings (Fig. 2E).

As a family member of the p53 family, p73 can induce apoptosis independent of p53. Western blotting of various prostate tissues revealed accumulation of cleaved (activated) caspase 3 in *p27$^{T187A/T187A}$;PB-Cre4;Rb1$^{lox/lox}$;Trp53$^{lox/lox}$* prostate tissues (Fig. 2E), suggesting that the increased p73 in this genotype induced apoptosis in the absence of p53. We next used TUNEL staining to demonstrate that DKO neoplastic lesions contained more apoptosis in *p27$^{T187A/T187A}$* mice than in *p27$^{+/+}$* mice (Fig. 3A,B,C). To determine whether p73 contributed to this apoptosis, we determine the effects of p73 knockdown (Fig. 3D) in AADKO prostate tumor cells. In untreated AADKO cell culture, 9% of the population showed sub-G1 DNA content. Knockdown of p73 reduced the sub-G1 population to 1.5%, which was confirmed by a 2nd shp73 (Fig. 3E). We further show that DKO prostate tumor cells contained little sub-G1 cells (0.6%), which was increased to 17% by Skp2 knockdown, additional knockdown of p73 reduced it to background levels (Fig. 3F). These findings delineate a p27-E2F1-p73-apoptosis pathway activated by p27T187A KI in DKO prostate tumorigenesis (Fig. S4).

p27T187A KI delays progression of DKO prostate tumorigenesis

DKO prostate tumorigenesis is invasive, metastatic, castration resistant, and becomes lethal within 7-10 months (26). Skp2 KO mice are significantly smaller and less fertile than WT controls. DKO prostate tumorigenesis in Skp2 KO mice cannot progress beyond PIN stages due to cell proliferation arrest and apoptosis (24). p27T187A KI mice do not have the abnormities seen in Skp2 KO mice. We next generated two cohorts of mice, *PB-Cre4;Rb1$^{lox/lox}$;Trp53$^{lox/lox}$* and *p27$^{T187A/T187A}$;PB-Cre4;Rb1$^{lox/lox}$;Trp53$^{lox/lox}$* to determine how DKO prostate tumorigenesis progressed in p27T187A KI mice.

In addition to inducing p53-independent apoptosis via an p27-E2F1-p73 axis, increased p27 inhibited cell proliferation, as measured by Ki67 (Fig. S5A,C) and pHH3 (Fig. S5B,D) staining, in DKO prostate tumorigenesis. We found that 80% of *PB-Cre4;Rb1$^{lox/lox}$;Trp53$^{lox/lox}$* mice contained gross prostate tumors compared to 50% of *p27$^{T187A/T187A}$;PB-*

Cre4;Rb1$^{lox/lox}$;Trp53$^{lox/lox}$ mice at 8-9 months of age (Fig. 4A,B). Only 2 of 30 *PB-Cre4;Rb1$^{lox/lox}$;Trp53$^{lox/lox}$* mice survived pass 9 months, while 13 of 38 *p27$^{T187A/T187A}$;PB-Cre4;Rb1$^{lox/lox}$;Trp53$^{lox/lox}$* mice survived pass 10 months ($p < 0.0001$, Fig. 4C). These findings demonstrate that the innocuous p27T187A mutation can delay progression of the aggressive DKO prostate tumorigenesis to significantly extend survival.

A specific inhibitor of SCF$^{Skp2/Cks1}$ selectively inhibits DKO over AADKO prostate tumor cells

With FDA approval for the use of a proteasome inhibitor, bortezomib, to treat multiple myeloma, targeting ubiquitin-mediated protein degradation has become a validated cancer therapy strategy (27, 28). The current challenge is to add specificity to this strategy, since unspecific inhibition of protein degradation generates serious side-effects. Inhibition of SCF$^{Skp2/Cks1}$ is substrate specific and technically feasible since the Skp2 and Cks1 joint pocket is known to recruit only p27T187p, p21S130p, and p57 by prediction and is suitable for small molecule inhibitors (6, 29, 30). Using a structure-based in silico screen, small molecules fitting in the Skp2/Cks1 joint pocket have been identified (Fig. S6A) (13). We employed these inhibitors to determine the pharmacologic effects of inhibiting the Skp2/Cks1-p27T187p interaction in DKO prostate tumor cells. Since these inhibitors block the same Skp2/Cks1-p27T187p interaction as p27T187A KI, we also tested them on AADKO prostate tumor cells to gain insight to its mechanism of action. In Fig. 5A, we titrated inhibitor compound 1 (C1) (13) to compare its effects on proliferation of DKO and AADKO prostate tumor cells, compared to DU145 cells (see below). At 1.25 μM, C1 strongly reduced DKO cell proliferation (by 80% relative to vehicle (DMSO) control) but weakly reduced AADKO proliferation (by 20%), and AADKO cells proliferated more slowly than DKO cells in the absence of C1 (Fig. S6B). This selectivity for DKO cells continued when C1 concentration was increased to 2.5 μM. These findings provide genetic validation for the designed mechanism of action of C1. At 5.0 μM, C1 also strongly

reduced AADKO proliferation (by 75% relative to DMSO control), suggesting that higher concentrations of C1 blocked ubiquitination of p21 and possibly p57 to exert additional antitumor activity in AADKO cells. Indeed, C1 treatment increased p27 only in DKO cells but increased p21 in both DKO and AADKO cells (Fig. 5B). These findings demonstrate a therapeutic advantage in pharmacological targeting of the Skp2/Cks1 joint pocket over p27T187A KI (Fig. S6A). Further studies are needed to determine whether the Skp2 and Cks1 joint pocket also target other proteins in addition to the p27 family and whether C1 has off-targets.

Inactivation of *RB1* and *TP53* significantly co-occur in mCRPC

To determine how often *RB1* and *TP53* are genetically inactivated together in prostate cancer in the clinics, we queried the genetic status of *RB1, TP53, PTEN, NKX3-1, and MYC* (five established prostate cancer drivers) in three cohorts of primary prostate cancer (totaling 599 samples) on cBioPortal (31). We did not find co-occurrence of genetic inactivation of *RB1* and *TP53* in any of the 599 specimens (Table S1). In the largest study (32), genetic inactivation of *TP53* co-occurred significantly with activation of *MYC*, providing a TCGA level validation for the existing knowledge that the synergy between these two oncogenic events drives prostate tumorigenesis (33).

Most primary prostate cancer is treated and cured by prostatectomy, but about one quarter of the patients develop metastatic prostate cancer after primary therapy or at presentation. These cases are treated with androgen deprivation therapies, but invariably the cancer would relapse in the form of metastatic castration resistant prostate cancer (mCRPC). Many mCRPCs are treated with inhibitors of residual androgen synthesis, such as abiraterone acetate, and 2nd generation AR antagonist, such as enzalutamide, but the efficacy of the treatment is not durable and the disease would progress to AR-independent prostate cancer. Some patients may respond to taxane chemotherapies, but resistance develop quickly. mCRPCs then becomes lethal, leading to 27,000 death every year in US alone. Recent

increases in biopsies of mCRPC at autopsy (34) and the most recent efforts to collect mCRPC biopsies at clinical trials (35) led to TCGA of mCRPC. We queried the same five genes in three cohorts of mCRPC totaling 228 samples (Table S1). Remarkably, co-occurrence for inactivation of *RB1* and *TP53* is statistically significant in two of the three mCRPC cohorts while none of the other co-occurrences reached statistical significance. Most of the co-occurred inactivation is likely biallelic (Figure S7). We propose that these TCGA findings identify DKO prostate tumorigenesis as a mouse model for mCRPC.

There are seven human prostate cancer cell lines in CCLE (Cancer Cell Line Encyclopedia). DU145, derived from a brain metastasis and is hormone-insensitive, contains truncating mutation K715* in *RB1* and inactivating mutation V274F in *TP53*. C1 at 5.0 μM inhibited DU145 proliferation and increased p27 and p21 in them to a degree comparable to DKO prostate tumor cells (Fig. 5A,B). Thus, specific inhibition of $SCF^{Skp2/Cks1}$ is a potential therapeutic strategy for mCRPC, which currently has no durable treatment.

AADKO prostate tumor organoids spontaneously disintegrate while $SCF^{Skp2/Cks1}$ inhibitor similarly inhibits DKO prostate tumor organoids

DU145 cell line was established about 40 years ago (36), and is the only prostate cancer cell line containing inactivating mutations in *Rb1* and *TP53*. Extended 2-dimensional (2D) culture of established cancer cell lines encourages secondary genomic alterations that are not present in the original cancer specimens (37), and 2D culture bears little resemblance to the prostate. Organoid cultures are emerging as an alternative since tumor cell organoids demonstrate stable genomic landscapes faithful to the original tumor specimens, and respond to therapeutics in three-dimensional acinus-like structures (38). Prostate tumor organoid cultures can be generated from mouse models (39, 40) as well as contemporary patients (41). Testing both on the same experimental platform is expected to increase the predictive value of the observed therapeutic effects in preparation for clinical trials.

We next adapted published protocols (39, 40) to generate DKO and AADKO prostate tumor organoids (Fig. 5C,D). At day 15 after plating, DKO and AADKO cells generated organoids with similar efficiencies and size ranges (Fig. S8 and Fig. 5E, quantified in the DMSO columns in Fig. 5G,H). This differed from the 2D cultures, where AADKO cells proliferated much more slowly than DKO cells (Fig. S5B). A prominent difference between DKO and AADKO organoid cultures is the 1.9 fold increase in debris piles in the latter in untreated cultures (Fig. 5F and quantified in the two DMSO columns in Figure 5H). Longitudinal monitoring over a six-day period revealed most DKO organoids grew larger while most AADKO organoids spontaneously disintegrated into debris piles (Fig. S8). These organoid phenotypes demonstrate the ability of organoid cultures to more closely model autochthonous DKO and AADKO prostate tumors.

We then titrated C1 to test its effects on DKO and AADKO prostate tumor organoids. At 1.25 μM, C1 reduced organoid forming efficiency by 1.7 fold for DKO organoids compared to 1.1 fold for AADKO organoids (Fig. 5G); and increased debris piles 2.9 fold for DKO organoids compared to 1.1 fold for AADKO organoids (Fig. 5H). This selectivity for DKO organoids largely disappeared when C1 concentrations were increased to 5.0 μM, although about 20% of small AADKO organoids remained in AADKO culture. These organoids findings provide a higher level of genetic and functional validation for the therapeutic potential of $SCF^{Skp2Cks1}$ inhibitors for pRb and p53 deficient prostate cancer, which are usually in advanced stages in the clinic.

In summary, we have shown genetic and molecular evidence that phosphorylation of Thr187 is required to prevent p27 accumulation in DKO prostate tumorigenesis. Without Thr187 phosphorylation, increased p27 triggers a p27-E2F1-p73-apoptosis pathway in DKO prostate tumorigenesis to delay its progression to lethality. We demonstrated the translational value of these findings by genetically validating the designed mechanism of action of a specific $SCF^{Skp2/Cks1}$ inhibitor, and functionally validating its advantageous therapeutic potential over

p27T187A KI for DKO prostate cancer cells. Progression to mCRPC frequently involve co-inactivation of *RB1* and *TP53*. pRb and p53 are the two major tumor suppressors responsible for most of the antitumor mechanisms in the cells. Their co-inactivation could explain why durable treatment remains elusive for mCRPC. While traditional prostate cancer cell lines containing inactivating mutations in *RB1* and *TP53* are scarce and likely have incurred genomic alteration not present in the original tumors, six recently established mCRPC organoid lines from contemporary patients contained frequent inactivation of *RB1* and *TP53*, and these organoid lines maintain stable genomic landscapes faithful to the biopsy specimens that they were derived from (41). These organoid lines can now be tested in parallel with our DKO organoid lines to translate our mouse findings to human mCRPC.

Materials and Methods

All mice used for experiments are on FVBxC57BL6Jx129Sv background. Mice were maintained under pathogen-free conditions in the Albert Einstein College of Medicine animal facility. Mouse experiments protocols were reviewed and approved by Einstein Animal Care and Use Committee, conforming to accepted standards of humane animal care.

For organoid cultures, 2000 dissociated cells from DKO or AADKO prostate tumors were plated according to published protocols (39, 40). Qualification in Fig. 5 was based on photographs of ten 10x-fields, each fields yielding 3-5 photographs focusing on consecutive planes inside Matrigel layers. Two duplicate wells were counted in this manner.

Detail Materials and Methods are in Supplementary Materials accompanying this article.

Acknowledgment

This work was supported by NIH grants RO1CA127901and RO1CA131421 (LZ), Albert Einstein Comprehensive Cancer Research Center (5P30CA13330) and Liver Research Center (5P30DK061153) provided core facility support. HZ is a recipient of DOD PCRP Postdoctoral

Fellowship (PC121837), and LZ was a Irma T. Hirschl Career Scientist Award recipient. We thank Dr. James Roberts for providing the p27T187A KI mice.

Author contributions: HZ and LZ conceived and designed the research; HZ, ZL, FB, HF, JC performed the experiments; JL evaluated prostate cancer pathology; HZ and LZ analyzed the data; HZ, JL, and LZ wrote the paper.

References

1. Starostina NG & Kipreos ET (2012) Multiple degradation pathways regulate versatile CIP/KIP CDK inhibitors. *Trends in cell biology* 22(1):33-41.
2. Vlach J, Hennecke S, & Amati B (1997) Phosphorylation-dependent degradation of the cyclin-dependent kinase inhibitor p27. *EMBO J* 16(17):5334-5344.
3. Montagnoli A*, et al.* (1999) Ubiquitination of p27 is regulated by Cdk-dependent phosphorylation and trimeric complex formation. *Genes Dev* 13(9):1181-1189.
4. Ganoth D*, et al.* (2001) The cell-cycle regulatory protein Cks1 is required for SCF^{Skp2}-mediated ubiquitinylation of p27. *Nat. Cell Biol.* 3:321-324.
5. Spruck C*, et al.* (2001) A CDK-independent function of mammalian Cks1: targeting of SCF^{Skp2} to the CDK inhibitor $p27^{Kip1}$. *Mol. Cell* 7:639-650.
6. Hao B*, et al.* (2005) Structural basis of the Cks1-dependent recognition of p27(Kip1) by the SCF(Skp2) ubiquitin ligase. *Mol. Cell* 20(1):9-19.
7. Malek NP*, et al.* (2001) A mouse knock-in model exposes sequential proteolytic pathways that regulate p27Kip1 in G1 and S phase. *Nature* 413(6853):323-327.
8. Fero ML, Randel E, Gurley KE, Roberts JM, & Kemp CJ (1998) The murine gene p27Kip1 is haplo-insufficient for tumour suppression. *Nature* 396:177-180.
9. Chu IM, Hengst L, & Slingerland JM (2008) The Cdk inhibitor p27 in human cancer: prognostic potential and relevance to anticancer therapy. *Nature reviews. Cancer* 8(4):253-267.

10. Timmerbeul I*, et al.* (2006) Testing the importance of p27 degradation by the SCFskp2 pathway in murine models of lung and colon cancer. *Proc. Natl. Acad. Sci. U S A* 103(38):14009-14014.

11. Park MS*, et al.* (1999) p27 and Rb are on overlapping pathways suppressing tumorigenesis in mice. *Proc. Natl. Acad. Sci. (USA)* 96:6382-6387.

12. Zhao H*, et al.* (2015) Substituting Threonine187 With Alanine in p27Kip1 Prevents Pituitary Tumorigenesis By Two-Hit Loss Of Rb1 And Enhances Humoral Immunity In Old Age. *J Biol Chem*:published online Jan 12, 2015.

13. Wu L*, et al.* (2012) Specific small molecule inhibitors of Skp2-mediated p27 degradation. *Chemistry & biology* 19(12):1515-1524.

14. Skaar JR, Pagan JK, & Pagano M (2014) SCF ubiquitin ligase-targeted therapies. *Nature reviews. Drug discovery* 13(12):889-903.

15. Hattori T*, et al.* (2007) Pirh2 promotes ubiquitin-dependent degradation of the cyclin-dependent kinase inhibitor p27Kip1. *Cancer Res* 67(22):10789-10795.

16. Kamura T*, et al.* (2004) Cytoplasmic ubiquitin ligase KPC regulates proteolysis of p27(Kip1) at G1 phase. *Nat. Cell Biol.* 6(12):1229-1235.

17. Miranda-Carboni GA*, et al.* (2008) A functional link between Wnt signaling and SKP2-independent p27 turnover in mammary tumors. *Genes Dev* 22(22):3121-3134.

18. Cao X*, et al.* (2011) WW domain-containing E3 ubiquitin protein ligase 1 (WWP1) delays cellular senescence by promoting p27(Kip1) degradation in human diploid fibroblasts. *J Biol Chem* 286(38):33447-33456.

19. Ji P*, et al.* (2004) An Rb-Skp2-p27 pathway mediates acute cell cycle inhibition by Rb and is retained in a partial-penetrance Rb mutant. *Mol. Cell* 16(1):47-58.

20. Zhang L & Wang C (2005) F-box protein Skp2: a novel transcriptional target of E2F. *Oncogene* 25(18):2615-2627.

21. Yung Y, Walker JL, Roberts JM, & Assoian RK (2007) A Skp2 autoinduction loop and restriction point control. *J. Cell Biol.* 178(5):741-747.

22. Binne UK*, et al.* (2007) Retinoblastoma protein and anaphase-promoting complex physically interact and functionally cooperate during cell-cycle exit. *Nat. Cell Biol.* 9(2):225-232.

23. Wang H*, et al.* (2010) Skp2 is required for survival of aberrantly proliferating Rb1-deficient cells and for tumorigenesis in Rb1+/- mice. *Nat Genet* 42(1):83-88.

24. Zhao H*, et al.* (2013) Skp2 Deletion Unmasks a p27 Safeguard that Blocks Tumorigenesis in the Absence of pRb and p53 Tumor Suppressors. *Cancer Cell* 24(5):645-659.

25. Lu Z*, et al.* (2014) Skp2 suppresses apoptosis in Rb1-deficient tumours by limiting E2F1 activity. *Nat Commun* 5:3463.

26. Zhou Z*, et al.* (2006) Synergy of p53 and Rb deficiency in a conditional mouse model for metastatic prostate cancer. *Cancer Res.* 66(16):7889-7898.

27. Bassermann F, Eichner R, & Pagano M (2014) The ubiquitin proteasome system - implications for cell cycle control and the targeted treatment of cancer. *Biochimica et biophysica acta* 1843(1):150-162.

28. Orlowski RZ & Kuhn DJ (2008) Proteasome inhibitors in cancer therapy: lessons from the first decade. *Clinical cancer research : an official journal of the American Association for Cancer Research* 14(6):1649-1657.

29. Bornstein G*, et al.* (2003) Role of the SCFSkp2 ubiquitin ligase in the degradation of p21Cip1 in S phase. *J. Biol. Chem.* 278(28):25752-25757.

30. Kamura T*, et al.* (2003) Degradation of p57Kip2 mediated by SCFSkp2-dependent ubiquitylation. *Proc Natl Acad Sci U S A* 100(18):10231-10236.

31. Gao J*, et al.* (2013) Integrative analysis of complex cancer genomics and clinical profiles using the cBioPortal. *Science signaling* 6(269):pl1.

32. Network. CGAR (2015) The Molecular Taxonomy of Primary Prostate Cancer. *Cell* 163(4):1011-1025.

33. Shen MM & Abate-Shen C (2010) Molecular genetics of prostate cancer: new prospects for old challenges. *Genes Dev* 24(18):1967-2000.

34. Grasso CS*, et al.* (2012) The mutational landscape of lethal castration-resistant prostate cancer. *Nature* 487(7406):239-243.

35. Robinson D*, et al.* (2015) Integrative clinical genomics of advanced prostate cancer. *Cell* 161(5):1215-1228.

36. Stone KR, Mickey DD, Wunderli H, Mickey GH, & Paulson DF (1978) Isolation of a human prostate carcinoma cell line (DU 145). *International journal of cancer. Journal international du cancer* 21(3):274-281.

37. Gillet JP, Varma S, & Gottesman MM (2013) The clinical relevance of cancer cell lines. *Journal of the National Cancer Institute* 105(7):452-458.

38. Sato T & Clevers H (2015) SnapShot: Growing Organoids from Stem Cells. *Cell* 161(7):1700-1700 e1701.

39. Karthaus WR*, et al.* (2014) Identification of multipotent luminal progenitor cells in human prostate organoid cultures. *Cell* 159(1):163-175.

40. Chua CW*, et al.* (2014) Single luminal epithelial progenitors can generate prostate organoids in culture. *Nat Cell Biol* 16(10):951-961, 951-954.

41. Gao D*, et al.* (2014) Organoid cultures derived from patients with advanced prostate cancer. *Cell* 159(1):176-187.

Figure Legends

Fig. 1. *p27*$^{T187A/T187A}$ mice accumulated p27 protein in DKO prostate. (A) H&E and p27 IHC staining, as marked on the left, of consecutive prostate sections of four genotypes, as indicated

above the photographs. (B) Protein levels were determined by Western blot with the indicated antibodies in prostate ventral and anterior lobes of the indicated genotypes. A/A is abbreviated from T187A/T187A. (C) DKO and AADKO prostate cells were transduced with lentiviruses expressing the indicated shRNA (Scrmbl, scrambled). Following antibiotic selection, the transduced cells were subject to Western blot for the indicated proteins. The same cells were subject to RT-qPCR to determine levels of p27 mRNA relative to GAPDH mRNA (D) and CHX chase to determine p27 protein stability relative to α-tubulin (E).

Fig. 2. p27T187A KI activated an E2F1-p73 axis. (A) DKO and AADKO prostate cells treated with the indicated shRNA (as in Fig. 1C) were subject to Western blot for the indicated proteins. (B) The same cells were used for RT-qPCR to determine levels of p73 mRNA relative to GAPDH mRNA. (C) ChIP assay using E2F1 antibody, or normal IgG as control, to determine recruitment of E2F1, or normal IgG as control, onto E2F1, p73, and GAPDH promoters in DKO and AADKO prostate cells. (D) p73 IHC staining of prostate sections of four genotypes as indicated above the photographs. (E) Protein levels were determined by Western blot with the indicated antibodies in prostate ventral and anterior lobes of the indicated genotypes.

Fig. 3. p27T187A KI increased apoptosis in DKO prostate tumorigenesis and p73 played a major role in the apoptosis. (A and B) Consecutive prostate sections of four genotypes, as indicated above the photographs, stained with H&E or TUNEL, as indicated on the left. (C) Quantification of apoptosis. Arrows in the photograph demonstrate how total apoptosis was quantified. About 200 cells on each section (mouse) were counted. The bargraph was based on the average of quantifications from three mice. p value is by two-sided *t* test. (D) RT-qPCR to determine knockdown efficiencies by two shp73 constructs. (E and F) Propidium iodide based DNA content FACS to detect and quantify apoptosis as sub-G1 cell% in the population, as marked above the brackets.

Figure 4. Progression of DKO prostate tumorigenesis was inhibited in *p27*$^{T187A/T187A}$ mice. (A) Representative H&E stained prostate sections of the indicated genotypes at the indicated ages. (B) Pathological diagnoses of prostate lesions as PIN of four stages, invasive carcinomas, and gross tumors. Numbers of mice in each age groups are indicated below the chart. (C) Kaplan-Meier survival analysis comparing the *p27*$^{+/+}$ and *p27*$^{T187A/T187A}$ cohorts of mice undergoing DKO prostate tumorigenesis. Hazard ratio = 2.514, 95% confidence interval = 2.077 to 6.222, p <0.0001 by log-rank test.

Figure 5. A specific inhibitor of SCF$^{Skp2/Cks1}$ selectively inhibited DKO prostate tumor cells in two-dimensional culture and organoid culture and inhibited human mCRPC cell line DU145 in two-dimensional culture. (A) Proliferation chart showing cell numbers relative to the vehicle (DMSO) following treatment with Skp2/Cks1 pocket inhibitor Compound 1 (C1) at three concentrations after 2 days in monolayer cultures of the indicated cells. (B) Western blot following treatment with C1 (5 μM) for 2 days. (C) Organoid cultures of DKO prostate tumor cells after 15 days in culture. Organoids of various sizes (a, b, and c in red) were cropped out and shown at the original photograph size in (E). (D) Organoid cultures of AADKO prostate tumor cells after 15 days in culture. Debris piles likely result from organoids that grew to certain sizes and then disintegrated. Two examples of debris piles marked by a and b in blue and three unmarked debris piles were cropped out and shown in (F). (G) Counting of organoids and debris piles of various sizes following treatment with C1 at various concentrations for 15 days with vehicle (DMSO) control. (H) Fractions of organoids of the indicated sizes and debris piles.

Zhao_Fig 1

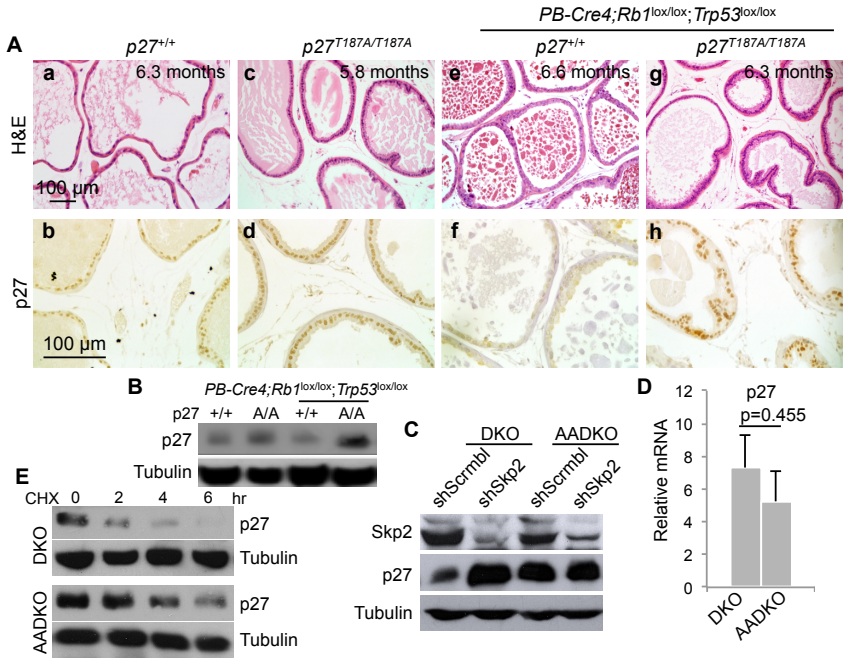

Zhao_Fig 2

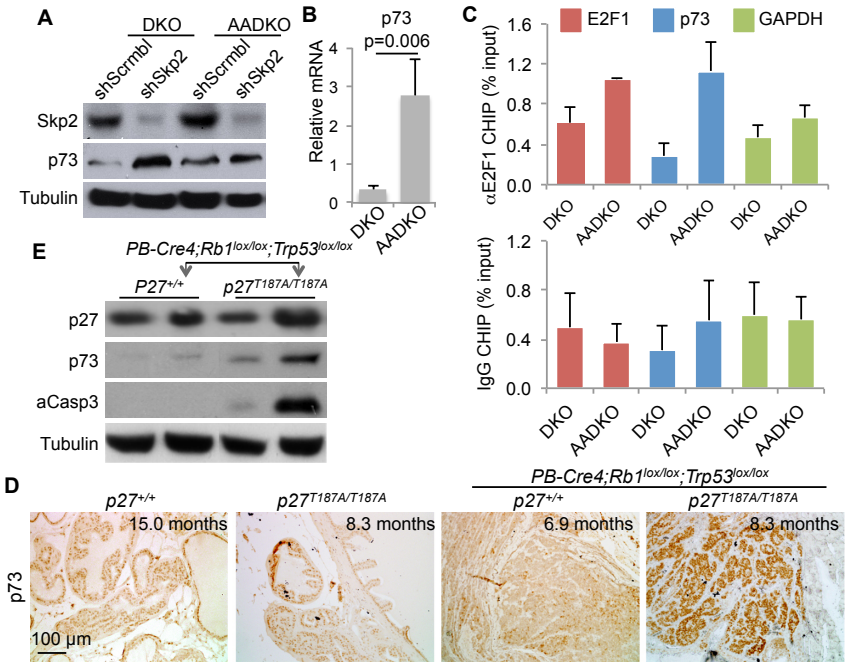

Zhao_Fig 3

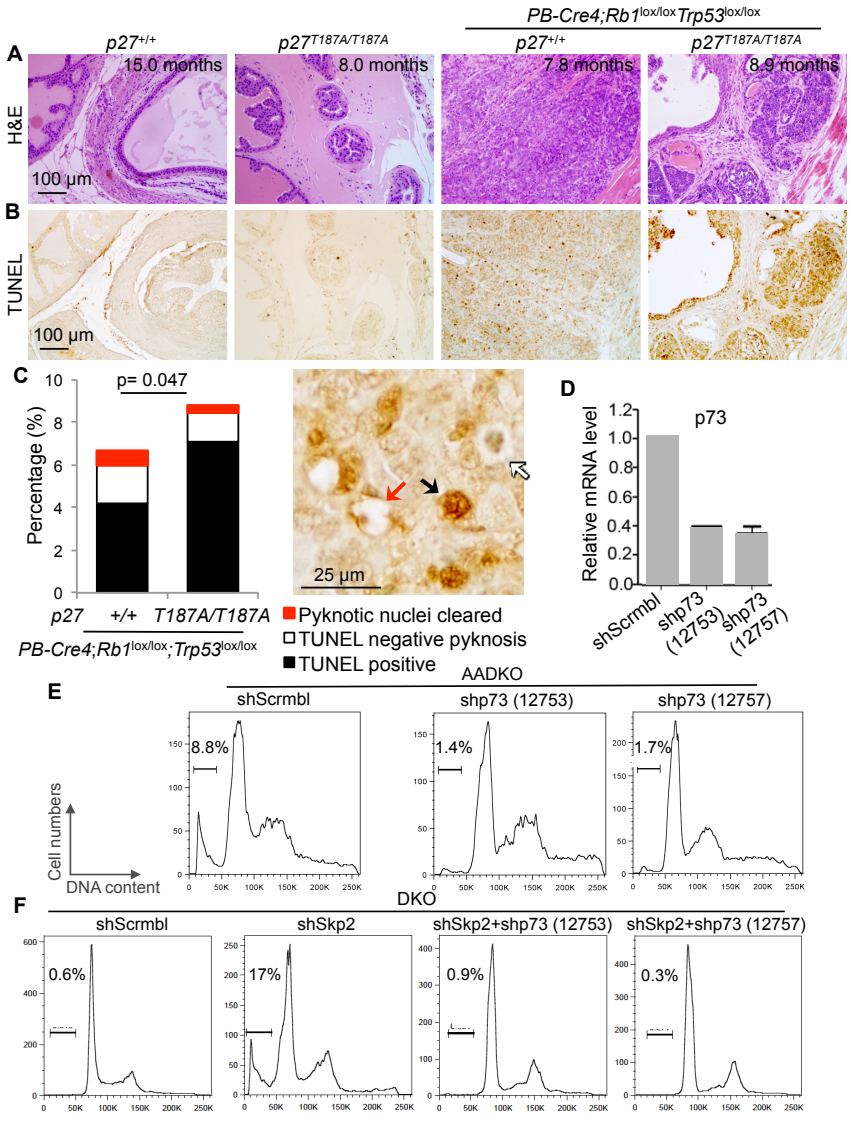
A
B
C
D
E
F
H&E
TUNEL
p27+/+
p27T187A/T187A
PB-Cre4;Rb1lox/lox Trp53lox/lox
15.0 months
8.0 months
7.8 months
8.9 months
100 μm
25 μm
p= 0.047
Percentage (%)
p27 +/+ T187A/T187A
PB-Cre4;Rb1lox/lox;Trp53lox/lox
Pyknotic nuclei cleared
TUNEL negative pyknosis
TUNEL positive
p73
Relative mRNA level
shScrmbl
shp73 (12753)
shp73 (12757)
AADKO
8.8%
1.4%
1.7%
Cell numbers
DNA content
DKO
shSkp2
shSkp2+shp73 (12753)
shSkp2+shp73 (12757)
0.6%
17%
0.9%
0.3%

Zhao_Fig 4

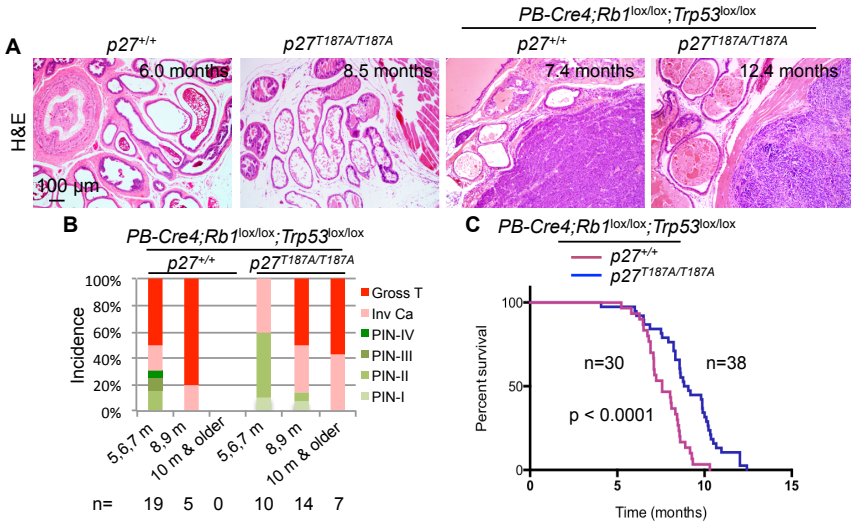

Zhao_Fig 5

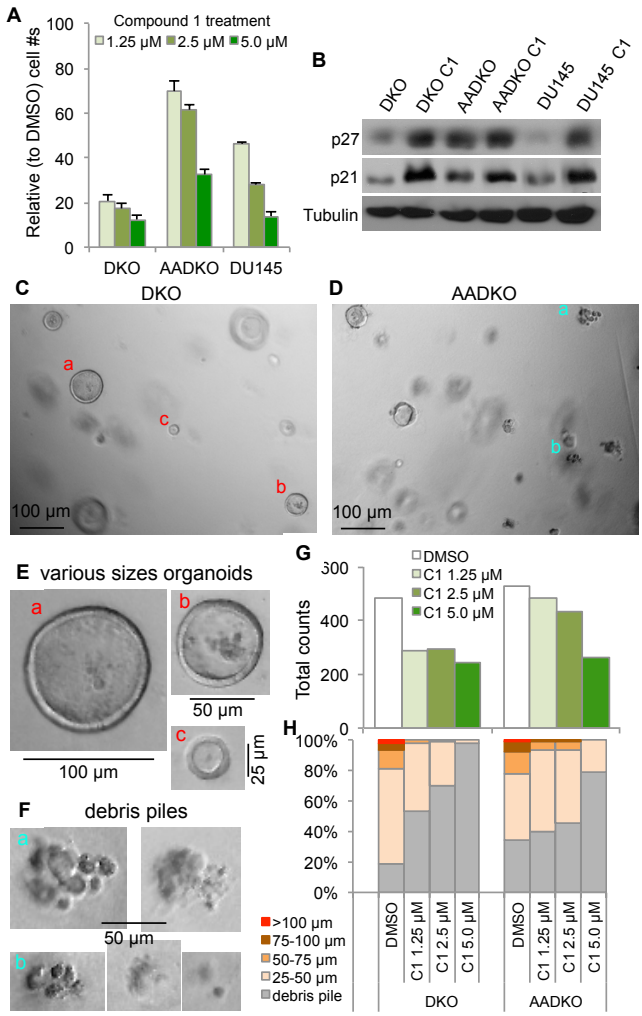

Supplementary Materials

p27T187A knockin mutation identifies Skp2/Cks1 pocket inhibitors for advanced prostate cancer

Hongling Zhao [1], Zhonglei Lu [1], Frederick Bauzon [1], Hao Fu [1], Jinhua Cui [1], Joseph Locker[2], and Liang Zhu[1]

[1]Department of Developmental and Molecular Biology, and Ophthalmology & Visual Sciences, and Medicine, The Albert Einstein Comprehensive Cancer Center and Liver Research Center, Albert Einstein College of Medicine, Bronx, NY 10461, USA. [2]Department of Pathology, University of Pittsburgh School of Medicine, Pittsburgh, PA 15261, USA

Inventory

Table S1. Pairwise relationships among *RB1*, *TP53, PTEN, NKX3-1* and *MYC* in primary prostate cancer and metastatic castration resistant prostate cancer (mCRPC)

	Primary prostate cancer			mCRPC		
Studies	MSKCC, 2010 [a]	Broad/Cornell 2012	TCGA, 2015	MSKCC, 2010 [a]	Michigan, 2012	Robinson et al, 2015
Specimen #s	157	109	333	28	50 [b]	150
RB1 inactivation [c]	3.2%	0.0%	0.9%	10%	29%	8.6%
TP53 inactivation [c]	1.9%	6.4%	7.5%	10%	54%	50%
PTEN inactivation [c]	5.7%	7.3%	17%	39%	50%	40%
NKX3-1 inactivation [c]	3.8%	0.0%	16%	3.6%	18%	3.3%
MYC activation [d]	40%	1.8%	13%	50%	25%	18%
Co-occurrence [e]	PPt, RM, PM, PtM	PPt	**PM**, RM, RPt, PPt	**RP**, RN, PN, RPt,	RM, PPt, NM, RN, PN, RPt, RP	**RP**, PPt, NM, PM, RPt, PN,
Statistic significance [f]			***p* = 0.033**	***p* = 0.023**		***p* = 0.039**

We retrieved data reported by (1-5) and analyzed them on cBioPortal. [a] This study included both primary and mCRPC specimens. [b] mCRPC specimens were obtained at autopsy. [c] Inactivation of *RB1*, *TP53*, *PTEN*, and *NKX3-1* is queried by HOMDEL MUT. [d] Activation of MYC is queried by AMP MUT EXP > 2 PROT > 2 (larger than 2 SD from the mean). [e] Tendency towards co-occurrence is by Log Odds Ratio; R, P, Pt, N, and M are short for *RB1*, *TP53*, *PTEN*, *NKX3-1*, and *MYC*, respectively, to indicate the pairs. [f] *p* value is by Fisher Exact Test. $p < 0.05$ is considered statistically significant, which is highlighted by bold font. Other pairs show tendencies with *p* values between 0.083 and 0.575. Tendency pairs with *p* values between 0.631 (the next higher value) to 0.907 (the highest) are not shown.

RB1 and *TP53* often incur Shallow Deletions, suggesting biallelic inactivation for some Mutation samples, as shown by the Oncoprints for two studies in Fig. S7.

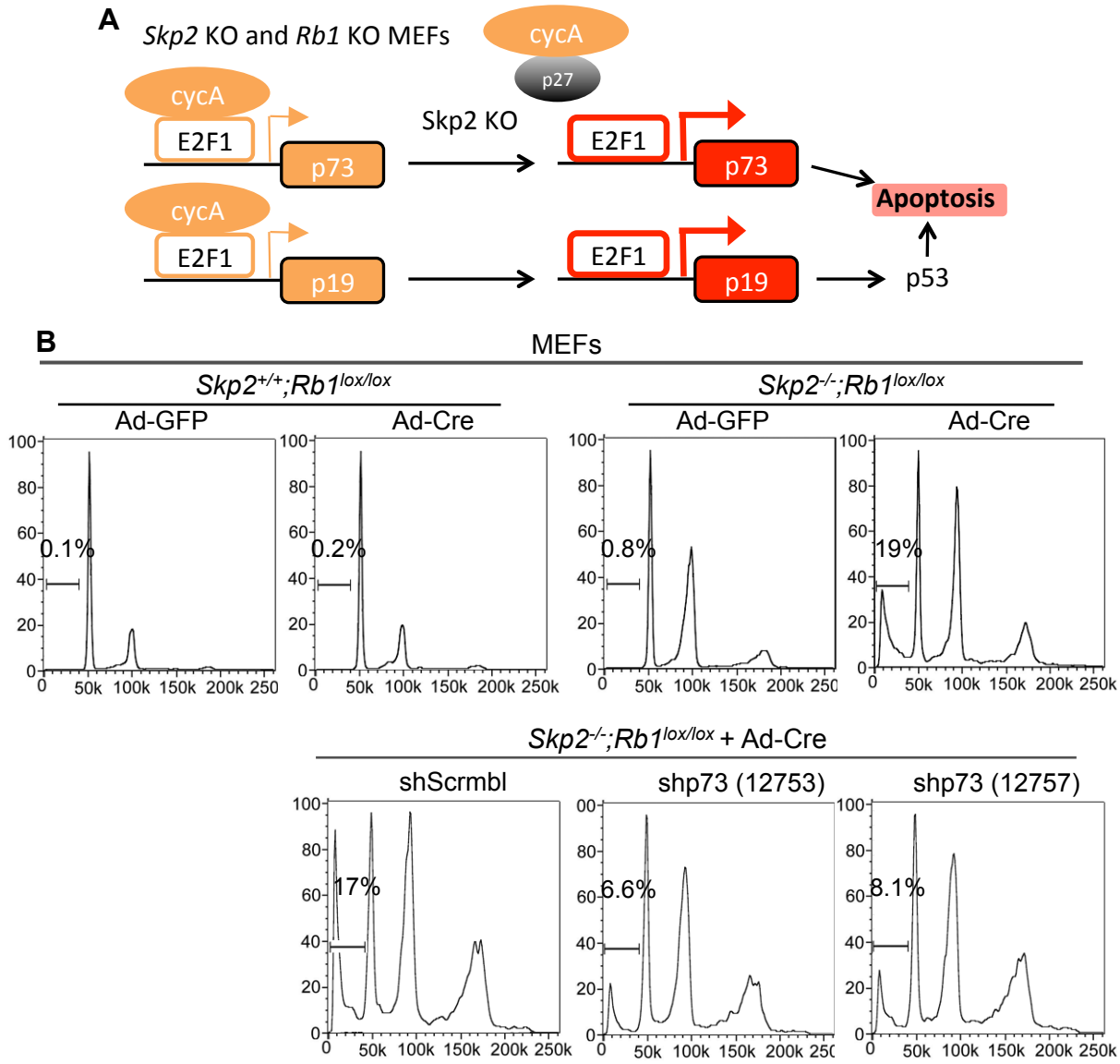

Fig. S1. Contribution of p73 to the apoptosis induced by *Rb1* deletion in Skp2 KO MEFs. (A) Cartoon depiction of how combined *Rb1* and Skp2 deletion led to further activation of E2F, which can induce p53-dependent and independent apoptosis. *Rb1* deletion activates E2F1 to increase expression of its target genes. The orange color indicates activated activity and expression when E2F1 is bound to cyclin A. Combined Skp2 deletion increased p27, which binds cyclin A competitively against E2F1 to relieve E2F1 from binding to and repression by cyclin A. The further elevated activity and expression is indicated by the red color. (B) Propidium iodide based DNA content FACS was used to detect and quantify apoptosis as sub-G1 cell populations shown above the brackets. Skp2 WT and Skp2 KO MEFs treated with Ad-GFP (as control) or Ad-Cre (to delete *Rb1*) were subjected to DNA content FACS to determine sub-G1 cell population sizes as indicated. (C) Same as in (A) except the indicated cells were additionally transduced with lentiviruses expressing shScrmbl (as control) or shp73 (to knockdown p73). Two separate shp73 constructs as indicated were used.

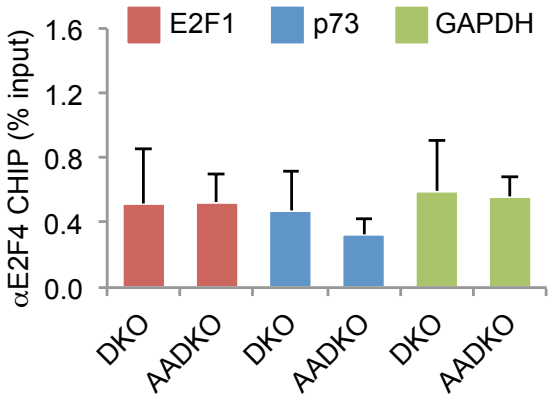

Fig. S2. Recruitment of E2F4 to E2F1, p73, or GAPDH promoters does not selectively increase in AADKO cells compared to DKO cells. ChIP experiment was performed with anti-E2F4 antibody to determine E2F4 occupancy on the indicated promoters in the indicated cells.

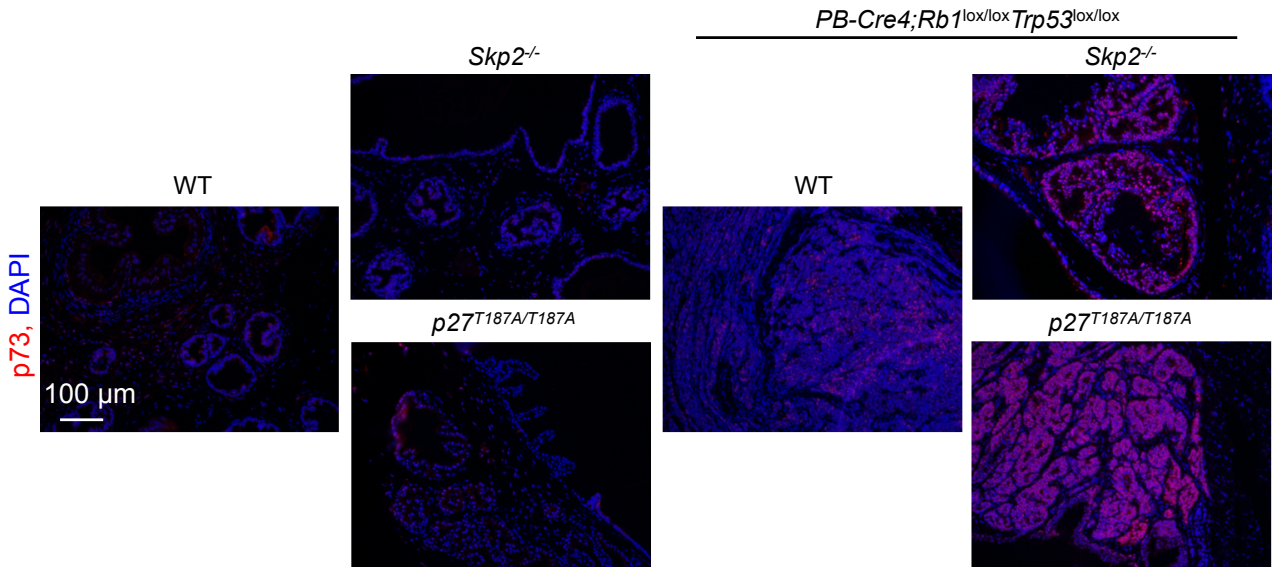

Fig. S3. p73 protein increased in DKO prostate tumorigenesis in Skp2 KO,or p27T187A KI, but not WT mice, nor in Skp2 KO or p27T187A KI mice. Prostate sections of the indicated genotypes were stained with anti-p73 with DNA counter stain by DAPI, as marked in red and blue, respectively.

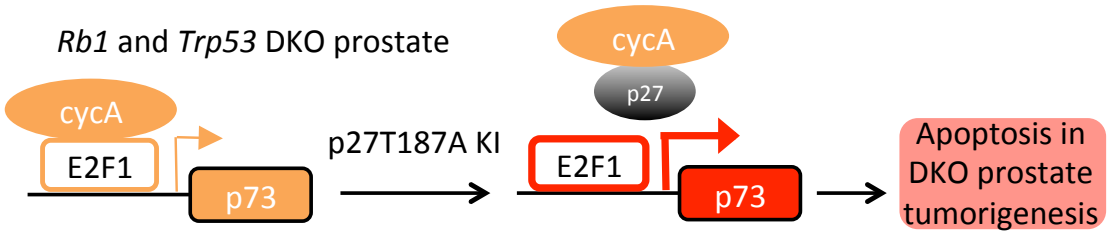

Fig. S4. p27T187A KI activates a p27-E2F1-p73-apoptosis pathway in DKO prostate tumorigenesis. The orange color indicates activated activity and expression. p27T187A KI increased p27, which relieves E2F1 from binding to and repression by cyclin A. The further elevated activity and expression is indicated by the red color.

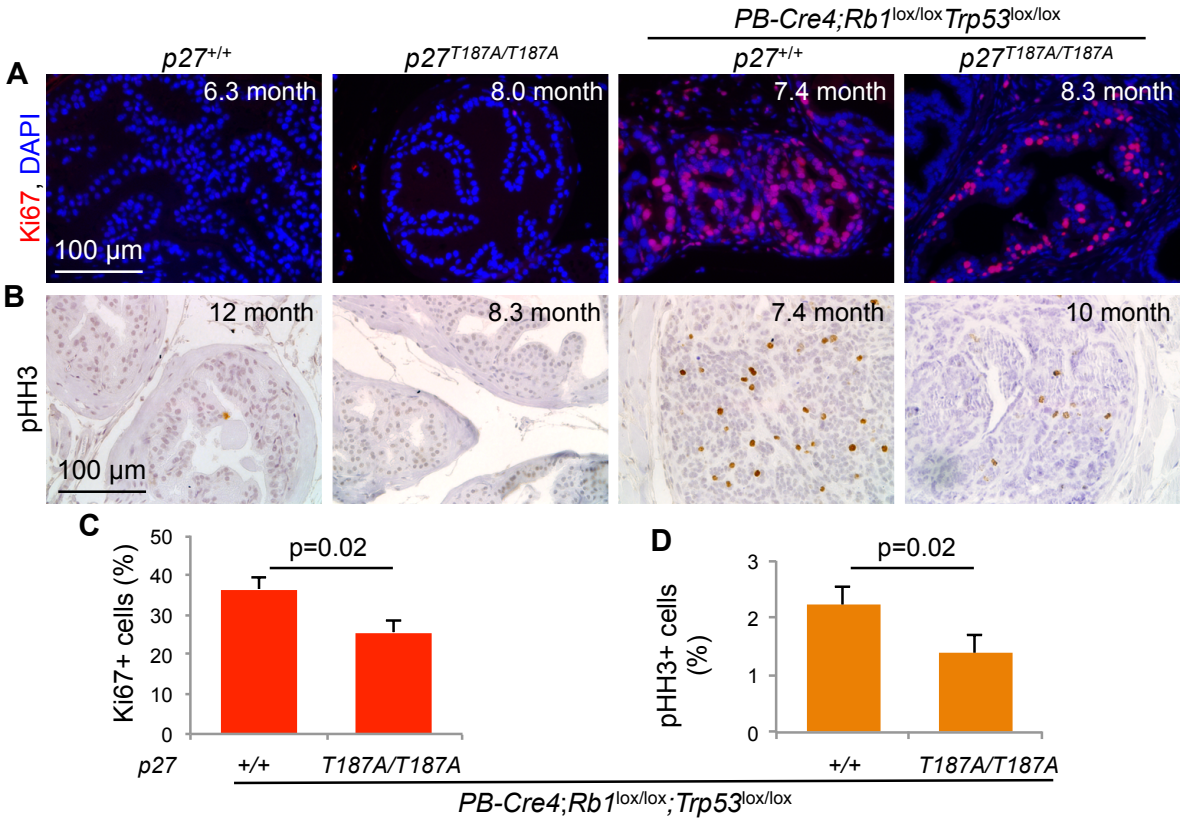

Fig. S5. p27T187A KI inhibits cell proliferation in DKO prostate tumorigenesis. (A) Cell proliferation was measured by Ki67 IF with DNA counter stain by DAPI as indicated by red and blue, respectively. Ki67 positive cells in DKO prostate tumorigenesis in p27 WT and p27T187A KI mice were quantified in (C). (B) Cell proliferation was measured by pHH3 IHC, positive cells in DKO prostate tumorigenesis in p27 WT and p27T187A KI mice were quantified in (D). Error bars represent SEM and p values are by two-sided *t* test.

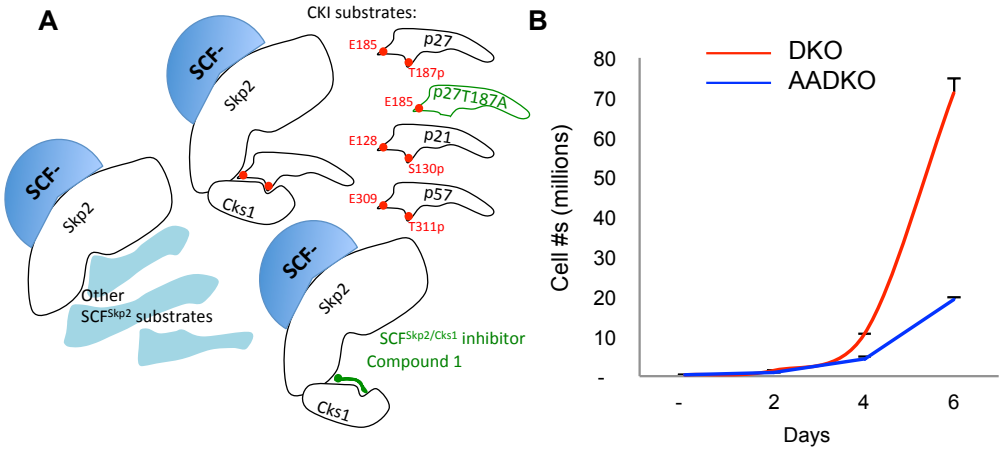

Fig. S6. Inhibition of p27 ubiquitination by $SCF^{Skp2/Cks1}$. (A) The designed inhibition mechanism for $SCF^{Skp2/Cks1}$ inhibitor Compound 1 (C1) compared to p27T187A KI. C1 can also inhibit ubiquitination of p21 and p57. (B) p27T187A KI inhibited proliferation of DKO prostate tumor cells in two-dimensional culture. Cell numbers were counted in triplicate plates every two days for six days.

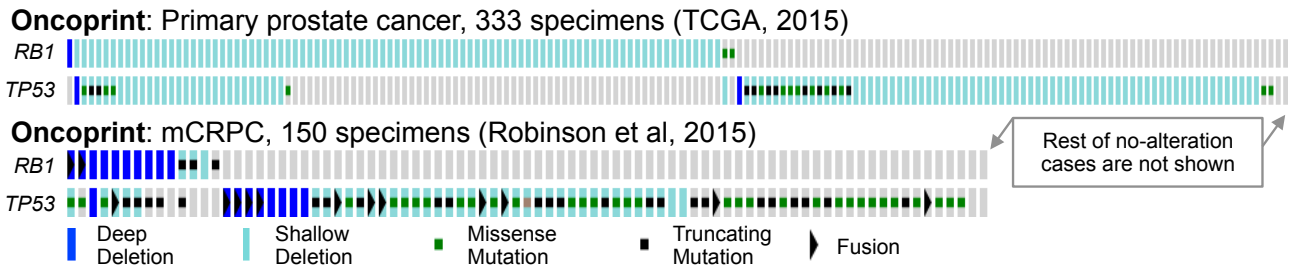

Fig. S7. Oncoprints of mutations and gene deletions of one study of primary prostate cancer (3) and one study of mCRPC (5). Related to Table S1.

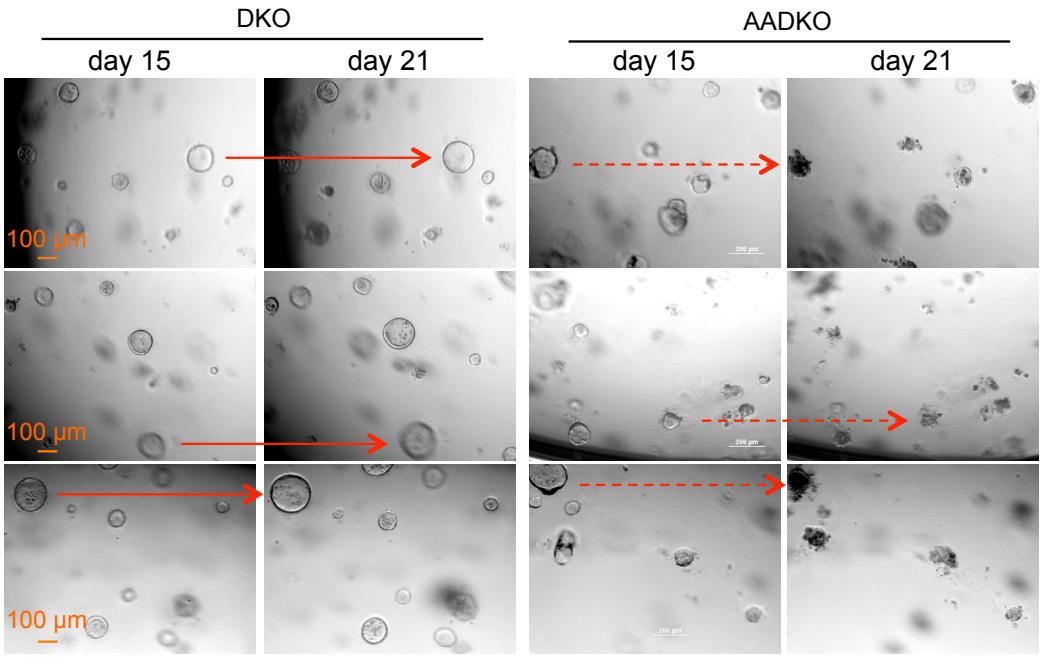

Fig. S8. DKO organoids grew larger while AADKO organoids spontaneously disintegrated during a 6-day period. The same areas of the organoid cultures were photographed on day 15 and day 21. Solid red arrows point to some examples of organoids growing larger, dashed red arrows point to some examples of organoids disintegrated into debris piles.

Materials and Methods

Mice

PB-Cre4 mice (6), *Rb1*$^{lox/lox}$ mice (7), *Trp53*$^{lox/lox}$ mice (8), and *p27*$^{T187A/T187A}$ mice (9) were described previously.

IHC and TUNEL Assays

Tissue sections and staining have been described previously (Zhao et al., 2013). Briefly, prostate glands were fixed in 10% Formalin (Fisher Scientific, SF 100-4), embedded in paraffin wax and sectioned. For immunohistochemistry (IHC) staining, slides were deparaffinized, hydrated, and incubated in a steamer for 20 minutes in sodium citrate buffer (Vector Labs, H3301) for antigen retrieval. Antibodies included: phospho-histone H3 (Cell Signaling Technology, #9701), Ki67 (Vector Labs, SP6), rabbit anti-p27 (Abcam, ab92741) and p73 (Abcam, ab40658). TUNEL staining was performed with an Apoptosis Detection Kit (Millipore, S7100).

Primary Prostate Cancer Cell Cultures, Organoid Cultures and Treatments

Primary prostate tumor cells were prepared from 0.3 cm x 0.3 cm tissue mass, which was minced with scalpels and dissociated in collagenase A in DMEM for 2 hours at 37°C. Primary prostate tumor cells were cultured in DMEM containing 10% FBS and their genotypes were confirmed by PCR genotyping of *Rb1*, *Trp53*, *p27*, and *PB-Cre4*. Prostate tumor cell organoid cultures were generated based on published protocols (10, 11). Prostate tumor pieces were minced and digested in 2.5 mg/ml collagenase D (#11088858001, Roche) in DMEM/F12 media (#10-092-CV, Corning) for 2 hours at 37°C, and followed by Trypsin digestion for 1 hour at 4°C. Dissociated cells were washed and seeded in growth factor reduced Matrigel (#356231, Corning) at 37°C. After 30 minutes incubation for Matrigel solidification, 100 µl complete DMEM/F12 medium were added on top of Matrigel. Media were changed every 3-4 days. Complete DMEM/F12 medium includes: 50 ng/ml EGF (#315-09, PeproTech Inc), 1 ng/ml FGF2 (#450-33, PeproTech Inc), 10 ng/ml FGF10 (#100-26, PeproTech Inc), 0.2 µg/ml

R-Spondin (#120-38, PeproTech Inc), 0.1 μg/ml Noggin (#250-38, PeproTech Inc), 500 nM A83-01 (SML0788, Sigma), 1x B27(17504-044, Life Technology), 1.25 mM N-acetyl-L-cysteine (A7250, Sigma), 10 mM Nicotinamide (#98-92-0, Acros Organics), 1x Glutamax (#35050-061, Life Technology), Primocin (#ant-pm-1, InvivoGen), 10 μM SB202190 (S7076, Sigma), 10 μM Y-27632 (S1049, Selleckchem), and 2 nM R1881 (R0908, Sigma). Knockdown of Skp2 or p73 was by lenti-shRNA vectors obtained from the Einstein shRNA core facility (shSkp2: 5'-GCAAGACTTCTGAACTGCTAT-3'; shp73 (12753): 5'-GCGCCTGTCATCCCTTCCAAT-3' and shp73 (12757): 5'-CAGCCTTTGGTTGACTCCTAT-3'); controlled by scrambled shRNA (shScrmbl). Generation of lentiviral stocks and transduction of cells were as described (12). Successful lentiviral transduction was ensured by puromycin (#BP2956-100, Fisher Scientific) resistance, followed by mRNA (RT-qPCR) and protein (Western blots) measurements. Compound 1 (C1, which inhibits interaction between Skp2/Cks1 and p27T187p (13)) was purchased from Xcess Biosciences Inc. (#432001-69-9). Prostate cancer cells were plated overnight and then treated with C1 for 2 days at the indicated concentrations.

Western Blot, CHX, RT-qPCR, ChIP Assays

Lysates of prostate tissues were prepared with RIPA buffer (50 mM Tris-HCl pH7.4, 1% NP40, 0.5% sodium deoxycholate, 0.1% SDS, 1 mM EDTA, 150 mM NaCl, and standard protease inhibitors). Prostate tissues were homogenized with Dounce glass homogenizer and briefly sonicated. Debris was removed by centrifugation for 10 minutes at 14,000 r.p.m. in an Eppendorf Centrifuge at 4 °C. Protein concentrations of the extracts were determined by Bio-Rad protein assay kit (#500-0006), and equal amounts of protein samples were loaded on 10% SDS gels and blotted onto PVDF membrane. For protein stability analysis, cells were plated into 60 mm dishes at 70%–80% confluence. CHX (#239764, Calbiochem) was added at 50 μg/ml. Antibodies used for Western blots are Skp2 (Santa Cruz Biotechnology, H435), p21 (Santa Cruz Biotechnology, SC-397) p27 (BD Bioscience, #610242), p73 (Abcam, ab40658), activated Caspase 3 (Cell Signaling Technology, #9661), and α-tubulin (Sigma-Aldrich, T6074). For RT-qPCR, cells were harvested at 16 h post plating. Total RNA was isolated with RNeasy kit (Qiagen) and reverse transcribed to cDNA with Superscript First Strand Synthesis System (Invitrogen, 18064-014). Real time-quantitative PCR was performed using SYBR green mastermix (Applied Biosystems, 4309155). Samples were run in triplicate and results were normalized with GAPDH in the same samples. Primers for p27 are sense: 5'-GCGGTGCCTTTAATTGGGTCT and antisense: 5'-GGCTTCTTGGGCGTCTGC T; p73 sense: 5'-AACGCCGAGCATCAATCC) and antisense: 5'-AGCCCAGACTCTGAGCACTT; GAPDH sense (5'-GGTTGTCTCCTGCGACTTCA and antisense 5'- GGTGGTCCAGGGTTTCTTAC. For ChIP analysis, briefly, cells were cross-linked with 1% formaldehyde in culture medium for 10 min at room temperature, which was stopped by addition of glycine to a final concentration of 0.125 M for 5 min at room temperature. Fixed cells were washed twice with PBS, pelleted and re-suspended in 1 ml of cell lysis buffer containing PMSF (5 mM HEPES pH8.0, 85 mM KCl, 0.5% Triton X-100,) and put on ice for 20 min before being pelleted again by centrifugation at 2500g for 5 minutes. Pellets were re-suspended with 600 μl nuclear lysis buffer containing PMSF (50 mMTris-HCl pH8.0, 10 mM EDTA, 1% SDS). DNA was sheared by sonication for 15 s x 4 in a 60 Sonic Dismembrator (Fisher), at a power setting of 10. Chromatins were precleared and incubated overnight at 4°C with 2 μg antibody. The chromatin and antibody mixture were then incubated with blocked protein A-Agrose beads at 4°C for 4 hr with rotation and followed by successive 10-minute washes in 1 ml of IP dilution buffer, dialysis buffer, TSE-500 buffer, LiCl detergent buffer, and TE buffer. After washing, the samples were eluted with elution buffer. The eluted material was purified by Qiagen PCR purification kit for qPCR. Antibody used for ChIP is E2F1 (Santa Cruz Biotechnology, SC-193X), E2F4 (Santa Cruz Biotechnology, SC-866X), IgG (Santa Cruz Biotechnology, SC-2027). Primer sequences for ChIP are: E2F1: sense 5-CTTTGGAGGTGAGCCTGAAGAG-3', antisense 5'-GGGTCTGGCGAAGCGAACA-3'; p73: sense 5'-TGAGAGTGCGGTTCTATTGGC-3', antisense 5'-GCCCTGAACATCTGCGTCTC-3'; GAPDH: sense 5'-GAGTTCTGGGAGTCTCGTGG-3', antisense 5'-CTCTTCGGGTGGTGGTTCA-3'.

Cell Proliferation Assay.

For prostate cell proliferation assay, $2X10^5$ cells were plated in 6 cm plates in triplicate, and cell numbers were counted every 2 days under the microscope with hemocytometers for indicated days. For prostate cell proliferation assay following C1 treatment, $1X10^5$ prostate tumor cells were plated overnight and then treated with C1 for 2 days at the indicated concentrations. For prostate tumor organoid culture, 2000 indicated prostate cells were seeded in 100 µl Matrigel in 48-well plate. After 30 minutes incubation at 37°C, complete DMEM/F12 media with indicated concentration of C1 were added to indicated wells.

Flow Cytometry Analysis for sub-G1 Cell Populations

Cells were plated for 16 hours. Cells were washed with PBS, trypsinized with 0.25% trypsin-EDTA at 37°C for 3-5 minutes, and resuspended with 0.5 ml PBS. Then cells were fixed with ice-cold 80% EtOH at 4°C overnight. The fixed cells were spun down and resuspended in 0.5 ml 0.25 mg/ml RNAse A and 30 µg/ml propidium iodide in PBS. Cells were filtered using 40 µm cell strainer before DNA content analysis using DXP10 Calibur at Einstein FACS core facility. Data were analyzed using Flowjo software.

Statistical Analyses

In Kaplan-Meier survival analysis, p value, hazard ratio and 95% confidence interval of hazard ratio were analyzed by log-rank test (GraphPad Prism 6 Software). Differences in Ki67, phospho-histone H3, TUNEL positive cells, cell proliferation and colony formation between indicated samples were analyzed by Student's *t*-test. All statistical analyses are two-sided. $p<0.05$ is considered as statistically significant.

Supplemental references

1. Taylor BS*, et al.* (2010) Integrative genomic profiling of human prostate cancer. *Cancer Cell* 18(1):11-22.
2. Barbieri CE*, et al.* (2012) Exome sequencing identifies recurrent SPOP, FOXA1 and MED12 mutations in prostate cancer. *Nat Genet* 44(6):685-689.
3. Network. CGAR (2015) The Molecular Taxonomy of Primary Prostate Cancer. *Cell* 163(4):1011-1025.
4. Grasso CS*, et al.* (2012) The mutational landscape of lethal castration-resistant prostate cancer. *Nature* 487(7406):239-243.
5. Robinson D*, et al.* (2015) Integrative clinical genomics of advanced prostate cancer. *Cell* 161(5):1215-1228.
6. Wu X*, et al.* (2001) Generation of a prostate epithelial cell-specific Cre transgenic mouse model for tissue-specific gene ablation. *Mechanisms of development* 101(1-2):61-69.
7. Sage J, Miller AL, Perez-Mancera PA, Wysocki JM, & Jacks T (2003) Acute mutation of retinoblastoma gene function is sufficient for cell cycle re-entry. *Nature* 424(6945):223-228.
8. Jonkers J*, et al.* (2001) Synergistic tumor suppressor activity of BRCA2 and p53 in a conditional mouse model for breast cancer. *Nat Genet* 29(4):418-425.
9. Malek NP*, et al.* (2001) A mouse knock-in model exposes sequential proteolytic pathways that regulate p27Kip1 in G1 and S phase. *Nature* 413(6853):323-327.
10. Karthaus WR*, et al.* (2014) Identification of multipotent luminal progenitor cells in human prostate organoid cultures. *Cell* 159(1):163-175.
11. Chua CW*, et al.* (2014) Single luminal epithelial progenitors can generate prostate organoids in culture. *Nat Cell Biol* 16(10):951-961, 951-954.
12. Sun D, Melegari M, Sridhar S, Rogler CE, & Zhu L (2006) A multi-miRNA hairpin method that improves gene knockdown efficiency and provides linked multi-gene knockdown. *BioTechniques* 41:59-63.
13. Wu L*, et al.* (2012) Specific small molecule inhibitors of Skp2-mediated p27 degradation. *Chemistry & biology* 19(12):1515-1524.

Reply Reply All Forward

Cell Symposia: Hallmarks of Cancer: Poster Acceptance Letter

Content-CHAL2014 [Content-CHAL2014@elsevier...

To: Hongling Zhao

Monday, August 18, 2014 7:58 AM

You forwarded this message on 8/18/2014 9:11 AM

Poster Acceptance Letter

Abstract reference number: CHAL2014_0167

Date: 18th August 2014

Email: hongling.zhao@einstein.yu.edu

Dear H. Zhao ,

Thank you for submitting an abstract to present at **Cell Symposia: Hallmarks of Cancer**. On behalf of the Organising Committee I am delighted to inform you that your abstract entitled "**Identifying effective antitumor mechanisms when both pRb and p53 are genetically inactivated**" has been accepted for **poster presentation** at the Conference.

If you have requested an oral slot, the review committee will finalise the decision on your abstract for short talk presentation in the next two weeks. We will contact you again by 29th August to confirm if your paper has been accepted for a short talk presentation

Title:	**Identifying effective antitumor mechanisms when both pRb and p53 are genetically inactivated**
Authors:	**H. Zhao, Z. Lu, L. Zhu**
Presenting Author:	**H. Zhao**

Please check the above details of your presentation carefully, as all conference material will be printed with this information. If there are any corrections please inform us as soon as possible by email to: Content-CHAL2014@elsevier.com

It is a condition of abstract acceptance that you or a nominated presenting co-author registers for the

Abstract for Cell Symposium, Hallmarks of Cancer: Asia, November 9-11, 2-14-Beijing, China

Identifying effective antitumor mechanisms when both pRb and p53 are genetically inactivated

Genetic inactivation of both major tumor suppressors pRb and p53 irreparably disables most cells' antitumor mechanisms. TCGA documents recurrent genetic inactivation of RB1 and TP53. They often co-occur and the co-occurrences become more frequent in more advanced cancer, which likely explain why advanced cancer are more likely to resist current anticancer therapies. Skp2 mediates ubiquitination of p27 to activate cyclin/CDKs, of Akt1 to promote anaerobic glycolysis, and of E-cadherin to promote cell migration. We used pRb and p53 doubly deficient mouse tumor models to determine the antitumor effects of targeting Skp2. Results show that Skp2 deletion blocked pRb and p53 doubly deficient pituitary and prostate tumorigenesis. On this platform, we identify multiple antitumor mechanisms, including mitotic block by p27, apoptosis by p73, blocking anaerobic glycolysis by targeting LDH-A, and dynamic control of EMT. We suggest that these antitumor mechanisms be considered in designing therapies for advanced and multi-therapy resistant cancer.

Reply Reply All Forward

Congratulations!

Mary Anne Clifford

To: Hongling Zhao

Cc: Liang Zhu

Tuesday, October 21, 2014 1:33 PM

You forwarded this message on 10/21/2014 1:47 PM.

October 21, 2014

Hongling Zhao, M.D., Ph.D.
Department of DMB
Ullmann - 521

Dear Hongling:

I am delighted to inform you that you have been selected by the Einstein Awards Committee as a recipient of one of the Dennis Shields Postdoctoral Research Prizes. Competition for these prizes was intense, and you should be extremely proud of this achievement.

Dean Spiegel will be presenting each awardee with a prize of $5,000 at a ceremony to be held at a date and time soon to be announced. In the spirit of the occasion, each awardee will be afforded the opportunity to give a 15-minute presentation of his/her work. Winners of travel awards for poster presentations will be announced at the close of the ceremony.

Please accept my congratulations on your truly outstanding achievement. I know that I speak for the entire Einstein community in wishing you continued success in your research, and I look forward to hearing your presentation.

With best wishes,

Jonathan M. Backer, M.D.
Director